## Title

Chemical tuning of $[Ni(hmp)(ROH)Cl]_4$ single molecule magnets and their self assembly onto gold

## Permalink

https://escholarship.org/uc/item/4qr2507q

## Author

Ma, James Minh

## Publication Date

2008

UNIVERSITY OF CALIFORNIA, SAN DIEGO

# Chemical Tuning of $[Ni(hmp)(ROH)Cl]_4$ Single Molecule Magnets and their Self Assembly onto Gold

A Thesis submitted in partial satisfaction of the requirements for the
degree Master of Science

in

Chemistry

by

James Minh Ma

Committee in charge:

Professor David N. Hendrickson, Chair
Professor Judy E. Kim
Professor Clifford P. Kubiak

2008

The Thesis of James Minh Ma is approved, and it is acceptable in quality and form for publication on microfilm and electronically:

Chair

University of California, San Diego

2008

To Sara, my family, Ms. Ward, and Rosental

# Table of Contents

## Chapter One

## Chapter Two

## Chapter Three

# List of Figures

## Chapter One

## Chapter Two

**Chapter Three**

# List of Tables

## Chapter Two

## Chapter Three

# Acknowledgements

I would like to first thank Professor Hendrickson introducing me to the field of molecular magnetism. I appreciate the work by Dr. Steven Barlow on the TEM analysis of the nanoparticles and Dr. Tom Mates for his XPS analysis of gold surfaces. Many thanks also go out to my labmates: Chris Beedle who first recruited me to the lab and taught me everything I know about magnetism, Katie Heroux who taught me X-ray crystallography and has been instrumental in the structural analysis of my compounds, Patrick Feng for his lively discussions about everything and brainstorming sessions, Casey Stephenson for being a fellow master’s student and his help in organic chemistry, and Sam Wilson who first trained me and introduced me to nickel chemistry. Ben Lear and John Goeltz of the Kubiak lab have also been extremely kind and gracious with spending the time to teach me how to do electrochemistry and surface IR measurements. Sara Thoi has also been very helpful in trouble shooting problems with my organic chemistry techniques and has been my motivation to finish my graduate studies. I would also like to thank Professor Kim who kept my interests in chemistry and has been my source for advice since my undergraduate years. I would also like to thank Ms. Ward, my first chemistry teacher, for motivating my interests toward chemistry. Lastly, I would like to thank Mr. Rosental, who always believed in the goodness of people and second chances for people to redeem themselves.

# ABSTACT OF THE THESIS

## Chemical Tuning of $[Ni(hmp)(ROH)Cl]_4$ Single Molecule Magnets and their Self Assembly onto Gold

by

James Minh Ma

Master of Science in Chemistry

University of California, San Diego 2008

Professor David N. Hendrickson, Chair

A series of tetra-nuclear cubane single molecule magnet (SMM) complexes were synthesized with the general formula $[Ni(hmp)(ROH)Cl]_4$ where ROH is an alcohol group or water. The following alcohol groups were explored to examine to effect of chemical modification on the magnetic characteristics of the compound and open the possibility of new chemistries: propyl alcohol, isobutyl alcohol, propargyl alcohol, water, benzyl alcohol, 2-thiophenemethanol, and 2-(methylthio)ethanol. Chemical modification of the compound varies the level of interaction between neighboring molecules and introducing other functional groups allow for post-modification of the complex. The analysis of both of molar paramagnetic susceptibility $\chi_M T$ versus temperature data and reduced magnetization measurements confirm the ferromagnetic coupling in the $Ni_4$ cubane molecule to give an S=4 ground state. AC susceptibility measurements were done to observe the kinetic effects of the barrier for reversal of magnetization.

Synthesis of self assembled monolayers (SAMs) of SMMs on gold surfaces and gold nanoparticles was explored. $[Ni(hmp\text{-}Cl)(MeOH)Cl]_4$, $[Mn^{II}_2Mn^{III}_2(mdea)_2(Hmdea)_2(O_2CPhBr)_2Cl_2]$**,** and $[Mn^{II}_2Mn^{III}_2(mdea)_2(Hmdea)_2(O_2CPhN_3)_4]$ were synthesized and possesses the functionality to undergo Suzuki or “Click” coupling reactions. The magnetic properties of the compounds were characterized and indicated ferromagnetic coupling to form S=4 and S=9 compounds, respectively. Suzuki coupling was carried out on the $Ni_4$ compound with gold surfaces and gold nanoparticles functionalized with 4-mercaptophenylboronic acid. XPS and IRRAS were used to monitor reaction progress and to verify the presence of the $Ni_4$ but results are inconclusive. Magnetic measurements were conducted on the functionalized AuNP and indicated a significant change in the magnetic susceptibility.

# Chapter One

# Introduction to Single Molecule Magnets

## 1.1 Introduction

Magnetic materials have been of intense interest for the last 3,000 years starting from naturally occurring materials such as loadstone. The technology associated with magnetic materials has evolved considerably since their early applications in devices such as magnetic compasses and are now commonplace in modern technologies such as nanoparticles used for drug delivery[1] and information storage technologies.[2] Recent developments in nanotechnologies have led to a need for device miniaturization. However, this goal is complicated due to the increasing role of quantum effects as particles approach the nanometer scale.[3] Quantum effects in magnetism have been theorized since the 1980's.[4, 5] However, initial "top down" approaches used to synthesize magnetic particles generally lead to materials with non-uniform sizes and shapes that make them difficult to characterize.[6] Chemists will play an ever increasing role in the design and development of nanoscale materials that was initiated by application of the "bottom up" approach to synthesis. This chemical synthesis approach allows for increased control of the size, shape, and environment (solvent molecules, molecular distributions etc.) within a crystal lattice and has produced some fascinating new materials such as spin-crossover complexes[7-11] and single-molecule magnets (SMMs)[12] that exhibit interesting magnetic and quantum phenomena.

The first SMM $[Mn_{12}O_{12}(OAc)_{16}(H_2O)_4] \cdot 2CH_3COOH \cdot 4H_2O$ ($Mn_{12}$-Ac) was synthesized by Lis[13] in 1980, but was not established as an SMM until 1993.[14-16] $Mn_{12}$-Ac is composed of four ferromagnetically coupled $Mn^{IV}$ ions centrally arranged in a distorted cube which is interconnected by oxide ions to eight ferromagnetically coupled $Mn^{III}$ ions.

$Mn_{12}$-Ac possesses an $S = 10$ ground state resulting from antiferromagnetic coupling between the inner $Mn^{IV}$ core ($S = 6$) and the outer $Mn^{III}$ ring ($S = 16$).

SMMs behave as individual magnetic particles and possess a significant barrier toward magnetization reversal as the result of a large spin ground-state ($S$) and significant easy-axis (Ising) axial magnetic anisotropy.[15-17] This anisotropy is reflected by a negative value of the axial zero-field splitting (ZFS) parameter ($D$), resulting in a theoretical barrier to magnetization reversal of $DS^2$ and $D(S^2\text{-}1/4)$ for integer and half-integer systems, respectively. The zfs term removes the degeneracy of the 2S+1 spin states in the absence of an external magnetic field and leads to a preferred orientation of the magnetic moment. For polynuclear transition metal complexes, zfs is a function of the zfs of the individual ions in their ground state. The orbital contributions from the single ions can be quenched by Jahn-Teller tetragonal elongation or by crystal fields leading to a small contribution by first approximation. Furthermore, spin-orbit coupling can lead to excited state mixing resulting in some contribution to the overall zfs and can be approximated using second order perturbation theory.[18]

In the case where two or more metal ions exist in a complex with appreciable zfs, the zfs becomes a function of the single ion contributions as well as the pair wise interactions between those metal ions

$$D = \sum_{i} d_i D_i + \sum_{i<j} d_{ij} D_{ij} \tag{1.1}$$

where $D_i$ is the zfs for the individual ion, $D_{ij}$ are the interactions between metal ions, and d is the expansion coefficient. However, interactions between metal ions are small whether they are through-space or through-bond. Therefore, the expression for the zfs of the molecule can be approximated as the linear combination of individual zfs tensors of the individual metal ions:[19]

$$D \approx \sum_i d_i\, D_i \tag{1.2}$$

The importance of the zfs of individual ions has therefore focused SMMs synthesis toward transition metal ions with inherently large zfs such as Ni, Mn, and Fe to generate the barrier for reversal of magnetization.

The energy barrier results in a preferred directionality for the system which is known as the easy axis. The easy axis lies along the z-axis of the molecule and results in a magnetic bistability which allows the molecule to exist in either a “spin-up” or “spin-down” state.[16] A diagram of the energy barrier for $Mn_{12}$-Ac is given in Figure 1. At room temperature, there is random population of the 2S+1 spin states leading to equal populations of molecules in the “spin-up” and “spin-down” states. However, the population distribution can be biased toward a particular spin orientation at low temperatures and in an externally applied magnetic field. Once oriented, the spins are unable to thermally relax and “climb” over the energy barrier. Thus, in order for the magnetic moment to go from a “spin up” to “spin down” state it must due so via quantum mechanical tunneling.

Intense studies of SMMs have revealed interesting quantum phenomena such as Quantum Tunneling of Magnetization (QTM), exchange bias, spin-spin cross relaxation effects, and Berry phase.[20-24] These effects have spurred extreme interest among chemists and physicists to synthesize and characterize new SMMs. A common set of tools have

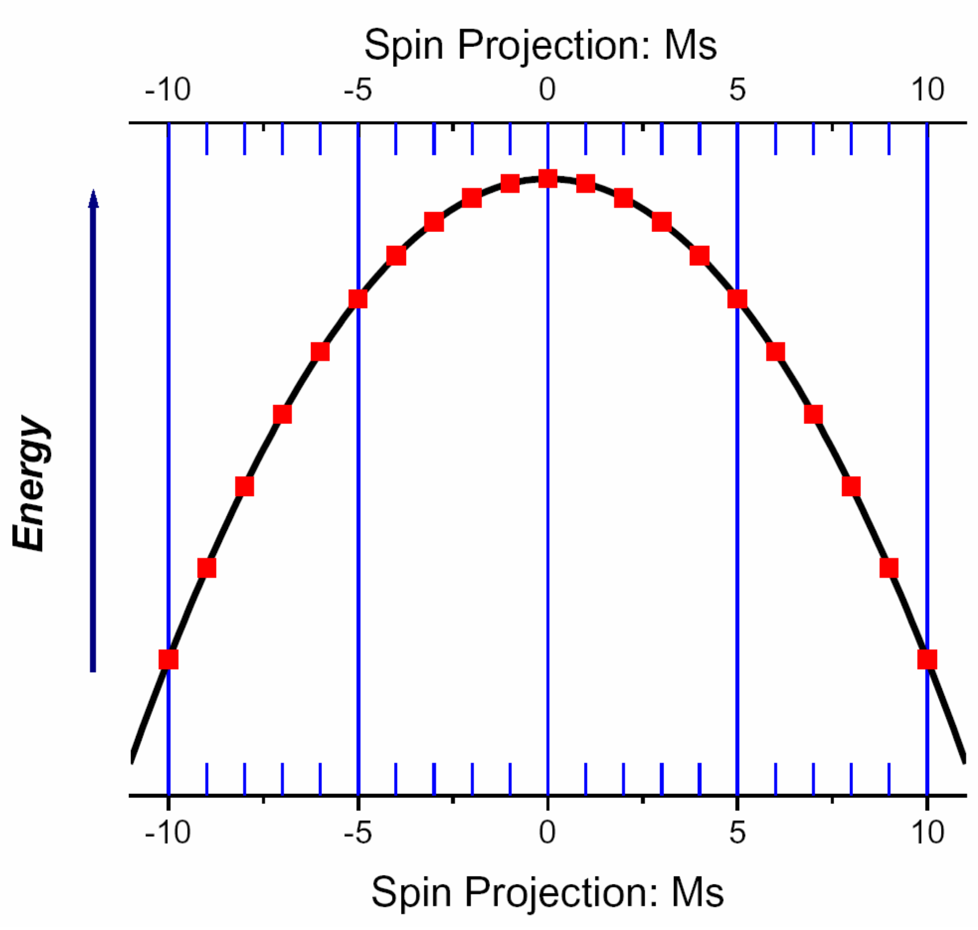

**Figure 1.** Potential energy diagram of $Mn_{12}$-Ac. Each red point represents a potential spin state.

been developed to characterize SMMs which include experiments such as variable temperature ($\chi_m$T vs. T) variable field (*M/Nß* vs. *H/T*) (reduced magnetization) direct current (DC) magnetic susceptibility, magnetization versus field ($M/M_s$ vs. *H*) hysteresis, and alternating current magnetic (AC) magnetic susceptibility.

## 1.2 Variable Temperature DC Magnetic Susceptibility

SMMs consist of paramagnetic transition metals centers which interact to yield a high spin ground state. Therefore, significant magnetic exchange interactions exist between the metal centers and are modulated by their bridging ligands. In the simplest case of isotropic coupling J of spins $S_j$ and $S_{i,,}$ the following spin Hamiltonian is used to represent the pairings magnetic exchange interactions:

$$\hat{H} = \sum_{i>j} -2J_{ij}\hat{S}_i\hat{S}_j \tag{1.3}$$

Ferromagnetic exchange between spin centers have positive J values and lead to spin alignment, thus summing the contribution of the individual spins. The opposite is true of antiferromagnetic exchange where J values are negative and act to pair opposing spin, thus leading to a low spin ground state.

The Kambe vector model can be used to simplify the above spin Hamiltonian to obtain directly the eigenvalues.[25] For a simple 2 metal ion system, the Kambe model can be easily applied. The total spin is defined as $\hat{S}_T = \hat{S}_A + \hat{S}_B$ where $\hat{S}_A$ and $\hat{S}_B$ are the spins for the two metal ions. A substitution can be made into the spin Hamiltonian and the Hamiltonian now can be expressed as:

$$\hat{H} = -J(\hat{S}_T^2 - \hat{S}_A^2 - \hat{S}_B^2)/2 \tag{1.4}$$

The corresponding energy eigenvalues $E(S_T)$ for the Hamiltonian are now defined as:

$$E(S_T, S_A, S_B) = -(J/2)[S_T(S_T+1)-S_A(S_A+1)-S_B(S_B+1)] \qquad (1.5)$$

The energies obtained for the spin states of the system are then put into the Van Vleck equation to fit experimental $\chi_M T$ data. The Van Vleck equation for magnetic susceptibility relates the exchange term J of a given spin state with the magnetic susceptibility $\chi_M T$. The Van Vleck equation takes the form

$$\chi_M T = \frac{Ng^2\beta^2}{3k}\frac{\sum_{S_T} S_T(S_T+1)(2S_T+1)\exp(-E_{S_T}^{(0)}/kT)}{\sum_{S_T}(2S_T+1)\exp(-E_{S_T}^{(0)}/kT)} + TIP \qquad (1.6)$$

where N is Avogadro's number, k is Boltzmann's constant, β is Bohr magneton, T is the absolute temperature, and TIP is the temperature independent paramagnetism. This approach allows for the determination of the magnetic exchange constants and the spin ground state.

### 1.3 Variable Field DC Magnetic Susceptibility

Determination of the axial zero-field splitting parameter D and the spin state of a system can be carried out by what is called a "reduced magnetization" experiment. A sample is scanned in multiple magnetic fields typically ranging from 0.1-5 T and with temperatures between 5-1.8 K. At higher temperatures (~300K) and in the absence of an applied magnetic field (B), SMMs show no net magnetization because there is sufficient Boltzman population of all energy states. However, at low temperatures (approaching 0K) and/or with the application of strong magnetic fields, individual magnetic moments will collectively orient, because the Zeeman term becomes larger than the thermal energy in the system. If there is no zfs or significant spin-orbit contribution, magnetization curves (iso-fields) in a M vs H/T plot will superimpose and will reach a maximum of two times the spin (2S) because all of the 2S+1 states are degenerate. Conversely, if there is considerable orbital and zfs contribution, the individual magnetization curves will not superimpose because zfs lifts the degeneracy of the 2S+1 states. In this case, information in regards to the magnitude of the zfs parameter and the ground state spin of a molecule can be evaluated employing the spin Hamiltonian:

$$\hat{H} = g\beta H \cdot \hat{S} + D[\hat{S}_z^2 - S(S+1)/3] + E[\hat{S}_x^2 - \hat{S}_y^2] \tag{1.7}$$

The first term accounts for Zeeman interactions, the second term is the second order zfs, and the third term the rhombic zfs. Application of the above Hamiltonian onto the 2S+1 spin basis set results in the energy eigenvalues $E_i$ that are then evaluated by substitution into the Van Vleck equation:

$$M = \frac{\sum_{i=-S}^{S} (\partial E_i / \partial H) \exp(-E_i / kT)}{\sum_{i=-S}^{S} \exp(-E_i / kT)} \tag{1.8}$$

It is important to note that certain assumptions are made in application of this model. First, the model assumes the molecules populate a single, well isolated, spin state with no thermally accessible excited states. Second, it assumes that there are no significant intermolecular or dipolar interactions between molecules which can give rise to mixing of higher lying states into the ground state.

### 1.4 Alternating Current Magnetic Susceptibility

The energy barrier in an SMM can also be examined by employing alternating current (AC) magnetic susceptibility experiments. A sample is placed in a small (~3 G) oscillating field with no external DC field and is cooled to low temperatures (< 5K). The governing equation for the response is as follows[12]:

$$M_{AC} = M_0\cos\theta\cos(\omega t)+M_0\sin\theta\sin(\omega t)= \chi' H_0\cos(\omega t)+ \chi'' H_0\sin(\omega t) \qquad (1.9)$$

where the real in-phase component is $\chi'$ which represents the dispersive magnetic response and the out-of-phase component is $\chi''$ which accounts for the energy dissipated due to absorption from the applied magnetic field. SMMs are known to show an out-of-phase susceptibility due to the presence of their inherent barrier toward the reversal of magnetization. The frequency and temperature dependence exhibited by SMMs is a consequence of the inability of the magnetic moment to stay aligned with the oscillating AC field. This response is more pronounced in higher frequencies (i.e. the onset of the out-of-phase component of the AC susceptibility will occur at higher temperatures and will result in a larger $\chi_m''$ maximum than lower frequencies). Furthermore, systems with a larger energy barrier $DS_z^2$ will show the onset of out-of-phase susceptibility at higher temperatures. Though frequency dependent out-of-phase signals are a hallmark of SMMs, they do not definitively confirm SMM behavior.

### 1.5 Magnetization Hysteresis and Quantum Tunneling of Magnetization (QTM)

In a magnetization hysteresis experiment, the magnetization value at particular field is not always proportional to the magnitude of the applied field. Rather, the magnetization value is related to the history of the magnetic moment in the applied field as seen in Figure 2. When an external field is applied to a classical magnet (Figure 2), the magnetization will reach saturation magnetization saturation ($M_s$) at a finite field strength and any increase in field strength will not affect the magnetization maximum of

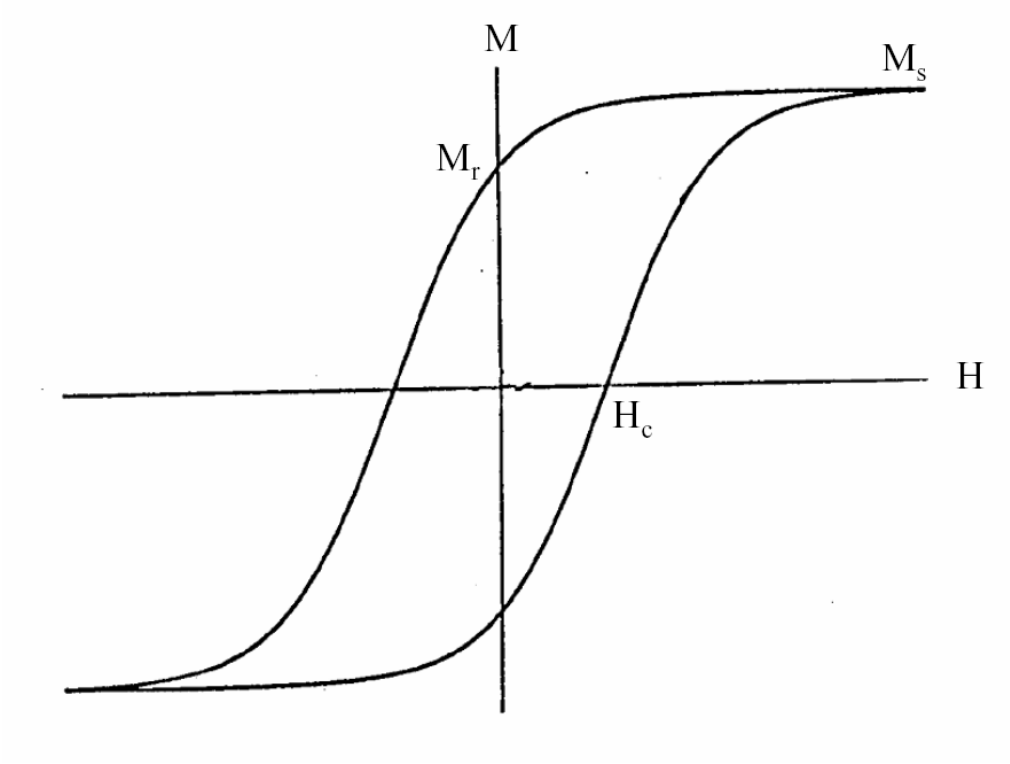

**Figure 2.** Hysteresis plot of a classical magnet.

the sample. If the field is turned off, the magnetization of the sample will decrease but not return to 0. The magnetization remaining under zero field is the remnant magnetization ($M_r$). An opposing field is necessary to return the magnetization of the sample to zero. This field is known as the coercive field ($H_c$). The same effect can be seen when the field is applied in the opposite direction and a mirror image of opposite sign is produced. The full sweep of the field in both directions results in the magnetic hysteresis loop seen in Figure 2.

A similar experiment can be carried out on SMMs to obtain hysteresis loops. Hysteresis loops for classical magnets arise from the annihilation and reformation of domain walls within the sample and is a macroscopic property. Quantum effects are observed in SMMs because SMMs are on the order of a few nanometers. A hysteresis plot of $Mn_{12}$-Ac is presented in Figure 3.[26] If the hysteresis measurement is done below the blocking temperature of the molecule, QTM can be observed. At temperatures greater than the blocking temperature, there is thermal relaxation of spin and tunneling events are not observed. Below the blocking temperature of a sample, spins are forced into either the “spin-up” or “spin-down” state and cannot thermally equilibrate. Tunneling events are observed as vertical “steps” in the hysteresis plot when the appropriate field is applied to create spin resonance and degeneracy is present between different $M_s$ states.

The system cycles between on and off resonant states as the field is swept in the hysteresis measurement. When the system is resonant, the spin levels of the “spin up” and “spin down” states are degenerate. The degeneracy of spin states allows for tunneling events to occur. A diagram of when tunneling is allowed and disallowed can be seen in Figure 4. The fields at which tunneling events occur are governed by the Hamiltonian:

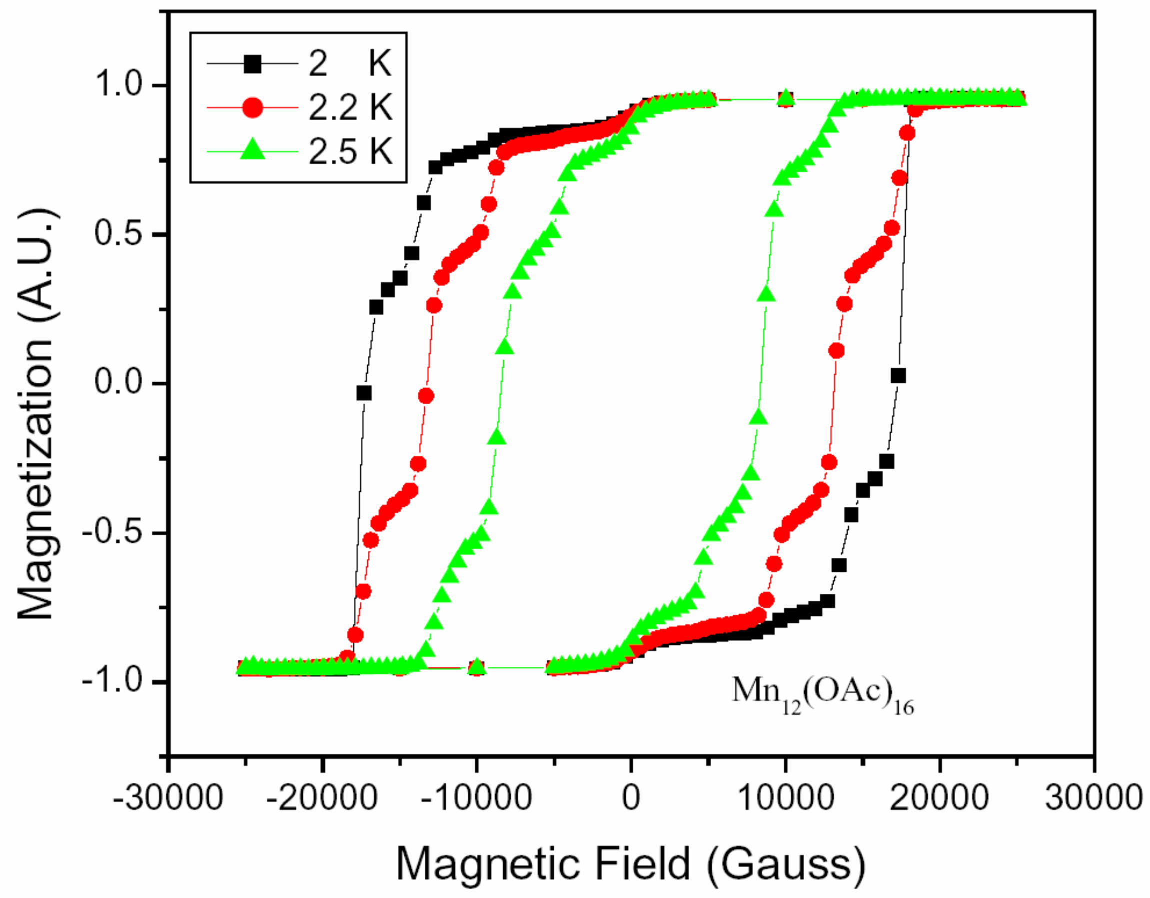

**Figure 3**. The hysteresis plot of $Mn_{12}$-Ac carried out at several temperatures. The tunneling events are seen as the vertical "steps".[27]

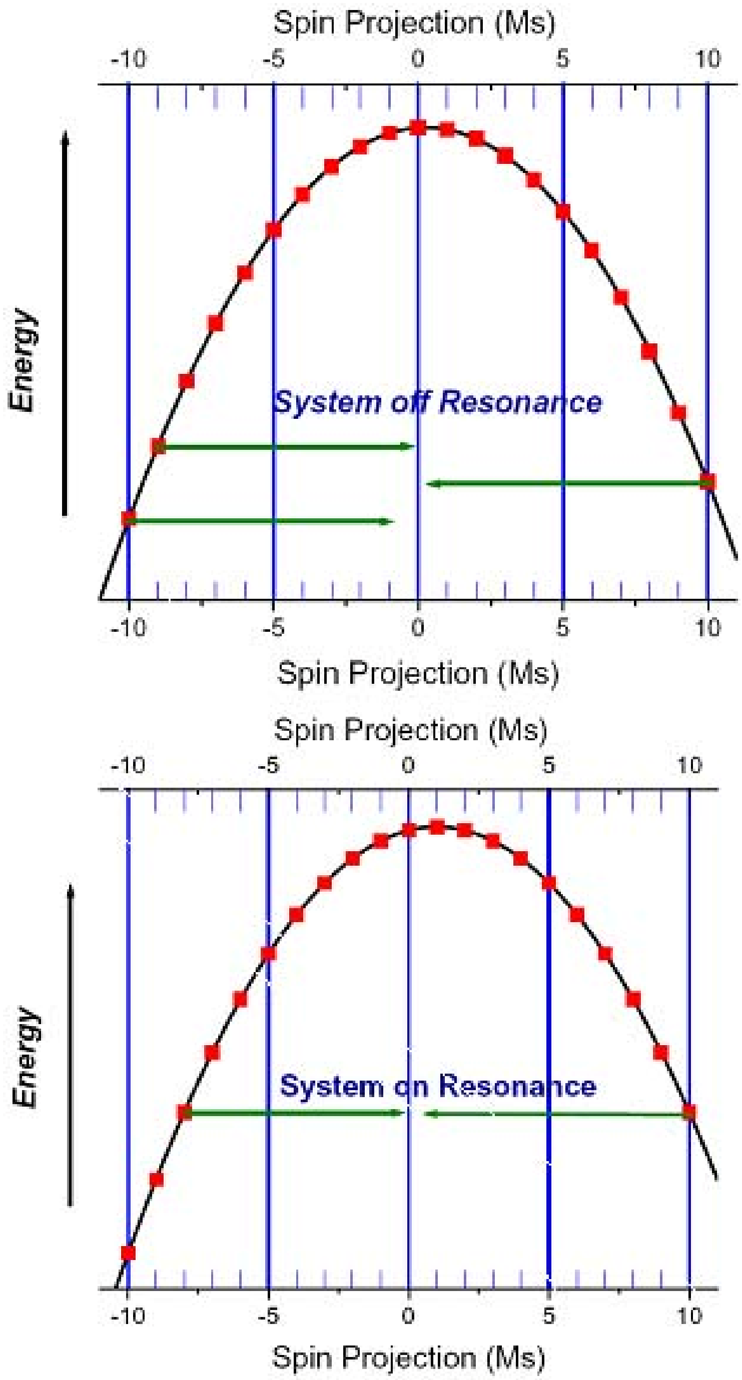

**Figure 4**. Diagram of an S=10 molecule with the spin state off (top) and on (bottom) resonance. No tunneling events occur when the system is off resonance.

$$\hat{H} = g\beta \mathrm{H} \cdot S + DS_z^2 + BS_z^4 + \hat{H}_T \qquad (1.10)$$

where the first term accounts for Zeeman interactions, the second and third terms represents the second and fourth order zfs term, and the last term $\hat{H}_T$ represents the transverse component of the spin operator. Transverse terms include the rhombic zfs E term and the fourth order transverse zfs $B_4^4$, both of which can cause quantum tunneling.

For systems such as $Mn_{12}$-Ac and $Ni_4$ cubanes where four fold symmetry exists, the rhombic E term is forbidden and the $B_4^4$ term is the dominant transverse term. For a term to be allowed it must be symmetric to all operations in the irreducible representation of the space group.

Tunneling can occur between unequal spin levels such as $M_s$=10 to $M_s$=-9 due to the distortion of the spin energy levels by the applied field. Tunneling can also occur between equivalent levels such as $M_s$=10 to $M_s$=-10 and for an $M_s$=10 system, this is ground state tunneling. Ground state tunneling is typically observed in zero magnetic field. However, it has been observed that for some systems that the ground state tunneling event is shifted away from H=0. This phenomenon is known as exchange bias. The $[Ni(hmp)(ROH)Cl]_4$ family of SMMs is an extensively studied system known to show exchange bias.[28, 29]

The relative simplicity of the $Ni_4$ system compared to $Mn_{12}$-Ac has allowed for detailed study of the molecule through high frequency electron paramagnetic resonance (HFEPR). This molecule continues to be an active area of research and is one of the focuses of this thesis.

## 1.6 Developments in Ni4 SMMs

The $Ni_4$ cubane family of molecules has been a productive family of molecules or studying important physical properties inherent to SMMs. The general formula is $[Ni(hmp)(ROH)X]_4$ where $hmp^-$ is the monoanion of 2-hydroxymethylpyridine, ROH is an alcohol ligand, and X is a halide ion. They are relatively simple systems composed of only 4 exchange coupled metal ions and are particularly suited to indepth study for the following reasons: 1) the peripheral alcohol ligands and solvate molecules of the $Ni_4$ family are easily exchanged; 2) in several of the $Ni_4$ complexes, the site symmetry in the crystal is high ($S_4$); 3) in certain cases (dmb) there are no solvate molecules. This reduces the number of microenvironments and gives sharp HFEPR signals; 4) isostructural $Zn_4$ complexes can be made. This has allowed the study by HFEPR of the properties of one $Ni^{II}$ ion in the $NiZn_3$ complex; 5) each $Ni^{II}$ has S=1 and therefore (2S+1)=3. This leads to a Hamiltonian matrix for a $Ni_4$ complex that is 81 x 81 in size. Thus it is possible to diagonalize the whole Hamiltonian matrix to discover which terms lead to the tunneling of the magnetization. This cannot be done for other SMMs such as $Mn_{12}$-Ac or $Fe_8$.

The effects of modification of the peripheral alcohol ligands were previously studied.[29, 30] A series of $[Ni(hmp)(ROH)X]_4$ molecules was synthesized using methanol (MeOH), ethanol (EtOH), 2-2'-dimethyl-1-butanol (dmb), and 3-cyclohexyl-1-propanol (chp) to examine the effect of increasing the steric bulk surround the $Ni_4$ molecule. It was found that the larger alcohol ligands provided a greater level of insulation between molecules that significantly affects intermolecular interactions, and thus, leads to distinct differences in exhibited magnetic behavior in this series of complexes. Subtle changes in the size and bulk of the aliphatic groups of the peripheral alcohol ligands, and the ability of the aliphatic groups to reside in varying crystallographic conformations (disorder), plays a crucial role on crystal packing and molecular site symmetry.

The $Ni_4$-MeOH, $Ni_4$-EtOH and $Ni_4$-chp complexes all have two symmetry independent molecules in their crystal lattice. In all three cases, one molecule is in a general position while the other resides on a special position. The $Ni_4$-dmb crystal lattice contains one symmetry independent molecule. The $Ni_4$-MeOH and $Ni_4$-EtOH complexes both cocrystallize with water solvate molecules, while the $Ni_4$-dmb and $Ni_4$-chp complexes contain no solvent molecules in their crystal lattice. The effect of long and short range intermolecular exchange interactions, through classical and non-classical hydrogen bonding significantly affect the magnetic ordering temperatures in this series of complexes.

Low temperature (<1.8 K) AC magnetic susceptibility measurements revealed that the magnetic ordering temperature in these molecules is, in part, related to the insulating ability of the coordinated alcohol ligand. [29, 30] The $Ni_4$-MeOH complex has the highest magnetic ordering temperature of 1100 mK, followed by $Ni_4$-dmb at 290 mK, and $Ni_4$-chp at ~80 mK. The higher magnetic ordering temperatures observed in the $Ni_4$-MeOH and $Ni_4$-EtOH complexes are due to the greater effect of long range interactions between molecules. This increased effect arises from close Cl···H contacts between the $Ni_4$ complexes and water solvate molecules and Cl···H contacts between neighboring $Ni_4$ complexes via hmp protons and chloride ions..[30] These interactions are minimized in the The $Ni_4$-dmb and $Ni_4$-chp complexes.

In addition, oriented single-crystal magnetization hysteresis ($M/M_s$ vs. H/T) measurements revealed the presence of exchange bias in the $Ni_4$ series. The magnitude of exchange bias can be correlated to the changing insulation ability of the coordinated alcohol ligands. The $Ni_4$-MeOH complex has an exchange bias of -330 mT, the shift for $Ni_4$-dmb is 12 mT, and for $Ni_4$-chp is -20 mT. The tunneling events for $Ni_4$-MeOH can be seen in Figure 5 as the vertical steps in the magnetization hysteresis loops. The derivative plot of the remaining compounds is provided in Figure 6 where $Ni_4$-dmb and $Ni_4$-chp are complexes 3 and 4, respectively. The on-resonance tunneling events are given as peaks in the derivative plot. The larger alcohol ligands reduce intermolecular exchange interactions which results in a smaller exchange bias.[30]

Molecular site symmetry and intermolecular exchange interactions play a vital role in determining quantum tunneling rates in SMMs. The $Ni_4$-chp complex exhibits very fast tunneling rates due to its lower symmetry. This complex crystallizes in the space group $C_2/c$ with two symmetry independent molecules. One molecule possesses $C_1$ symmetry and the other $C_2$ symmetry. All of the other $Ni_4$ complexes have $S_4$ site symmetry. The lower symmetry in the $Ni_4$-chp complex gives rise to symmetry allowed second order transverse anisotropy Hamiltonian terms and enhanced tunneling rates. While exchange bias and ordering temperatures can be attributed to the level of insulation between molecules and the magnitude of intermolecular interactions, the origin of fast tunneling in the high symmetry complexes has not been determined. In order to determine what Hamiltonian terms are responsible for tunneling in the high symmetry complexes, oriented single-crystal high-frequency electron paramagnetic resonance (HFEPR) studies were performed.

HFEPR studies were initiated to determine the Hamiltonian parameters and the origin of the fast ground state QTM rate in the high symmetry $Ni_4$ complexes, and in

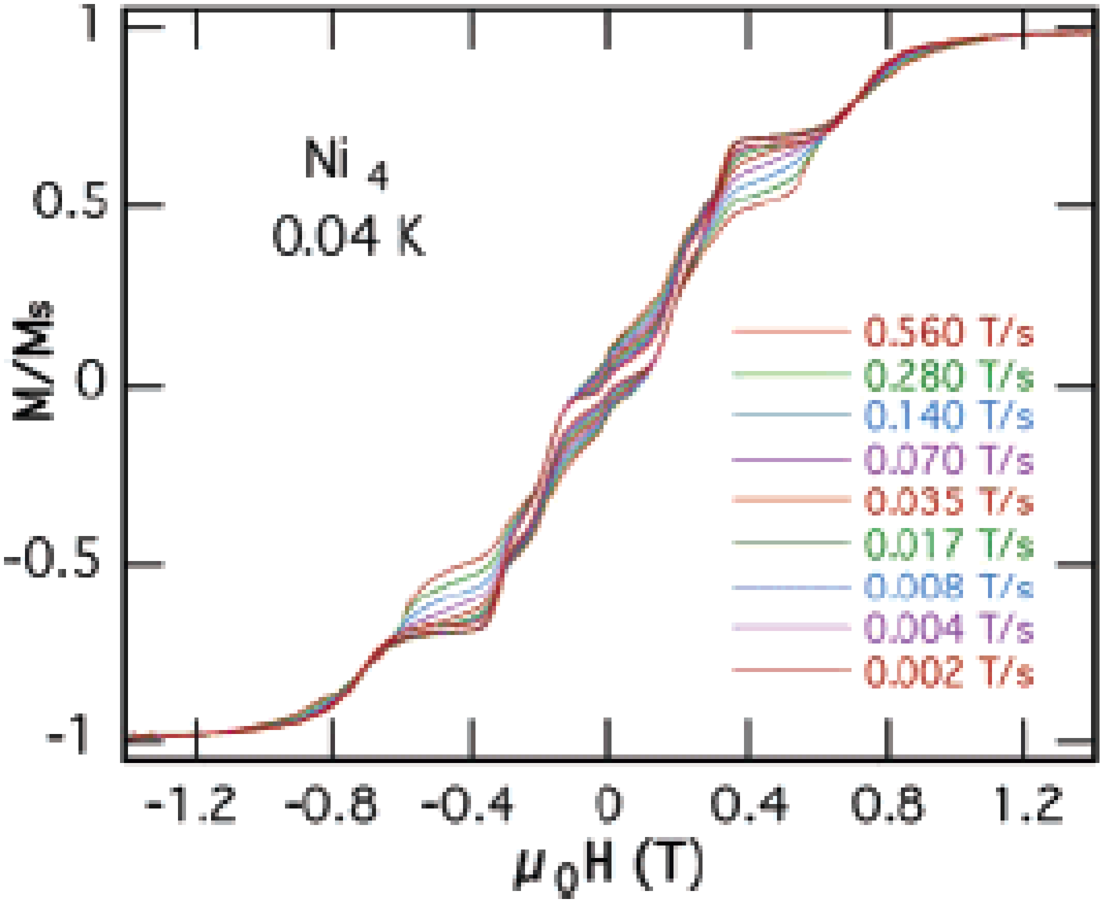

**Figure 5.** Magnetization versus applied field plot of a single crystal of [Ni(hmp)(MeOH)Cl]$_4$. The magnetic field was aligned along the easy axis of the molecules.[30] The system exhibits exchange bias with the first tunneling event occurring at -330 mT.

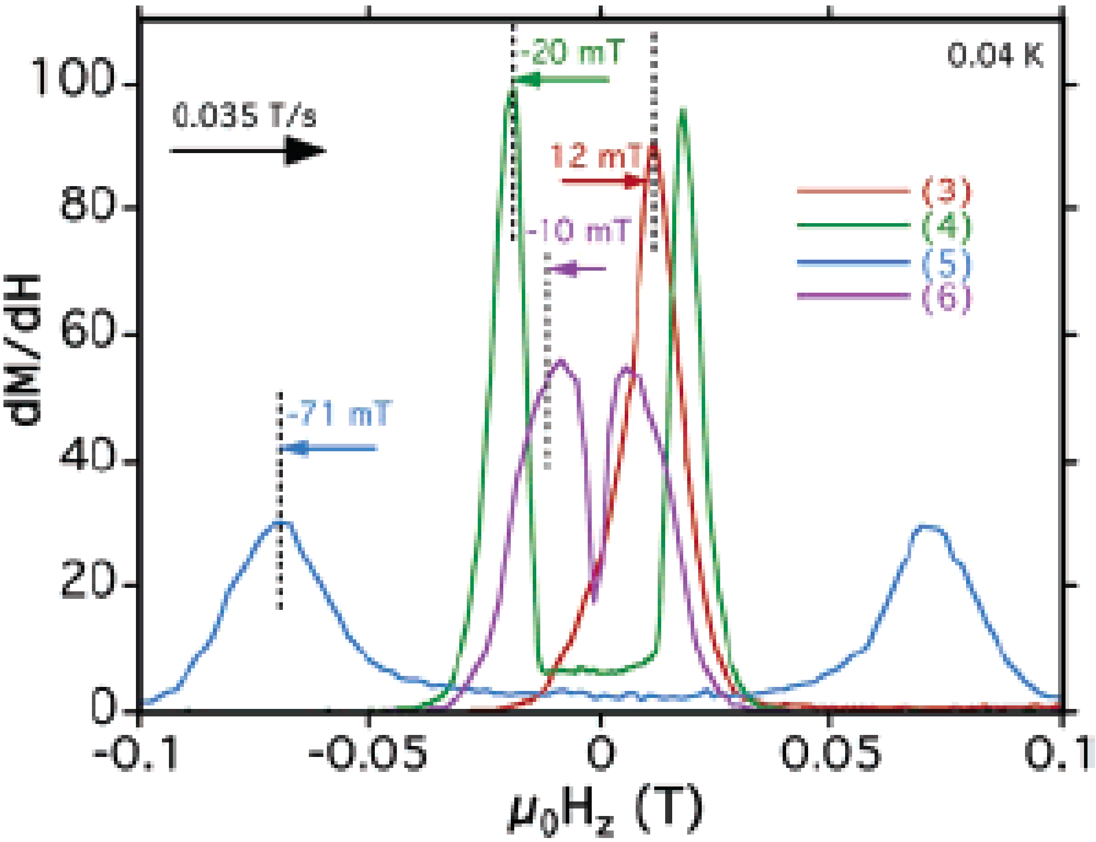

**Figure 6.** Plot of first derivative of magnetization versus applied field for the $Ni_4$ complexes containing dmb and chp. The labels in the plot for these compounds are 3 and 4, respectively. Peaks are the steps in the hysteresis plot and represent tunneling events. [30]

particular the $Ni_4$-dmb complex. The $Ni_4$-dmb, is a very important molecule in SMM research because it crystallizes with only one molecular orientation and contains no solvate molecules which is rare for SMMs. This is crucial, as it significantly limits intermolecular interactions and greatly reduces disorder within the crystal lattice. For comparison, the easy-axis HFEPR spectra of $Ni_4$-dmb, $Ni_4$-MeOH, and $Ni_4$-EtOH are provided in Figure 7. There is significant peak broadening and loss of features for $Ni_4$-MeOH and $Ni_4$-EtOH due to microenvironments within the crystal. While conversely, the solvate free dmb complex shows very sharp transitions and well developed fine structure.

The $S_4$ crystal site symmetry of the $Ni_4$-dmb complex precludes the inclusion of the rhombic second-order zfs Hamiltonian term $[E(\hat{S}_x^2 - \hat{S}_y^2)]$, so to fourth order approximation the spin Hamiltonian can be written as:

$$\hat{H} = D\hat{S}_z^2 + B_4^0\hat{O}_4^0 + B_4^4\hat{O}_4^4 + \mu_B\vec{B}\cdot\vec{g}\cdot\vec{S} \qquad (1.11)$$

It was initially proposed[29-32] that the origin of tunneling in the $Ni_4$-dmb complex was due to a transverse $B_4^4\hat{O}_4^4$ fourth order zfs term in the spin Hamiltonian. Very good theoretical fits to reduced magnetization data and frequency dependent HFEPR data could be achieved including a $B_4^4\hat{O}_4^4$ term employing an "effective spin model," or the giant spin approximation (GSA). The GSA assumes that $S$ and $M_s$ are good quantum numbers and that the energy separation between spin-multiplets can be approximated employing an effective Hamiltonian as presented in eqn. 1.11. However, it does not include the tensorial projections of individual single-ion zfs, isotropic Heisenberg exchange between metal centers, or the presence of low-lying excited states. The GSA model approximates

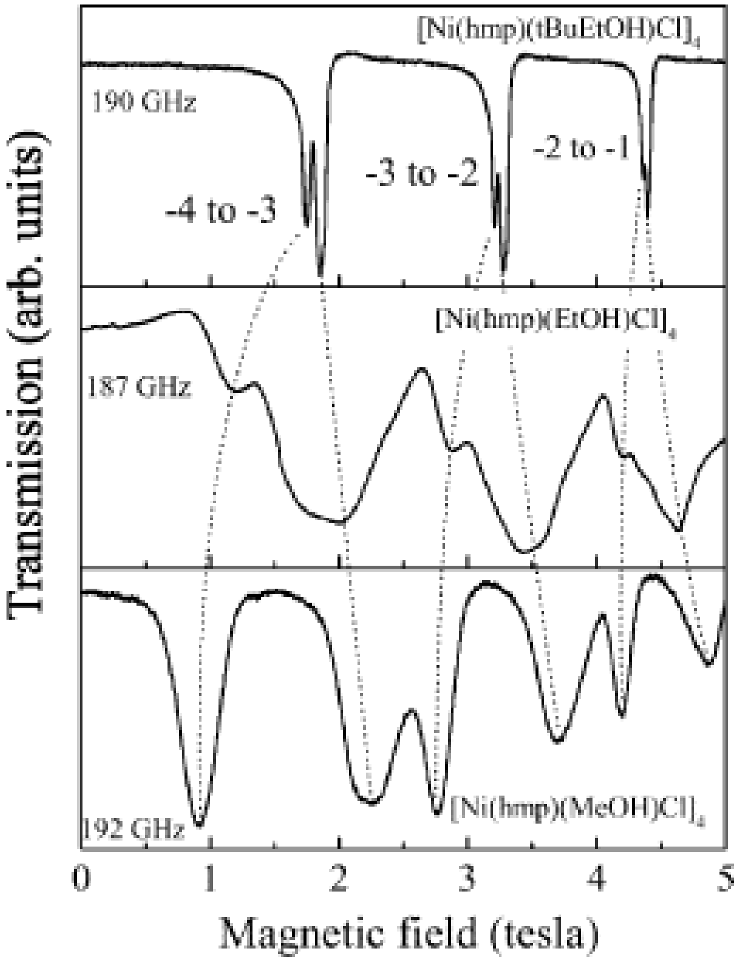

**Figure 7**. A comparison of the HFEPR spectra of the dmb, EtOH, and MeOH variations of [Ni(hmp)(ROH)Cl]$_4$. Spectra was obtained on single crystals at a frequency of 190 GHz, a temperature of 10 K, and along the easy axis of each of the molecules. The dashed lines indicate the splitting fine structure for each molecule.[29]

the system as a single large spin and ignores the internal magnetic degrees of freedom. Thus, in attempting to understand the physical basis for the inclusion of a fourth-order transverse term, it was revealed that in the high symmetry $Ni_4$ case the $B_4^4\hat{O}_4^4$ term has no physical meaning. Examination of the 2S+1 matrix associated with individual $Ni^{II}$ (S=1) ions yields a 3x3 matrix which inherently contains no fourth order Hamiltonian terms.

To determine the origin of transverse anisotropy responsible for tunneling in the $Ni_4$-dmb complex, HFEPR studies were conducted on a $Zn_4$ analogue of the $Ni_4$-dmb complex.[33] The diamagnetic zinc complex was doped with a small amount of $Ni^{II}$ that produced a crystal lattice in which only a small number of sites were occupied by nickel ions ($[Zn_{3.91}Ni_{0.09}(hmp)_4(dmb)_4Cl_4]$). From this, the individual single ion $Ni^{II}$ zfs (d) values could be obtained. The HFEPR study revealed that the relative magnitude of the local single-ion zfs term d is of the same magnitude as the exchange coupling parameter J between magnetic centers. Therefore, the single ions are operating in the medium exchange limit. At this limit, the interplay between J and d was found to give rise to mixing of states and is responsible for fast QTM in the high symmetry $Ni_4$ complexes.

Another important aspect of the $Ni_4$ family of molecules is its relatively small ground state spin. The 2S+1=3 matrix of each $Ni^{II}$ ion results in a 81x81 matrix that can easily be diagonalized employing standard computers. This cannot be done for many other SMMs such as the S=10 $Mn_{12}$-Ac and $Fe_8$ complexes as the resulting matrix is too large. Thus studies of the $Ni_4$ family of molecules have been an important area in SMM research for determining the origins of Hamiltonian parameters and testing the validity of theoretical models.

A continuing goal is to explore the effects of ligand modification on the physical properties of this family of complexes. Bulkier ligands than the ones previously explored could impart additional insulation to the molecule.[30] The use of non-aliphatic alcohols introduces a new type of ligand to the system with potentially interesting outcomes. Furthermore, alcohol ligands with additional functional groups can be utilized for post modification of the molecule.

Previous molecules primarily used simple aliphatic alcohols with difficult to modify alkane chains. Alcohol groups that present other functional groups may allow for the synthesis of new and interesting SMMs. It may be possible to link SMMs through the alcohol ligand to form multidimensional networks, to other molecules that may modify their properties, and to surfaces. A wide range of potential still exists through simple chemical modification and this thesis aims to address some of these concepts.

### 1.7 Applications of SMMs for Device Construction

The molecular dimensions of SMMs allow for packing of a large number of discrete spins in a given area. This has the obvious advantage of increasing the storage capacity of magnetic based information devices. In traditional macromolecular magnetic particles, the reduction in particle size reaches a practical limit known as the superparamagnetic limit. Anisotropy decreases with particle size and lowers the barrier for reversal of magnetization. At the superparamagnetic limit, the anisotropy of the system reaches a point where the thermal energy from the environment allows for the random reordering of spins. The particle becomes superparamagnetic and loses its ability to store information.[2, 6] It has been proposed that SMMs can be used to overcome this limit through chemical modification of their anisotropy. It has been shown that modification of metals and ligands used in SMMs alters their anisotropy without much increase in size.

Due to their small size, quantum effects also become predominate for SMMs. This enables unique possibilities for the use of SMMs in magnetic devices such as qubits for quantum computation.[34-37] The multiple spin states of a given molecule can be employed in addition to “spin-up” and “spin-down” characteristics to store and compute information.

Many challenges exist in creating useful SMM devices, one of which is how to package SMMs into electronics. SMMs are synthesized as crystalline materials and have limited use in this state. For information to be effectively stored in SMMs, ordered and accessible structures are necessary. Effort has been made to arrange SMMs much like the magnetic particles on the surface of hard drive storage media. Previous reports have cited the use of sulfur functionalized $Mn_{12}$ to attach to gold.[38-40] However, steric bulk or weak ligation of the sulfur-functionalized ligand inhibits strong SMM-gold interactions in those systems. Therefore, alternative reaction strategies to promote strong SMMs to gold interactions will be explored as a part of this thesis.

## 1.8 Outline of Thesis

The thesis explores the use of chemical modification to existing SMM families to explore the effects of incremental change in ligand environment and develop ways to post modify SMMs.

Chapter 2 discusses the synthesis, X-ray structural data, DC magnetic susceptibility, reduce magnetization, and AC magnetic susceptibility for a series of $[Ni(hmp)(ROH)Cl]_4$ molecules where R is an alcohol or water. The introduction of larger ligands sterically hinders interactions between molecules and modifies magnetic exchange characteristic. Alcohol ligands with additional functional groups were also explored with the goal of post modification.

Chapter 3 details the attempts to attach a SMM to gold. Suzuki and "Click" cross coupling reactions were explored as the strategy for attaching the molecules. A series of 3 SMMs were synthesized with the proper functional groups to utilize one of the aforementioned coupling reactions. The structural and magnetic characteristics of the compounds are discussed. Suzuki coupling of $[Ni(hmp\text{-}Cl)(MeOH)Cl]_4$ with gold surfaces and gold nanoparticles functionalized with 4-mercaptophenylboroinc acid were carried out. Spectroscopic techniques were used to attempt to verify the presence of the compound on the gold.

## References

1. Duguet, E.; Vasseur, S.; Mornet, S.; Devoisselle, J. M., Magnetic nanoparticles and their applications in medicine. *Nanomedicine* **2006,** 1, (2), 157-168.

2. Thompson, D. A.; Best, J. S., The future of magnetic data storage technology. *Ibm Journal of Research and Development* **2000,** 44, (3), 311-322.

3. Chudnovsky, E. M., Quantum hysteresis in molecular magnets. *Science* **1996,** 274, (5289), 938-939.

4. Chudnovsky, E. M.; Gunther, L., Quantum-theory of nucleation in ferromagnets. *Physical Review B* **1988,** 37, (16), 9455-9459.

5. Chudnovsky, E. M.; Gunther, L., Quantum tunneling of magnetization in small ferromagnetic particles. *Physical Review Letters* **1988,** 60, (8), 661-664.

6. Weller, D.; Moser, A., Thermal effect limits in ultrahigh-density magnetic recording. *Ieee Transactions on Magnetics* **1999,** 35, (6), 4423-4439.

7. Capes, L.; Letard, J. F.; Kahn, O., Photomagnetic properties in a series of spin crossover compounds [Fe(PM-L)(2)(NCX)(2)] (X = S, Se) with substituted 2 '-pyridylmethylene-4-amino ligands. *Chemistry-a European Journal* **2000,** 6, (12), 2246-2255.

8. Garcia, Y.; van Koningsbruggen, P. J.; Lapouyade, R.; Rabardel, L.; Kahn, O.; Wieczorek, M.; Bronisz, R.; Ciunik, Z.; Rudolf, M. F., Synthesis and spin-crossover characteristics of polynuclear 4-(2 '-hydroxy-ethyl)-1,2,4-triazole Fe(II) molecular materials. *Comptes Rendus De L Academie Des Sciences Serie Ii Fascicule C-Chimie* **1998,** 1, (8), 523-532.

9. Guionneau, P.; Letard, J. F.; Yufit, D. S.; Chasseau, D.; Bravic, G.; Goeta, A. E.; Howard, J. A. K.; Kahn, O., Structural approach of the features of the spin crossover transition in iron(II) compounds. *Journal of Materials Chemistry* **1999,** 9, (4), 985-994.

10. Kahn, O., Spin-crossover molecular materials. *Current Opinion in Solid State & Materials Science* **1996,** 1, (4), 547-554.

11. Roux, C.; Zarembowitch, J.; Itie, J. P.; Verdaguer, M.; Dartyge, E.; Fontaine, A.; Tolentino, H., Pressure-Induced Spin-State Crossovers in 6-Coordinate Cobalt(Ii) Complexes - a near-Edge X-Ray Absorption Study. *Inorganic Chemistry* **1991,** 30, (16), 3174-3179.

12. Dante Gatteschi, R. S., and Jacques Villain, *Molecular Nanomagnets*. Oxford University Press: New York, 2005.

13. Lis, T., Preparation, structure, and magnetic-properties of a dodecanenuclear mixed-valence manganese carboxylate. *Acta Crystallographica Section B-Structural Science* **1980,** 36, (SEP), 2042-2046.

14. Caneschi, A.; Gatteschi, D.; Sessoli, R.; Barra, A. L.; Brunel, L. C.; Guillot, M., Alternating-current susceptibiliy, high-field magnetization, and millimeter band EPR evidence for a ground S=10 state in $[Mn_{12}O_{12}(CH_3COO)_{16}(H_2O)_4]\cdot 2CH_3COOH\cdot 4H_2O$. *Journal of the American Chemical Society* **1991,** 113, (15), 5873-5874.

15. Sessoli, R.; Tsai, H. L.; Schake, A. R.; Wang, S. Y.; Vincent, J. B.; Folting, K.; Gatteschi, D.; Christou, G.; Hendrickson, D. N., High-Spin Molecules - [Mn12o12(O2cr)16(H2o)4]. *Journal of the American Chemical Society* **1993,** 115, (5), 1804-1816.

16. Sessoli, R.; Gatteschi, D.; Caneschi, A.; Novak, M. A., Magnetic Bistability in a Metal-Ion Cluster. *Nature* **1993,** 365, (6442), 141-143.

17. Christou, G.; Gatteschi, D.; Hendrickson, D. N.; Sessoli, R., Single-molecule magnets. *Mrs Bulletin* **2000,** 25, (11), 66-71.

18. Ballhausen, C. J., *Introduction to Ligand Field Theory*. McGraw-Hill: 1962.

19. Moryia, T., *Magnetism*. Academic Press: 1963.

20. del Barco, E.; Kent, A. D.; Hill, S.; North, J. M.; Dalal, N. S.; Rumberger, E. M.; Hendrickson, D. N.; Chakov, N.; Christou, G., Magnetic quantum tunneling in the single-molecule magnet Mn-12-acetate. *Journal of Low Temperature Physics* **2005,** 140, (1-2), 119-174.

21. del Barco, E.; Kent, A. D.; Rumberger, E. M.; Hendrickson, D. N.; Christou, G., Symmetry of magnetic quantum tunneling in single molecule magnet Mn-12-acetate. *Physical Review Letters* **2003,** 91, (4).

22. Gonzalez, G.; Leuenberger, M. N., Berry-phase blockade in single-molecule magnets. *Physical Review Letters* **2007,** 98, (25).

23. Leuenberger, M. N.; Mucciolo, E. R., Berry-phase oscillations of the kondo effect in single-molecule magnets. *Physical Review Letters* **2006,** 97, (12).

24. Wegewijs, M. R.; Romeike, C.; Schoeller, H.; Hofstetter, W., Magneto-transport through single-molecule magnets: Kondo-peaks, zero-bias dips, molecular symmetry and Berry's phase. *New Journal of Physics* **2007,** 9.

25. Kambe, K., On the paramagnetic suceptibilities of some polynuclear complex salts. *Journal of the Physical Society of Japan* **1950,** 5, (1), 48-51.

26. Sessoli, R.; Tsai, H. L.; Schake, A. R.; Wang, S.; Vincent, J. B.; Folting, K.; Gatteschi, D.; Christou, G.; Hendrickson, D. N., High-spin molecules: $[Mn_{12}O_{12}(O_2CR)_{16}(H_2O)_4]$. *J. Am. Chem. Soc.* **1993,** 115, (5), 1804-1816.

27. Mertes, K. M.; Suzuki, Y.; Sarachik, M. P.; Myasoedov, Y.; Shtrikman, H.; Zeldov, E.; Rumberger, E. M.; Hendrickson, D. N.; Christou, G., Mn-12-acetate: a prototypical single molecule magnet. *Solid State Communications* **2003,** 127, (2), 131-139.

28. Wernsdorfer, W.; Aliaga-Alcalde, N. r.; Hendrickson, D. N.; Christou, G., Exchange-biased quantum tunnelling in a supramolecular dimer of single-molecule magnets. *Nature* **2002,** 416, (6879), 406.

29. Yang, E.-C.; Wernsdorfer, W.; Hill, S.; Edwards, R. S.; Nakano, M.; Maccagnano, S.; Zakharov, L. N.; Rheingold, A. L.; Christou, G.; Hendrickson, D. N., Exchange bias in Ni4 single-molecule magnets. *Polyhedron* **2003,** 22, (14-17), 1727-1733.

30. Yang, E. C.; Wernsdorfer, W.; Zakharov, L. N.; Karaki, Y.; Yamaguchi, A.; Isidro, R. M.; Lu, G. D.; Wilson, S. A.; Rheingold, A. L.; Ishimoto, H.; Hendrickson, D. N., Fast magnetization tunneling in tetranickel(II) single-molecule magnets. *Inorganic Chemistry* **2006,** 45, (2), 529-546.

31. Hendrickson, D. N.; Yang, E. C.; Isidro, R. M.; Kirman, C.; Lawrence, J.; Edwards, R. S.; Hill, S.; Yamaguchi, A.; Ishimoto, H.; Wernsdorfer, W.; Ramsey, C.; Dalal, N.; Olmstead, M. M., Origin of the fast magnetization tunneling in tetranuclear nickel single-molecule magnets. *Polyhedron* **2005,** 24, (16-17), 2280-2283.

32. Kirman, C.; Lawrence, J.; Hill, S.; Yang, E. C.; Hendrickson, D. N., Origin of the fast magnetization tunneling in the single-molecule magnet [Ni(hmp)(t-BuEtOH)Cl](4). *Journal of Applied Physics* **2005,** 97, (10).

33. Yang, E. C.; Kirman, C.; Lawrence, J.; Zakharov, L. N.; Rheingoid, A. L.; Hill, S.; Hendrickson, D. N., Single-molecule magnets: High-field electron paramagnetic resonance evaluation of the single-ion zero-field interaction in a (Zn3NiII)-Ni-II complex. *Inorganic Chemistry* **2005,** 44, (11), 3827-3836.

34. Affronte, M.; Troiani, F.; Ghirri, A.; Candini, A.; Evangelisti, M.; Corradini, V.; Carretta, S.; Santini, P.; Amoretti, G.; Tuna, F.; Timco, G.; Winpenny, R. E. P., Single molecule magnets for quantum computation. *Journal of Physics D-Applied Physics* **2007,** 40, (10), 2999-3004.

35. Affronte, M.; Troiani, F.; Ghirri, A.; Carretta, S.; Santini, P.; Corradini, V.; Schuecker, R.; Muryn, C.; Timco, G.; Winpenny, R. E., Molecular routes for spin cluster qubits. *Dalton Transactions* **2006**, (23), 2810-2817.

36. Cornia, A.; Costantino, A. F.; Zobbi, L.; Caneschi, A.; Gatteschi, D.; Mannini, M.; Sessoli, R., Preparation of novel materials using SMMs. In *Single-Molecule Magnets and Related Phenomena*, 2006; Vol. 122, pp 133-161.

37. Leuenberger, M. N.; Loss, D., Quantum computing in molecular magnets. *Nature* **2001,** 410, (6830), 789-793.

38. Abdi, A. N.; Bucher, J. P.; Rabu, P.; Toulemonde, O.; Drillon, M.; Gerbier, P., Magnetic properties of bulk Mn(12)Pivalates(16) single molecule magnets and their self assembly on functionnalized gold surface. *Journal of Applied Physics* **2004,** 95, (11), 7345-7347.

39. Coronado, E.; Forment-Aliaga, A.; Romero, F. M.; Corradini, V.; Biagi, R.; DeRenzi, V.; Gambardella, A.; delPennino, U., Isolated Mn12 Single-Molecule Magnets Grafted on Gold Surfaces via Electrostatic Interactions. *Inorg. Chem.* **2005,** 44, (22), 7693-7695.

40. Zobbi, L.; Mannini, M.; Pacchioni, M.; Chastanet, G.; Bonacchi, D.; Zanardi, C.; Biagi, R.; Del Pennino, U.; Gatteschi, D.; Cornia, A.; Sessoli, R., Isolated single-molecule magnets on native gold. *Chemical Communications* **2005**, (12), 1640-1642.

# Chapter Two

## Chemical Tuning of $[Ni(hmp)(ROH)Cl]_4$ Single Molecule Magnets

## 2.1 Introduction

Single molecule magnets (SMMs) are nanoscale superparamagnetic transition metal clusters that exhibit magnetic and quantum phenomena. In previous studies, SMMs have been shown to exhibit spin parity[1], exchange bias,[2, 3] quantum tunneling of the magnetization (QTM),[4] spin-spin cross relaxation,[5] and berry phase.[4]

The first single molecule magnet discovered was $[Mn_{12}O_{12}(O_2CCH_3)_{16}(H_2O)_4] \bullet 2CH_3COOH \bullet 2H_2O$, or $Mn_{12}$-Ac, in 1993.[6-8] Since then, many systems of SMMs have been developed of varying topologies and compositions. One of particular interest has been the family of $[Ni(hmp)(ROH)X]_4$ molecules.[2, 9] The molecule consists of four $Ni^{II}$ ions occupying opposite vertices of a distorted cubane. The remaining sites of the cubane are occupied by four $\mu_3$-oxygen ions originating from the deprotonated alcohol arm of 2-hydroxymethylpyridine ($hmp^-$). The molecular cluster can be approximated as a tetrahedron of $Ni^{II}$ ions. The ROH group is a coordinated alcohol ligand and $X^-$ is a halide ion. Chemical modification of this system was achieved through ligand exchange of the alcohol and/or the use of a variety of Ni-halide salts. The molecular core for each variation is similar allowing for their comparison. These studies have been useful in determining the effect of the size of the alcohol ligand on structural and magnetic properties of a molecule and for understanding the origins of tunneling for this system.

A series of $[Ni(hmp)(ROH)X]_4$ molecules were synthesized using methanol (MeOH), ethanol (EtOH), 3,3-dimethyl-1-butanol (dmb), 3-cyclohexyl-1-propanol (chp) to examine the effect of increasing the steric bulk surround the $Ni_4$ molecule.[2, 9] It was found that the larger alcohol ligands provided a greater level of insulation for the molecule and that directly translated into different observed physical properties. The level of intermolecular interactions could be seen by observing the magnetic ordering temperatures based on low temperature (<1.8 K) AC susceptibility measurements. The $Ni_4$-MeOH complex has the highest magnetic ordering temperature of 1100 mK, followed by $Ni_4$-dmb at 290 mK., and $Ni_4$-chp at ~80 mK. The higher magnetic ordering temperatures are due to the greater effect of long range interactions between molecules in systems with lower insulation.[9]

In addition, by a magnetization hysteresis measurement revealed the presence of exchange bias for the 3 systems. The magnitude of exchange bias can be correlated to the changing size of the alcohol ligands. The $Ni_4$-MeOH version has an exchange bias of -330 mT, the shift for $Ni_4$-dmb is 12 mT, and for $Ni_4$-chp the shift is -20 mT. Greater insulation of the molecule results in a smaller exchange bias as the extent of exchange bias can be related to the level of intermolecular interactions.[9]

Although some level of predictable modification to magnetic characteristics can be achieved through exchange of the alcohol ligand, the origin of tunneling was not well understood until the in depth study of $[Ni(hmp)(dmb)Cl]_4$ through HFEPR. The molecule crystallizes in one molecular orientation with no solvate molecules which is uncommon for SMMs. These properties remove disorder in the system and make it a good candidate for HFEPR studies. In addition, a $Zn_4$-dmb analogue was synthesized and was doped with a small amount of $Ni^{II}$ so that the single ion contributions could be determined. Through these studies, it was determined that the origin of tunneling for this system is due to state mixing brought on by interactions between individual ion anisotropy d and exchange coupling J between metal centers. This has been an important study in SMM research as this situation is similar to many other SMM systems such as $Mn_{12}$-Ac.[10-13]

The $[Ni(hmp)(ROH)Cl]_4$ cubane family of complexes has been shown to be a useful tool for understanding magnetic exchange in SMMs but only a handful of potential alcohol ligands have been explored. There exist many other alcohol ligands that could further modulate the level of insulation and in turn affect intermolecular magnetic exchange interactions. Although several alcohol ligands of increasing chain length have been previously reported, these alcohols largely consisted of primary alcohols on an aliphatic chain. Alcohols with conjugation, heteroatoms, and/or with other functional groups can offer a new dimension to the $Ni_4$ system. A possibility is that these new types of alcohol ligands may offer the ability to chemically modify the $Ni_4$ complex after it has already been fully synthesized. Heteroatoms such as sulfur can be advantageous in promoting interactions of SMMs with gold, allowing for the exploration of SMMs attached to conducting materials. In addition, due to difficulties in predicting how the complexes will arrange themselves in the crystal lattice, it is important to empirically explore the potential of various alcohol groups with the goal of obtaining a well formed crystal with few microenvironments. Therefore, the goal of this project has been to explore these possibilities and to structurally and magnetically characterize new $[Ni(hmp)(ROH)Cl]_4$ complexes.

## 2.2 Experimental

### Synthesis

All procedures were carried out under aerobic conditions. Reagents were purchased from Sigma-Aldrich and used as is unless otherwise noted. $[Ni(hmp)(MeOH)Cl]_4$ was made according to a published procedure.[2] All of the following complexes were made using the reaction strategy of dissolving $[Ni(hmp)(MeOH)Cl]_4$ in an organic solvent with a large excess of the desired alcohol. Specific reaction conditions are outlined as follows.

**$[Ni(hmp)(PrOH)_{.75}(H_2O)_{.25}Cl]_4$** • $H_2O$ **(1** • $H_2O$**).** $[Ni(hmp)(MeOH)Cl]_4$ (2.13mmol , 2.0g) was dissolved in 50 mL $CH_2Cl_2$ and 1-propanol (670mmol, 40.2g). Once the components are fully dissolved, the solution was filtered and allowed to slowly to evaporate. Green crystals formed after several weeks. Select IR: 3424 $cm^{-1}$(s), 1607 $cm^{-1}$(m), 1441 $cm^{-1}$(m), 1289 $cm^{-1}$(m), 1077 $cm^{-1}$(s), and 763 $cm^{-1}$(m). Elemental Analysis calculated: 38.88 %C 4.55 %H 5.5 %N. Experimental: 34.78 %C 3.90 %H 5.95 %N.

**$[Ni(hmp)(isobutylOH)Cl]_4$** •2MeOH **(2** • 2MeOH**).** $[Ni(hmp)(MeOH)Cl]_4$ (2.13mmol , 2.0g) was dissolved in 50 mL $CH_2Cl_2$ containing isobutyl alcohol (220mmol, 16.0g). Once dissolved, the solution was filtered and allowed to slowly to evaporate. Green crystals formed after several weeks. Select IR: 3411 $cm^{-1}$(s), 1607 $cm^{-1}$(m), 1440 $cm^{-1}$(w), 1288 $cm^{-1}$(w), 1070 $cm^{-1}$(s), and 756 $cm^{-1}$(m). Elemental Analysis calculated: 43.4 %C 6.18 %H 5.05 %N. Experimental: 35.62 %C 3.95 %H 6.00 %N.

**$[Ni(hmp)(C_3H_3OH)Cl]_4$** •MeOH **(3** • MeOH**).** $[Ni(hmp)(MeOH)Cl]_4$ (1mmol , 0.91g) was made from $NiCl_2$ that was dried in an oven for 48 hrs and anhydrous methanol. It was dissolved in 75 mL of $CH_2Cl_2$ and propargyl alcohol (0.34mmol, 19.26g). The reaction was carried out under flowing $N_2$. The solution was filtered and layered with $Et_2O$. Green block crystals formed in a few days. Select IR: 3392 $cm^{-1}$(m), 1606 $cm^{-1}$(m), 1441 $cm^{-1}$(m), 1067 $cm^{-1}$(s), and 760 $cm^{-1}$(m). Elemental Analysis calculated: 41.87 %C 3.80 %H 5.29 %N. Experimental: 34.04 %C 3.07 %H 6.01 %N.

**$[Ni(hmp)(H_2O)Cl]_4$** • $4C_4H_8O_2$ **($4$ • $4C_4H_8O_2$).** $[Ni(hmp)(MeOH)Cl]_4$ was dissolved in 50 mL of 1,4-dioxane and brought to reflux. The crystals are initially insoluble but dropwise addition of ca. 2 mL of $H_2O$ brought the solids into solution. The solution was filtered and allowed to cool in a covered flask. Green block crystals formed overnight. Select IR: 3338 $cm^{-1}$(s), 1600 $cm^{-1}$(m), 1450 $cm^{-1}$(m), 1305 $cm^{-1}$(m), and 1121 $cm^{-1}$(m). Elemental Analysis calculated: 38.8 %C 5.54 %H 4.53 %N. Experimental: 38.1 %C 38.1 %H 4.89 %N.

**$[Ni(hmp)(benzylOH)Cl]_4$ (5).** $[Ni(hmp)(MeOH)Cl]_4$ (2.13mmol , 2.0g) was dissolved in 50 mL $CHCl_3$ and benzyl alcohol (100mmol, 10.8g). The solution was filtered and allowed to slowly to evaporate. Green crystals formed after several weeks. Select IR: 3209 $cm^{-1}$(s), 1606 $cm^{-1}$(m), 1440 $cm^{-1}$(m), 1285 $cm^{-1}$(w), 1073 $cm^{-1}$(s), 770 $cm^{-1}$(m). Elemental Analysis calculated: 50.30 %C 4.55 %H 4.51 %N. Experimental: 50.59 %C 4.08 %H 4.85 %N.

**$[Ni(hmp)(TPMeOH)Cl]_4$ (6).** $[Ni(hmp)(MeOH)Cl]_4$ (2.13mmol , 2.0g) was dissolved in 50 mL $CH_2Cl_2$ containing 2-thiophenemethanol (250mmol, 28g). The solution was filtered and allowed to slowly evaporate. Green crystals formed after several weeks. Select IR: 3170 $cm^{-1}$(s), 1605 $cm^{-1}$(m), 1570 $cm^{-1}$(w), 1481 $cm^{-1}$(w), 1438 $cm^{-1}$(m), 1287 $cm^{-1}$(m), 1071 $cm^{-1}$(m), 1013 $cm^{-1}$(m), and 707 $cm^{-1}$(w). Elemental Analysis calculated: 41.89 %C 3.51 %H 4.44 %N 10.17 %S. Experimental: 41.59 %C 3.38 %H 4.47 %N 10.83 %S.

**$[Ni(hmp)(MeSEtOH)Cl]_4$ (7).** $[Ni(hmp)(MeOH)Cl]_4$ (2.13mmol , 2.0g) was dissolved in 50 mL $CH_2Cl_2$ and 2-(methylthio)ethanol (250mmol, 23g). The solution was filtered and allowed to slowly evaporate. Green crystals formed after several weeks. Select IR: 3434 $cm^{-1}$(s), 3230 $cm^{-1}$(s), 1606 $cm^{-1}$(m), 1440 $cm^{-1}$(m), 1288 $cm^{-1}$(w), 1046 $cm^{-1}$(s), and 764 $cm^{-1}$(w).

## X-ray Crystallography

Diffraction data were collected using a Bruker Smart Apex CCD diffractometer at 100 K (for complexes **1**, **3**, and **6**), 208 K (for complex **4**), and 218 K (for complexes **2**, **5**, and **7**). The data were integrated using the Bruker SAINT software and SADABS was employed to correct for absorption differences. The structures were solved using direct methods (SHELXS-97), developed by successive difference Fourier syntheses, and refined by full matrix least-squares on all $F^2$ data. All non-hydrogen atoms were refined anisotropically and the hydrogen atoms were idealized based on 1.2-1.5 times the equivalent isotropic U values for the C atoms to which they were bound.

Due to large amounts of disorder in complex **1**, several atoms were refined isotropically including: C6, C11-12, C15, C23, C25-27, C29, C30, C32, and O6. Also, one propyl arm was disordered over two positions and refined in two parts (Part 1=C31, C33; Part 2=C31A, C33) to a final occupancy of 58%. For complex **2**, carbon atoms 18, 19, 20, 48, 49, and 50 of the isobutyl groups are positionally disordered leading to larger than normal thermal ellipsoids. The sulfur atoms of the thiophene groups in complex **6** are positionally disordered over the 2 and 5 positions, commonly seen in thiophene structures. Disordered carbon and sulfur atoms of three of the alcohol ligands in **7** were modeled by refining carbon atoms 18, 18′, 19, and 19′ at half occupancy and by using free variables which were refined to the following occupancies: C37, 30%; C38, 60%; C28, 60%; S1, 42%; C17, 53%; and S2, 58%.

Disordered solvent molecules in **1**, **2**, and **3** were treated by the PLATON program SQUEEZE, the details of which can be found in the cif. The electron density accounted for 1 water, 2 methanol, and 1 methanol solvate molecules per $Ni_4$ cubane for **1**, **2,** and **3**, respectively. All of the 1,4-dioxane solvate molecules in complex **4** were ordered and refined anisotropically.

## Magnetic Studies

DC magnetic susceptibility data were collected on ground microcrystalline samples locked in eicosane to prevent torquing of the sample in the magnetic field. A Quantum Design MPMS-5 SQUID magnetometer equipped with a 5.5 T magnet was used to analyze the samples. The experiments were done between 300-1.8 K in fields ranging from 0.1 to 50 kG. Magnetic susceptibility data were corrected for the sample holder, sample rod, and eicosane. A diamagnetic correction was applied to the observed magnetic susceptibilities using Pascal's constants.[14]

AC magnetic susceptibility data were collected with a 3 Oe AC field from 10-997 Hz with no applied DC field. The experiments were carried out at 1.8-5 K using a Quantum Design MPMS-2 SQUID magnetometer equipped with a 3 T magnet.

### Other Physical Measurements

Elemental analysis data were collected by Numega Resonance Laboratories (San Diego, CA). IR spectra were collected samples on powder samples locked in a KBr pellet on a Thermo-Nicolet Avatar 360 spectrometer.

## 2.3 Results and Discussion

### Synthesis

A level of synthetic control was achieved through ligand exchange to create a series of 7 molecules with the general formula $[Ni(hmp)(ROH)Cl]_4$ where ROH is an alcohol based ligand. It was found that under the aerobic conditions, $H_2O$ from the atmosphere or “wet” solvents could serve as a competing ligand thus preventing the full substitution of the methanol ligand with the desired alcohol. This is seen in the case of complex **1** with the partial substitution by propyl alcohol. Therefore, a large excess of the alcohol ligand was necessary and in some cases $Et_2O$ diffusion was the preferred method of crystallization to prevent absorption of $H_2O$ from the atmosphere. This competition from water was also seen in complex **3,** but employing these techniques eventually led to the full substitution of the molecule.

Difficulty was experienced when trying to substitute the methanol group with alcohol ligands with longer aliphatic chains. Partial substitution of molecule occurred or the molecule would form a powdery precipitate that failed to form diffraction quality crystals. This is likely due to the labile nature of the larger ligands. Attempts were also made to use solid alcohols at room temperature such as napthanol. However, the large excess used to initiate ligand exchange resulted in recrystallization of the alcohol and formed an inseparable product.

Ligands with multiple functional groups were explored to develop new avenues of chemistry for nickel cubane SMMs. Propargyl alcohol was utilized in complex **3** to eventually employ "Click Chemistry", a 1,3-cyclo-addition of azides to terminal acetylenes, to post-functionalize the SMMs or develop a new line of ligands.[15] Attempts were made to post functionalize the SMM through the coupling reaction but failed. Azidobenzene was used as a Click partner with complex **3** and resulted in the removal of the propargyl ligand. Two products were formed in the reaction; a crystalline product which was later identified to be complex **4** and a black precipitate that is the product of the addition of propargyl alcohol to azidobenzene. The propargyl alcohol is therefore likely too weakly coordinated to successfully allow for post modification of the $Ni_4$ system.

The 2-thiophenemethanol ligand for complex **6** was investigated for two purposes. First, the ligand's sulfur atom can be used to attach SMMs to gold substrates through Au-S bonds. Second, polythiophene is a well studied conducting polymer which can be potentially used to link SMMs together in conducting chains.[16-18] Complex **7** was synthesized using 2-(methylthio)ethanol to exploit the same Au-S interactions for attachment to gold.

## Description of Structures

All of the synthesized complexes have the same core structure as their parent compound $[Ni(hmp)(MeOH)Cl]_4$**.** The core of each complex is 4 $Ni^{II}$ ions occupying alternating positions of a distorted cube with $\mu_3$-oxo atoms occupying the remaining 4 vertices. Each octahedral $Ni^{II}$ ions is coordinated by 3 $\mu_3$-oxo atoms originating from the deprotonated arms of the $hmp^-$ ligands, a nitrogen atom from $hmp^-$, a $Cl^-$ ion, and a protonated oxygen atom from either an alcohol ligand or a water ligand. ORTEP representations of complexes **1-7** are provided in Figures 1-8. A list of the supporting crystallographic information for each compound can be found in Tables 1-4. As the complexes are isostructural with its parent complex, only differences are highlighted below. [2, 9]

Complex **1** $[Ni(hmp)(PrOH)_{.75}(H_2O)_{.25}Cl]_4 \bullet H_2O$ is shown in Figure 1 with its disordered cocrystallized water solvate molecule treated with SQUUEZED and is omitted for clarity. In complex **1**, water competed with propyl alcohol despite the addition of a large excess of alcohol ligand. Due to this partial substitution, the symmetry of the molecule is lowered from the $S_4$ molecular symmetry found in other $Ni_4$ cubanes to $C_1$. The shorter length of water compared to propyl alcohol lessens the insulation from neighboring molecules. Furthermore, the water molecule offers a hydrogen bonding pathway for intermolecular interactions through the O(5)··Cl(1) hydrogen bond of the coordinated water ligand and the coordinated $Cl^-$ ion of its neighbor. The hydrogen bond contact distance between the O··Cl is 3.12 Å, which falls into the regime of moderate hydrogen bonding interactions.[19] There is some disorder in the propargyl alcohol ligands as evidenced by their large and irregularly shaped thermal ellipsoids. There is one molecular orientation with all molecules in the unit cell related by a mirror plane.

Greater insulation of the SMM is achieved in complex **2**

**Table 1.** Crystal Data and Structure Refinement Parameters for Complexes **1** and **2**

| | **1** | **2** |
|---|---|---|
| **Empirical formula** | C32.50 H52 Cl4 N4 Ni4 O9 | C42 H68 Cl4 N4 Ni4 O10 |
| **Formula weight** | 1019.42 | 1164.56 |
| **Temperature** | 100(2) K | 218(2) K |
| **Wavelength** | 0.71073 Å | 0.71073 Å |
| **Crystal system** | Monoclinic | Triclinic |
| **Space group** | C2/c | P-1 |
| **Unit cell dimensions** | a = 18.619(13) Å | a = 12.6770(16) Å |
| | b = 17.068(12) Å | b = 13.7318(17) Å |
| | c = 28.03(2) Å | c = 16.065(2) Å |
| | a= 90°. | a= 70.930(2)° |
| | b= 91.552(13)°. | b= 86.935(2)° |
| | g = 90°. | g = 83.853(2)° |
| **Volume** | 8903(11) Å$^3$ | 2627.4(6) Å$^3$ |
| **Z** | 8 | 2 |
| **Density (calc.)** | 1.521 g/cm$^3$ | 1.486 g/cm$_3$ |
| **Absorption coefficient mm$^{-1}$** | 1.956 mm$^{-1}$ | 1.668 mm$^{-1}$ |
| **F(000)** | 4216 | 1228 |
| **Crystal color/habit** | green block | green block |
| **Theta range for data collection** | 2.16 to 28.21°. | 2.08 to 28.20° |
| **Reflections collected** | 8123 | 20769 |
| **Independent reflections** | 4637 [R(int) = 0.0267] | 11867 [R(int) = 0.0230] |
| **Completeness to theta = 25.00°** | 48.1 % | 91.8 % |
| **Data / restraints / parameters** | 4637 / 0 / 427 | 11867 / 0 / 541 |
| **Goodness-of-fit on F2** | 1.130 | 1.096 |
| **Final R indices [I>2sigma(I)]** | R1 = 0.0599, wR2 = 0.1880 | R1 = 0.0468, wR2 = 0.1337 |
| **R indices (all data)** | R1 = 0.0728, wR2 = 0.2084 | R1 = 0.0577, wR2 = 0.1397 |
| **Largest diff. peak and hole** | 1.045 and -0.735 e.Å$^{-3}$ | 1.006 and -0.834 e Å$^{-3}$ |

**Table 2.** Crystal Data and Structure Refinement Parameters for Complexes **3** and **4**

| | **3** | **4** |
|---|---|---|
| **Empirical formula** | C37 H40 Cl4 N4 Ni4 O9 | C40 H64 Cl4 N4 Ni4 O16 |
| **Formula weight** | 1061.37 | 1233.59 |
| **Temperature** | 100(2) K | 208(2) K |
| **Wavelength** | 0.71073 Å | 0.71073 Å |
| **Crystal system** | Monoclinic | Triclinic |
| **Space group** | C2/c | P-1 |
| **Unit cell dimensions** | a = 31.223(2) Å | a = 10.629(4) Å |
| | b = 16.6104(12) Å | b = 10.667(5) Å |
| | c = 19.3085(14) Å | c = 24.385(10) Å |
| | a= 90°. | a= 99.928(6)°. |
| | b= 119.1260(10)°. | b= 101.380(5)°. |
| | g = 90°. | g = 98.701(5)°. |
| **Volume** | 8747.6(11) Å$^3$ | 2620.2(19) Å$^3$ |
| **Z** | 8 | 2 |
| **Density (calc.)** | 1.612 g/cm$^3$ | 1.564 g/cm$^3$ |
| **Absorption coefficient mm$^{-1}$** | 1.995 mm$^{-1}$ | 1.686 mm$^{-1}$ |
| **F(000)** | 4336 | 1280 |
| **Crystal color/habit** | green plate | green block |
| **Theta range for data collection** | 1.49 to 28.24°. | 2.32 to 25.03°. |
| **Reflections collected** | 48674 | 34459 |
| **Independent reflections** | 10072 [R(int) = 0.0310] | 9188 [R(int) = 0.0816] |
| **Completeness to theta = 25.00°** | 100.0 % | 99.1 % |
| **Data / restraints / parameters** | 10072 / 0 / 506 | 9188 / 0 / 645 |
| **Goodness-of-fit on F2** | 0.988 | 1.046 |
| **Final R indices [I>2sigma(I)]** | R1 = 0.0295, wR2 = 0.0730 | R1 = 0.0532, wR2 = 0.0860 |
| **R indices (all data)** | R1 = 0.0345, wR2 = 0.0754 | R1 = 0.0909, wR2 = 0.0973 |
| **Largest diff. peak and hole** | 1.353 and -0.540 e.Å$^{-3}$ | 0.573 and -0.510 e.Å$^{-3}$ |

**Table 3.** Crystal Data and Structure Refinement Parameters for Complexes **5** and **6**

| | **5** | **6** |
|---|---|---|
| **Empirical formula** | C52 H52 Cl4 N4 Ni4 O8 | C44 H44 Cl4 N4 Ni4 O8 S4 |
| **Formula weight** | 1237.62 | 1261.72 |
| **Temperature** | 213(2) K | 100(2) K |
| **Wavelength** | 0.71073 Å | 0.71073 Å |
| **Crystal system** | Triclinic | Triclinic |
| **Space group** | P-1 | P-1 |
| **Unit cell dimensions** | a = 12.121(2) Å | a = 17.4468(13) Å |
| | b = 13.378(3) Å | b = 18.4072(14) Å |
| | c = 18.598(4) Å | c = 19.7902(15) Å |
| | a = 79.202(3)° | a = 63.9810(10)°. |
| | b = 79.785(3)° | b = 76.1130(10)°. |
| | g = 65.318(3)° | g = 61.9690(10)°. |
| **Volume** | 2675.1(9) Å$^3$ | 5036.8(7) Å$^3$ |
| **Z** | 2 | 4 |
| **Density (calc.)** | 1.536 g/cm$^3$ | 1.664 g/cm$^3$ |
| **Absorption coefficient mm$^{-1}$** | 1.642 mm$^{-1}$ | 1.905 mm$^{-1}$ |
| **F(000)** | 1272 | 2576 |
| **Crystal color/habit** | green block | green plate |
| **Theta range for data collection** | 1.69 to 28.36° | 1.32 to 27.57°. |
| **Reflections collected** | 21015 | 43057 |
| **Independent reflections** | 12053 [R(int) = 0.0264] | 22016 [R(int) = 0.0381] |
| **Completeness to theta = 25.00°** | 90.1 % | 94.5 % |
| **Data / restraints / parameters** | 12053 / 0 / 649 | 22016 / 0 / 1228 |
| **Goodness-of-fit on F2** | 1.064 | 1.024 |
| **Final R indices [I>2sigma(I)]** | R1 = 0.0319, wR2 = 0.0868 | R1 = 0.0497, wR2 = 0.1195 |
| **R indices (all data)** | R1 = 0.0365, wR2 = 0.0896 | R1 = 0.0755, wR2 = 0.1320 |
| **Largest diff. peak and hole** | 0.674 and -0.601 e Å$^{-3}$ | 1.419 and -0.884 e.Å$^{-3}$ |

**Table 4.** Crystal Data and Structure Refinement Parameters for Complex 7

| | 7 |
|---|---|
| **Empirical formula** | C36 H56 Cl4 N4 Ni4 O8 S4 |
| **Formula weight** | 1177.73 |
| **Temperature** | 218(2) K |
| **Wavelength** | 0.71073 Å |
| **Crystal system** | Triclinic |
| **Space group** | P-1 |
| **Unit cell dimensions** | a = 12.5795(18) Å |
| | b = 12.9903(18) Å |
| | c = 17.241(2) Å |
| | a= 72.786(2)°. |
| | b= 82.827(2)°. |
| | g = 63.347(2)°. |
| **Volume** | 2405.1(6) Å$^3$ |
| **Z** | 2 |
| **Density (calc.)** | 1.626 g/cm$^3$ |
| **Absorption coefficient mm$^{-1}$** | 1.988 mm$^{-1}$ |
| **F(000)** | 1216 |
| **Crystal color/habit** | green block |
| **Theta range for data collection** | 2.18 to 28.30°. |
| **Reflections collected** | 19046 |
| **Independent reflections** | 10865 [R(int) = 0.0196] |
| **Completeness to theta = 25.00°** | 99.6 % |
| **Data / restraints / parameters** | 10865 / 0 / 622 |
| **Goodness-of-fit on F2** | 1.043 |
| **Final R indices [I>2sigma(I)]** | R1 = 0.0402, wR2 = 0.1097 |
| **R indices (all data)** | R1 = 0.0456, wR2 = 0.1144 |
| **Largest diff. peak and hole** | 1.189 and -0.922 e.Å$^{-3}$ |

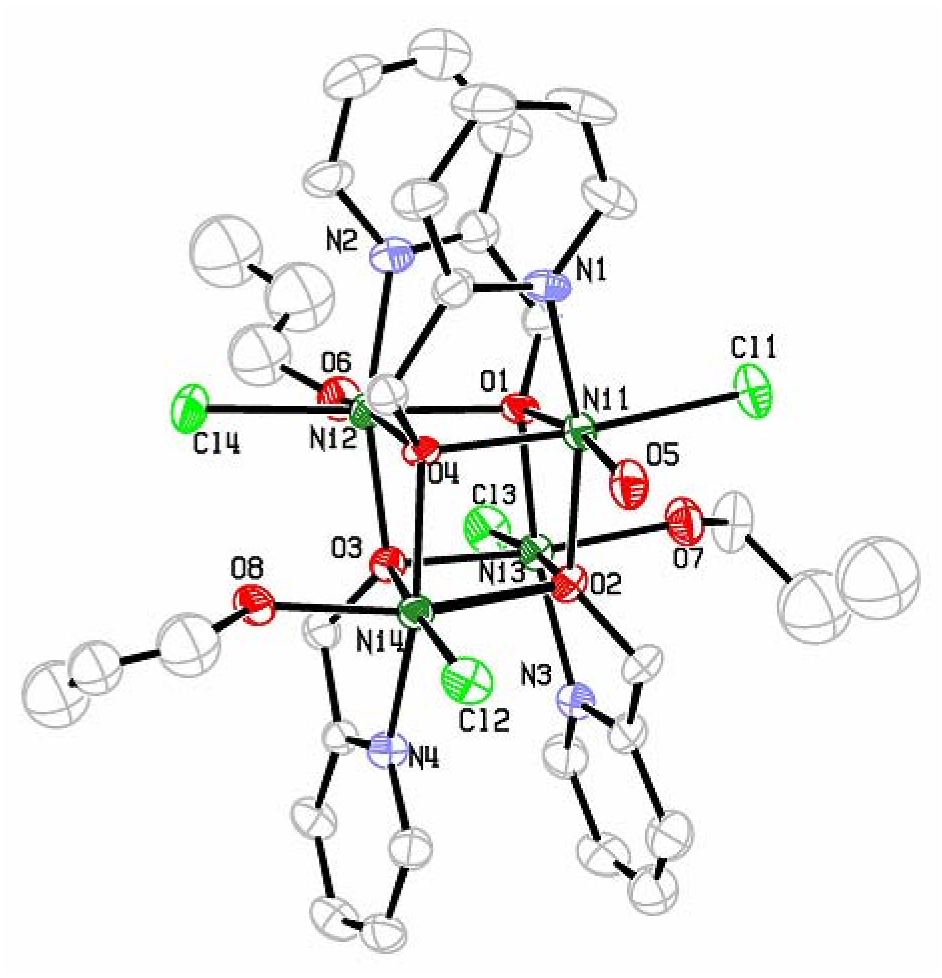

**Figure 1.** ORTEP of [Ni(hmp)(PrOH)$_{.75}$(H2O)$_{.25}$Cl]$_4$ • $H_2O$ (**1** •$H_2O$) with thermal ellipsoids at the 30% probability level. Hydrogen and solvate atoms omitted for clarity.

$[Ni(hmp)(isobutylOH)Cl]_4$ •2MeOH through the use of the bulkier isobutyl alcohol ligand. Complex **2** is depicted in Figure 2**.** The molecule is fully substituted with the isobutyl ligand. The system cocrystallizes with 2 disordered methanol solvate molecules. Ignoring the solvate molecules, the core $Ni_4$ molecule has $S_4$ symmetry. The molecule packs in the P-1 space group and there is a single molecular orientation in the unit cell related by an inversion center. No hydrogen bonding contacts were present with a closest contact distance O··Cl of 5.4 Å.

Complex **3** $[Ni(hmp)(C_3H_3OH)Cl]_4$ •MeOH is shown in Figure 3. Disorder is present in the propargyl alcohol ligands of complex as evidenced by their large and irregularly shaped thermal ellipsoids of the carbons atoms on the alcohol group. The propargyl alcohol is a weakly coordinating ligand and faces competition from water but full substitution was achieved. Complex **3** cocrystallizes with one disordered methanol solvate molecule. The molecule crystallizes with in the higher symmetry C2/c space group with a single molecular orientation.

Complex **4** $[Ni(hmp)(H_2O)Cl]_4$ • $4C_4H_8O_2$ is shown in Figure 4 and differs from the other complexes studied because the R group is not an alcohol ligand. The complex is fully substituted with water ligands that are stabilized in a hydrogen bonding network with 1,4-dioxane solvate molecules. There are four ordered dioxane molecules for every $Ni_4$ cubane. The dioxane molecules form sheets that insulate the $Ni_4$ molecule from neighboring $Ni_4$ molecules that lie in the plane containing the water and $Cl^-$ ligands. A packing diagram of the molecule can be seen in Figure 5.

The O(water)-O(dioxane) hydrogen bonds are 2.80 Å and 2.76 Å for the two different water ligands on a given side of the cluster. Although there is an H-bonding network that links together $Ni_4$ molecules in a plane, it is unlikely that dioxane can facilitate any magnetic exchange between neighboring cubanes. Dioxane is an electronically saturated molecule and is, therefore, expected to insulate the $Ni_4$ complex. As a result, complex **4** is a potentially well-insulated system through the packing of cocrystallized solvate molecules. The molecule crystallizes in the P-1 space group with one molecular orientation in the asymmetric unit. All molecules in the unit cell are related by an inversion operator. The structure and symmetry of this molecule make it a good candidate for more advanced analysis through HFEPR. To verify insulation for this molecule, addition analysis needs to be done to determine the magnetic ordering temperature and the exchange bias for this system.

Complexes **5** $[Ni(hmp)(benzylOH)Cl]_4$ and **6** $[Ni(hmp)(TPMeOH)Cl]_4$ are shown in Figures 6 and 7, respectively. They are different from the previous examples of the $Ni_4$ molecules as their R group is no longer a simple aliphatic chain. Coordinated to the complexes are cyclic carbon molecules with a primary alcohol group extending from the ring. A structurally different situation arises as this eliminates the methyl rotors present in the aliphatic systems. Reducing the rotational movement in the system could potentially allow for clearer HFEPR signals. The complex crystallizes with no solvent molecules and with only one molecular orientation. In turn, these properties make complex **5** similar to the $Ni_4$-dmb complex in regard to the decreased number of microenvironments in the crystal and thus make complex **5** a potentially good candidate for HFEPR studies.There is no hydrogen bonding in this system with the closest contact distances being Cl··Cl 6.04 Å and Cl··O 7.81 Å.

Complex **6** $[Ni(hmp)(TPMeOH)Cl]_4$ exhibits disorder in the 2 and 5 positions of

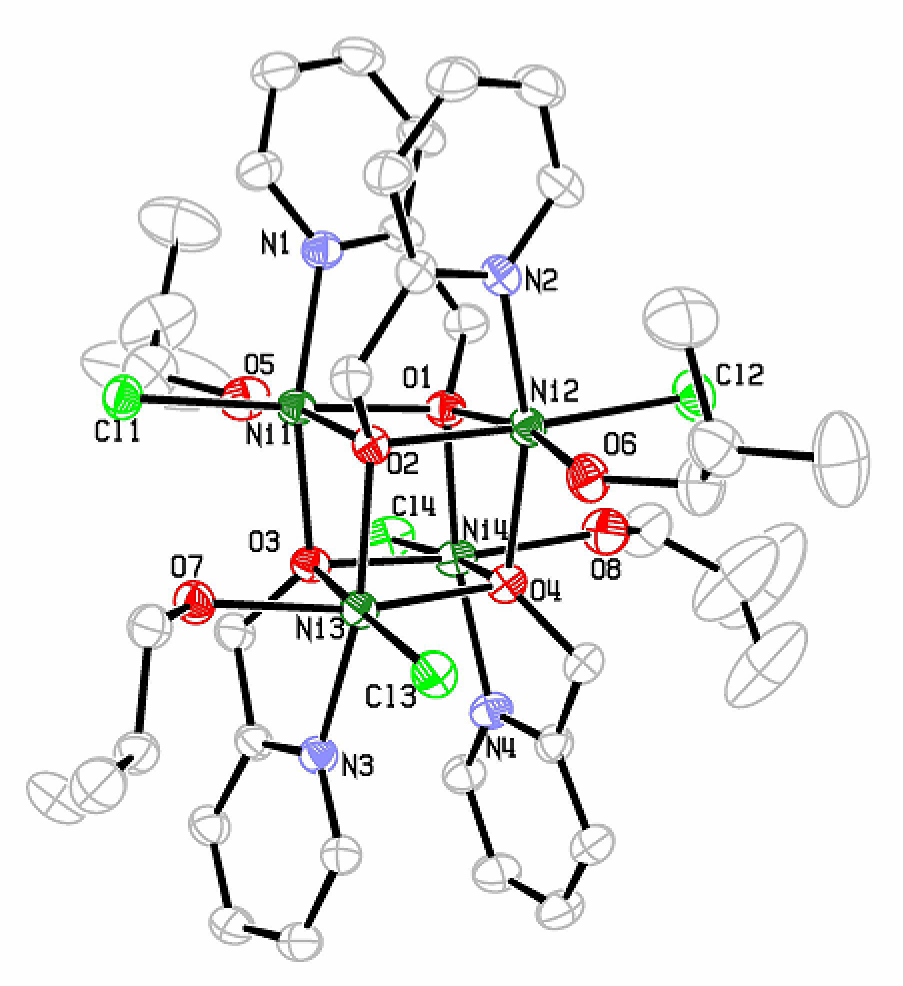

**Figure 2.** ORTEP of [Ni(hmp)(i-butylOH)Cl]$_4$ •2MeOH (**2** •2MeOH) with thermal ellipsoids at the 30% probability level. Hydrogen and solvate atoms omitted for clarity.

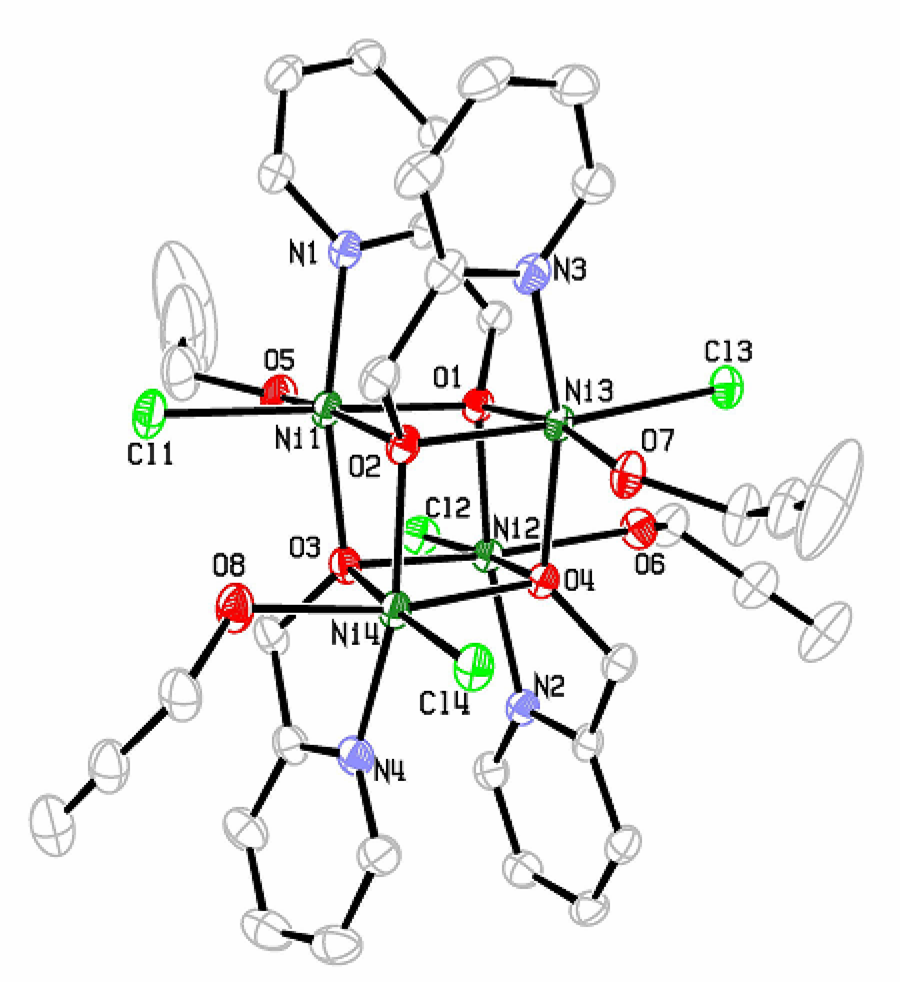

**Figure 3.** ORTEP of $[\mathrm{Ni(hmp)(C_3H_3OH)Cl}]_4$ •MeOH (**3** •1MeOH) with thermal ellipsoids at the 30% probability level. Hydrogen and solvate atoms omitted for clarity.

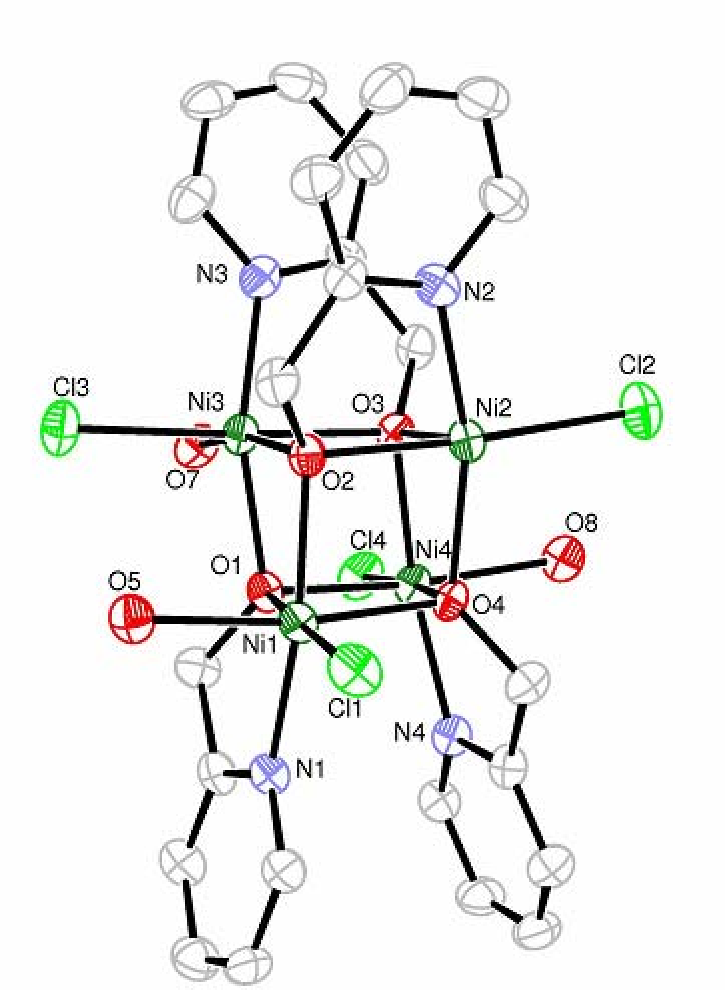

**Figure 4.** ORTEP of [Ni(hmp)($H_2O$)Cl]$_4$ •4($C_4H_8O_2$) (**4** •4$C_4H_8O_2$) with thermal ellipsoids at the 30% probability level. Hydrogen and solvate atoms omitted for clarity.

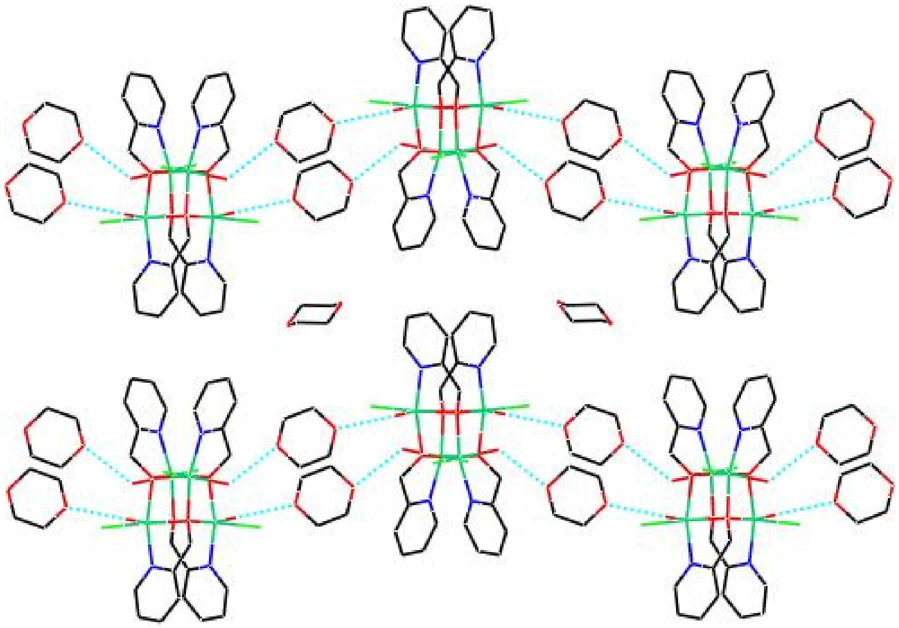

**Figure 5.** Crystal Packing diagram for **4 •4($C_4H_8O_2$).** Hydrogen bonding contacts are shown in green.

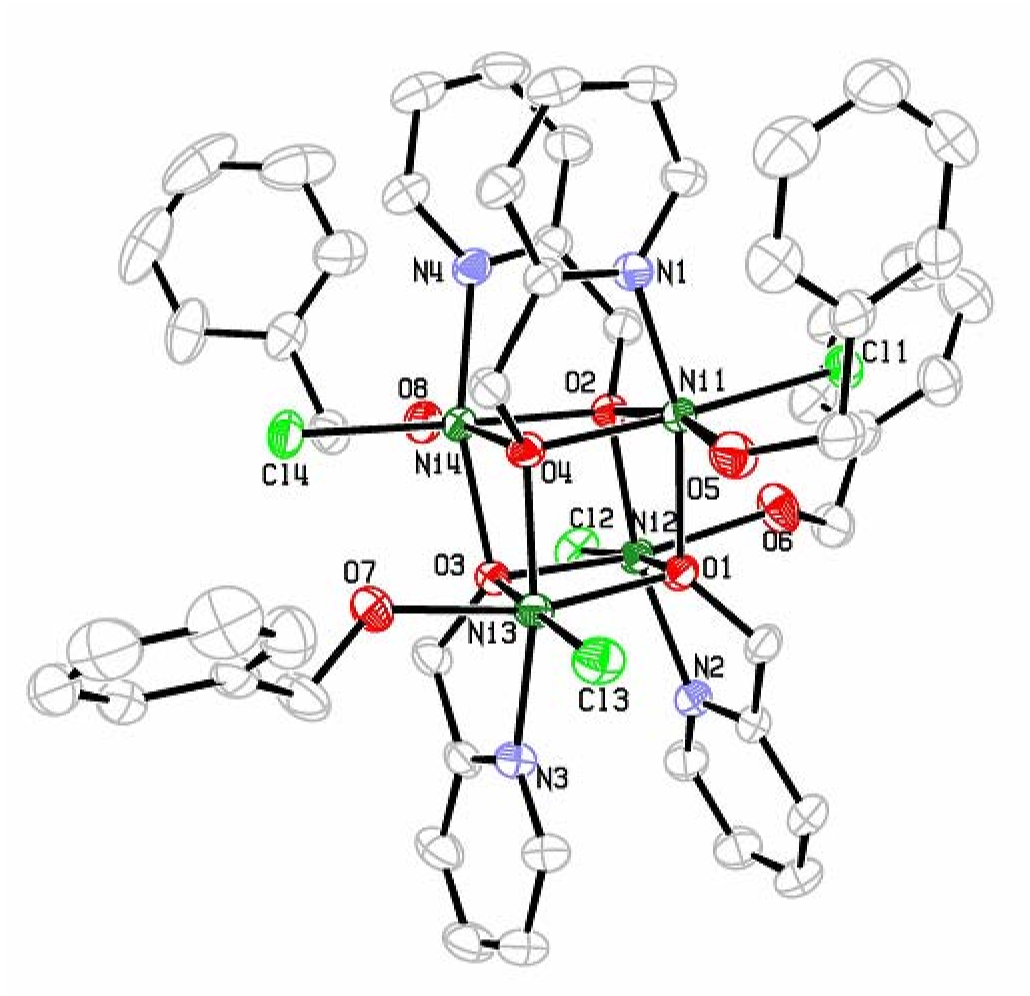

**Figure 6.** ORTEP of [Ni(hmp)(benzylOH)Cl]$_4$ (**5**) with thermal ellipsoids at the 30% probability level. Hydrogen atoms omitted for clarity.

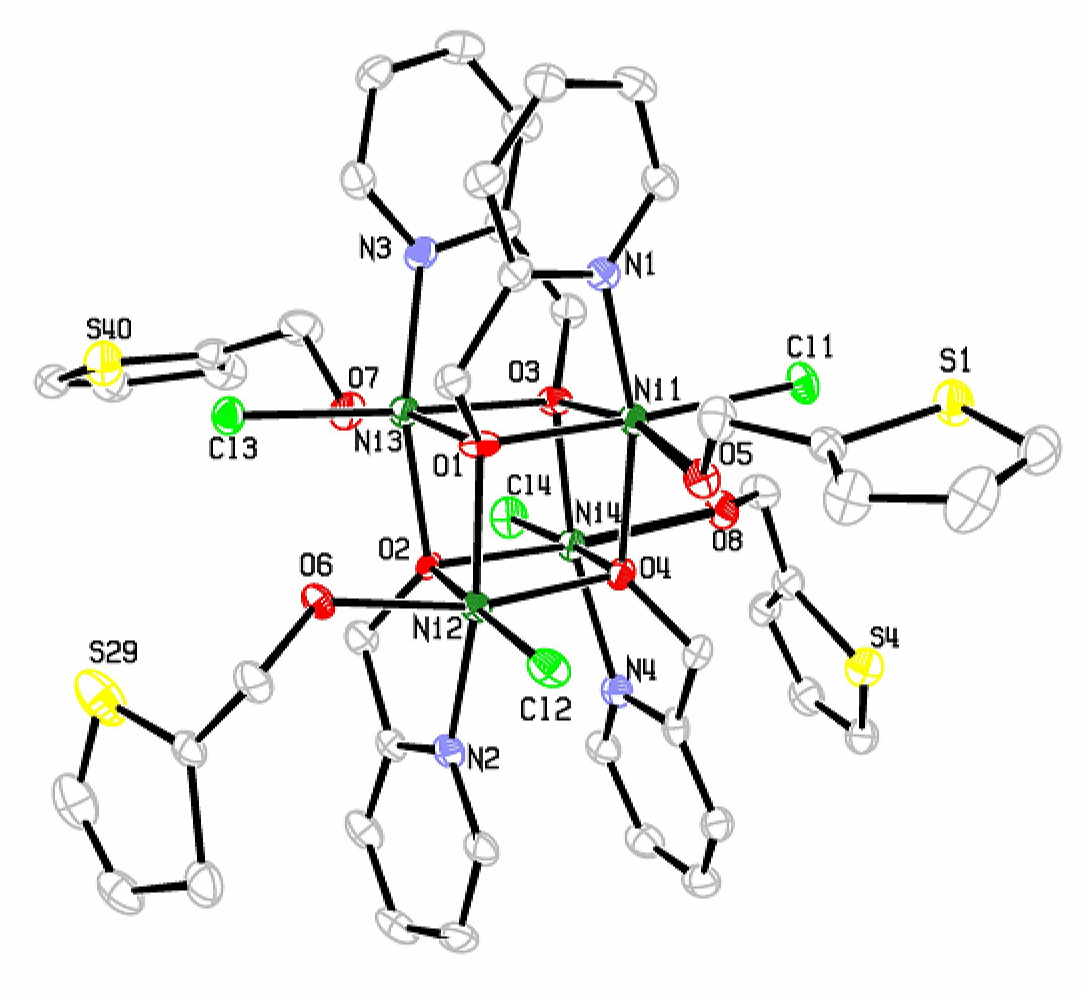

**Figure 7.** ORTEP of $[Ni(hmp)(TPMeOH)Cl]_4$ (**6**) with thermal ellipsoids at the 30% probability level. Hydrogen atoms omitted for clarity.

the thiophene rings where the sulfur atom is at 50% occupancy between both positions. This complex also crystallizes with two symmetry independent molecules in the unit cell. Though complex **6** has more disorder than **5**, it may be useful for supporting interactions with other types of molecules. The sulfur atom on the thiophene molecule has access to the exterior of the molecule. Although sterically hindered, one can take advantage of Au-S interactions to attach SMMs to gold surfaces. In addition, the 2 and 3 positions of the thiophene are unobstructed and are the points of polymerization for polythiophene.[16, 17] This could allow for the creation of multidimensional networks of SMMs if polymerization could successfully be achieved off those positions.

To alleviate some of the Au-S steric problems expected with the 2-thiophenemethanol ligand, complex **7** $[Ni(hmp)(MeSEtOH)Cl]_4$ was synthesized with 2-(methylthio)ethanol in an attempt to obtain a less sterically hindered sulfur atom. Complex **7** is depicted in Figure 8 with only one conformation of the disordered 2-(methylthio)ethanol arms shown. This ligand will present similar functionality to methylthiophenylcarboxylate ligand which has been successfully used with $Mn_{12}$ to attach the molecule to a gold surface. [20]

## DC Magnetic Susceptibility

The DC magnetic susceptibilities of compounds **1-7** were measured between 300 and 1.8 K and are plotted as $\chi_M T$ versus T. Plotting as $\chi_M T$ as opposed to just $\chi_M$ exposes potential deviations from paramagnetic behavior. Paramagnetic compounds follow Curie-Weiss behavior and the $\chi_M T$ results in a constant value as expressed by the equation:

$$\chi T = \frac{Ng^2\mu_B^2}{3k_B}S(S+1) \tag{2.1}$$

where $\mu_B$ is the Bohr magneton, $k_B$ is Boltzman's constant, and S is the spin value.

The $\chi_M T$ for compounds **1-7** are between 4.5 $cm^3$ $mol^{-1}$ K and 6.5 $cm^3$ $mol^{-1}$ K at 300 K. This value slowly increases as the temperature is lowered until approximately 100 K, at which point $\chi_M T$ increases more rapidly until it reaches a maximum of ~10.5 $cm^3$ $mol^{-1}$ K at 15 K. Below 15 K, the rapid decrease in $\chi_M T$ can be attributed largely to Zeeman effects. The large rise in $\chi_M T$ followed by the decrease below 15 K is similar to what was found for other S=4 $Ni_4$ cubane complexes and is indicative of strong ferromagnetic coupling between the $Ni^{II}$ ions. $Ni^{II}$ is the most common stable oxidation state of Ni and is S=1. Given that their $\chi_M T$ plots suggest ferromagnetic coupling between the $Ni^{II}$ S=1 centers and the similar architecture of **1-7** to published $Ni_4$ S=4 SMMs, it is likely that **1-7** will be S=4 as well.[2, 9] However, modeling of their magnetic data is necessary before their ground state is established.

Complexes **1-7** were analyzed using two models as with previously characterized $Ni_4$ cubane complexes.[2, 9] The first model assumes that the molecules are perfect cubes and exhibit $T_d$ symmetry. In turn, the model treats the magnetic exchange interactions between all the metal centers to be equivalent. This serves as an adequate model for some of the $[Ni(hmp)(ROH)Cl]_4$ systems because the $Ni^{II}$ ions have similar ligand environments. However, in most cases, the second model is superior as it takes into account the lower $S_4$ symmetry as opposed to the idealized $T_d$ symmetry as assumed in the previous model.

The spin Hamiltonian in the first model takes the form

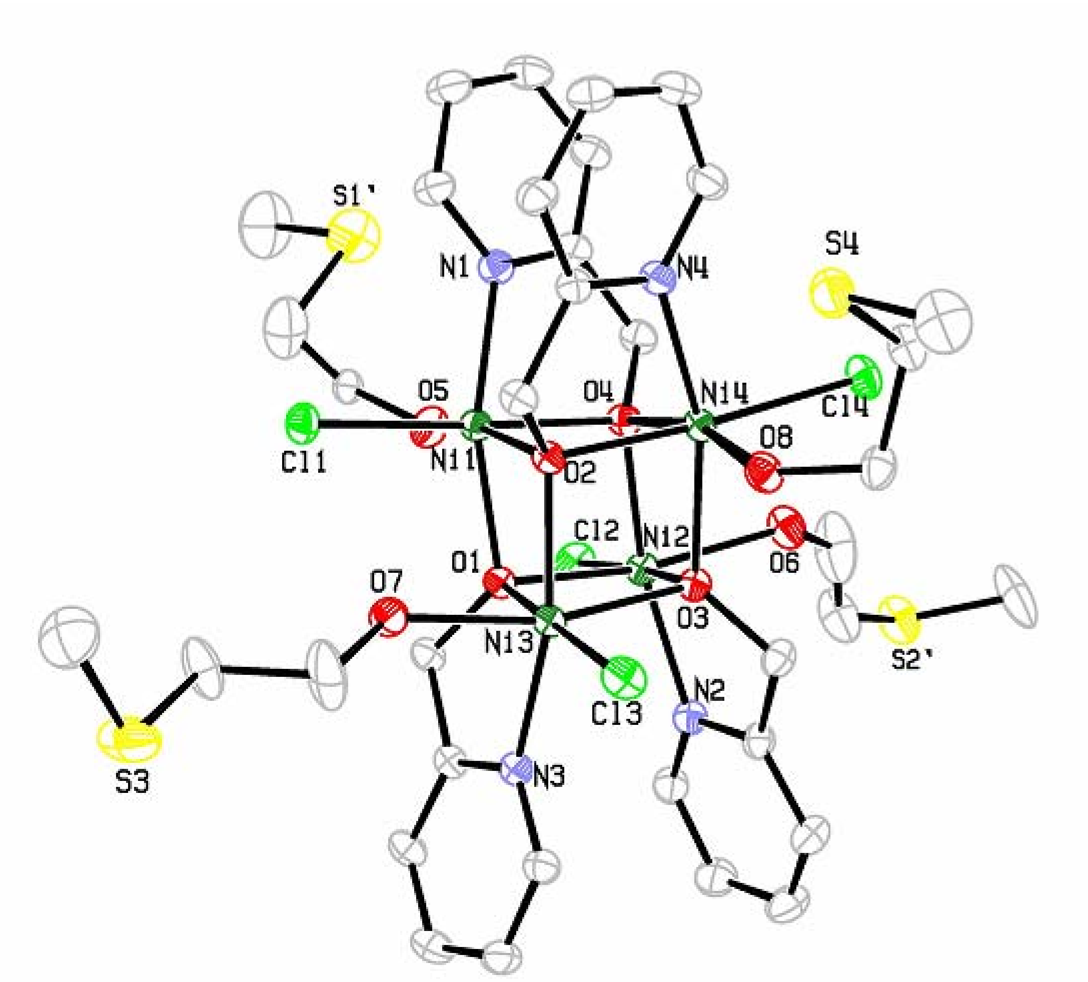

**Figure 8**. ORTEP of $[Ni(hmp)(MeSEtOH)Cl]_4$ (**7**) with thermal ellipsoids at the 30% probability level. Hydrogen atoms omitted for clarity.

$$\hat{H} = -2J(\hat{S}_1 \bullet \hat{S}_2 + \hat{S}_1 \bullet \hat{S}_3 + \hat{S}_2 \bullet \hat{S}_4 + \hat{S}_3 \bullet \hat{S}_4) \tag{2.2}$$

and accounts for the interaction of oxo-bridged metal ions. The Kambe vector technique gives the energy of the 19 different spin states of the $Ni_4$ molecules.

$$E(S_T) = -J[S_T(S_T + 1)] \tag{2.3}$$

A definition of $\hat{S}_T = \hat{S}_1 + \hat{S}_2 + \hat{S}_3 + \hat{S}_4$ is made to account for the 0, 1, 2, 3, and 4 states of $S_T$. The energies resulting from the fitted parameters were used in the Van Vleck equation to provide the modeled $\chi_M T$ data. This model was used to fit the $\chi_M T$ data for complex **4** and yielded a spin ground state of S=4 and a positive (ferromagnetic) coupling constant, J. The fit is shown as the solid red line and the experimental data as the black points in Figure 9.

For complex **4**, idealizing the symmetry of the system to be $T_d$ appears to be reasonable. The single J parameter model results in a good fit to experimental data. The spin ground state, g, and J parameters obtained are comparable to the parameters obtained for the $Ni_4$-dmb system and other $Ni_4$ systems.

The second model employs two J-values to take in account the lower symmetry that these complexes posses. The spin Hamiltonian takes the form:

$$\hat{H} = -2J_a(\hat{S}_1 \bullet \hat{S}_2 + \hat{S}_3 \bullet \hat{S}_4) - 2J_b(\hat{S}_1 \bullet \hat{S}_3 + \hat{S}_1 \bullet \hat{S}_4 + \hat{S}_2 \bullet \hat{S}_3 + \hat{S}_2 \bullet \hat{S}_4) \tag{2.4}$$

The spin Hamiltonian can be simplified by utilizing Kambe vector coupling such that $S_A = S_1 + S_2$, $S_B = S_3 + S_4$, and $S_T = S_A + S_B$. Using these definitions, the energy of a state can be expressed as:

$$\begin{aligned} E(S_T, S_A, S_B) = -J_A[S_A(S_A + 1) + S_B(S_B + 1)] \\ - J_2[S_T(S_T + 1) - S_A(S_A + 1) - S_B)(S_B + 1)] \end{aligned} \tag{2.5}$$

The same approach is then used in this second model as in the first where the energies can be substituted into the Van Vleck equation to fit the $\chi_M T$ results. This second model yields a better fit of the data for complexes **1**, **2**, **3**, **5**, **6**, and **7** as shown in Figures 10, 11, 12, 13, 14, and 15, respectively. The temperature independent paramagnetism (TIP) contribution to magnetic susceptibility for 4 $Ni^{II}$ was taken into account for all complexes and is fixed at 400 x $10^{-6}$ $cm^3mol^{-1}$.

There is deviation of the fitted data from the experimental data for complexes **2** and **3**. In addition, the fit of complex **1** resulted in a g value of 2.24 which is on the higher side for the $Ni_4$ cubane family of SMMs. These problems can be possibly attributed to impurities in the SQUID sample used. Elemental analysis data reveals that the bulk sample of the compounds used for analysis poorly matches the expected elemental composition as determined by X-ray crystallography. The mixed products have unknowns contributing to the DC magnetic susceptibility of the samples which the model cannot account for. All products in the reaction vessels for complexes **1**, **2**, and **3** appear to be crystalline and are therefore impossible to distinguish. A pure product needs to be obtained before an accurate fit can be made. The parameters determined from the fit of the data are shown in Figures 10, 11, and 12 should only be used as crude estimates.

The two J value model for complex **5** results in a good fit to experimental data as seen in Figure 13. The parameters obtained of S=4, g=2.12, $J_a$=7.58 $cm^{-1}$, and $J_b$= 2.39 $cm^{-1}$ are comparable to the $Ni_4$-dmb system and other $Ni_4$ SMMs. The parameters obtained for this compound can be trusted and indicates that the lower symmetry model employed for this system is appropriate. Attempts to fit this complex to a single J value model resulted in poor a fit.

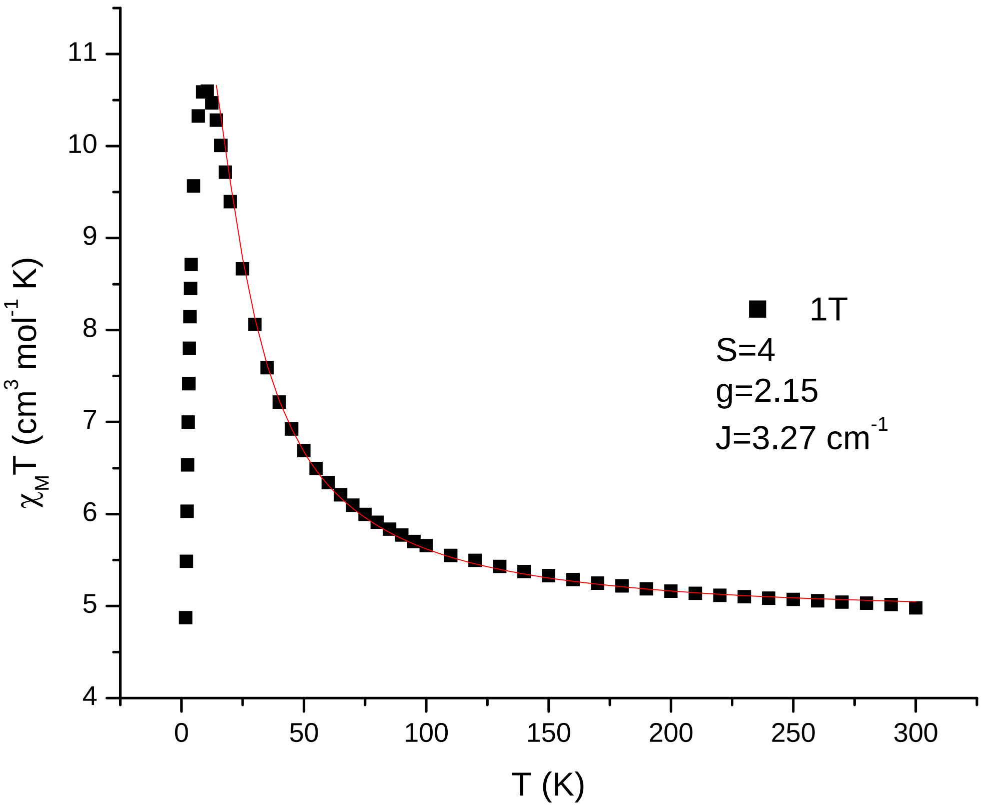

**Figure 9.** DC magnetic susceptibility of complex **4** [Ni(hmp)($H_2O$)Cl]$_4$ •4($C_4H_8O_2$). Fit shown in red.

For complexes **6** and **7** as seen in Figures 14 and 15**,** the maximum value of $\chi_M$T max is significantly lower at 7.8 cm$^{-1}$ and 8.5 cm$^{-1}$, respectively, compared to the $\chi_M$T max of ~11 cm$^{-1}$ seen in other Ni$_4$ systems. The lower $\chi_M$T max attributes to the lower g values obtained from fitting and is indicative of other effects occurring in the system. Elemental analysis matches fairly well to the predicted elemental composition

based on X-ray crystallography and therefore rules out diamagnetic impurities in the sample. It is possible that there are interactions due to the sulfur atoms on both molecules. The large electron rich sulfur atoms can help support antiferromagnetic exchange between molecules. However, disorder in the X-ray crystal structure prevents accurate determination of the S-S distance and further analytical techniques are necessary to decipher the origins of this behavior.

An additional DC magnetic susceptibility experiment used to analyze these complexes is the reduced magnetization technique. The sample is measured between 4 and 1.8 K at different magnetic field strengths varying between 0.1 and 5 T. This technique allows for another measure of the g value and spin ground state. In addition, it provides information on the axial zero-field splitting value D in the Hamiltonian term $DS_z^2$. The results are plotted as M/Nβ versus H/T where M is the magnetization, N is Avogadro's number, β is the Bohr magneton, H is the magnetic field, and T is temperature. For systems where there is no D value, the iso-fields will be superimposed and will saturate at the value of 2S at high magnetic fields. On the contrary, if a D value does exist for the complex, the iso-field data will not be superimposed. All of the complexes exhibited a non-zero D value as evidenced by the splitting of the iso-field lines. Modeling is necessary to determine the sign and magnitude of the D value.

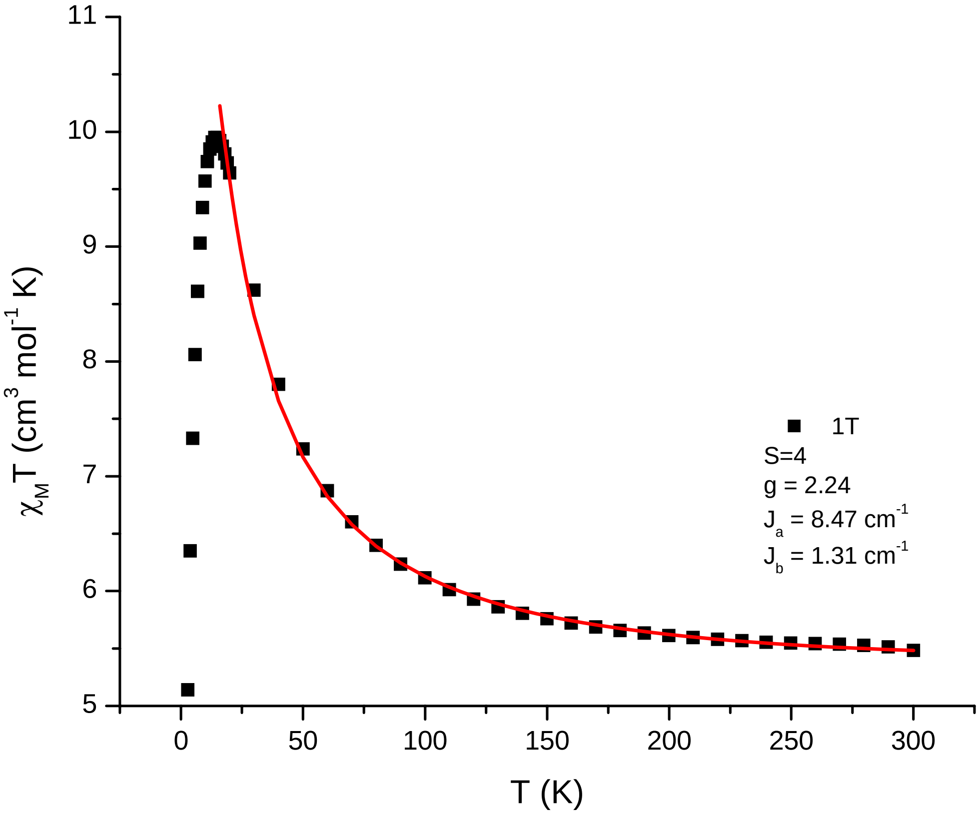

**Figure 10.** DC magnetic susceptibility of complex **1** [Ni(hmp)(PrOH)$_{.75}$(H2O)$_{.25}$Cl]$_4$. Fit shown in red.

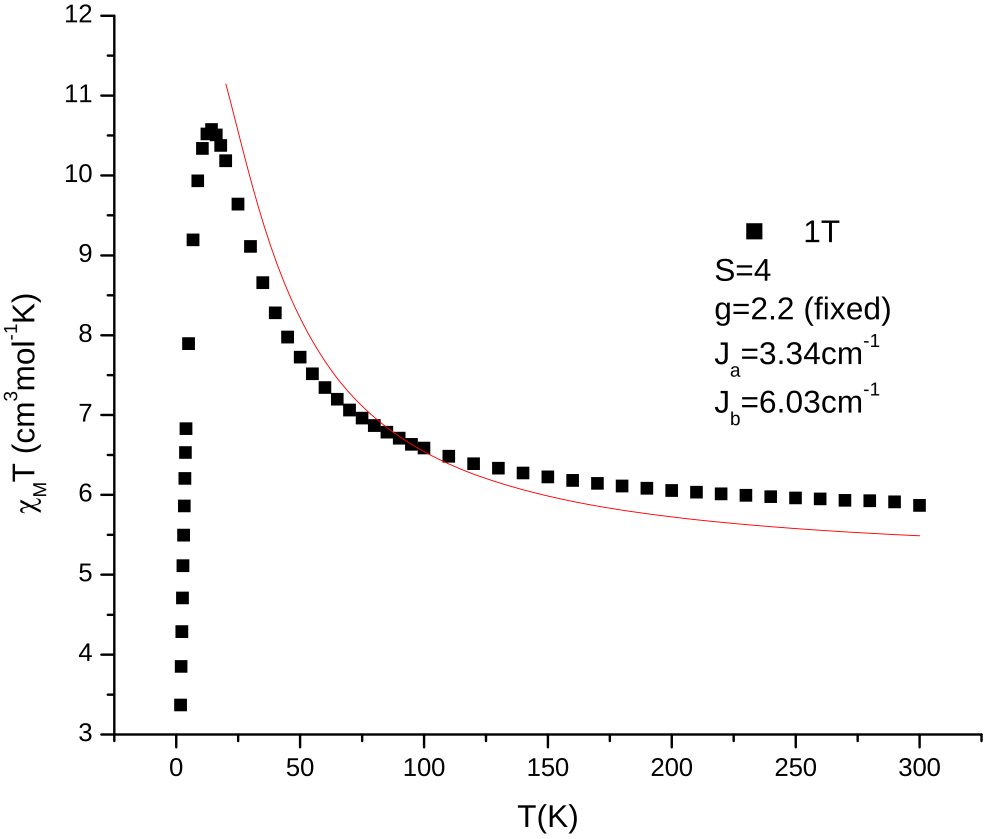

**Figure 11.** DC magnetic susceptibility of complex **2** [Ni(hmp)(i-butylOH)Cl]$_4$•2MeOH. Fit shown in red.

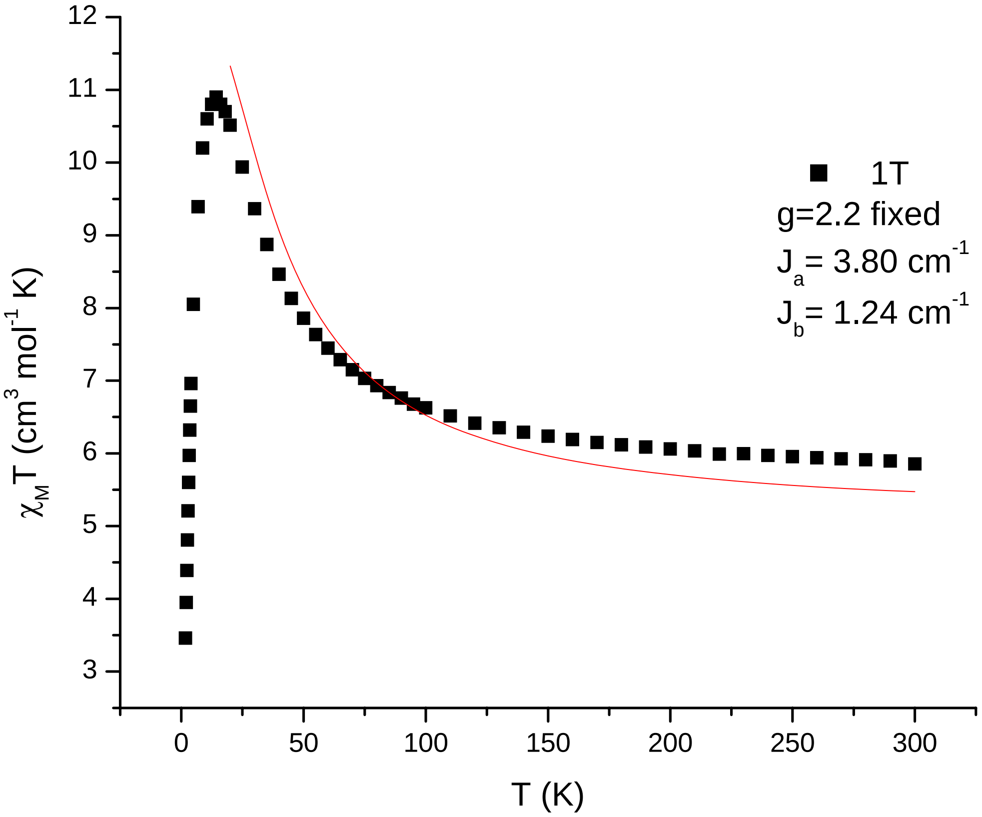

**Figure 12.** DC magnetic susceptibility of complex **3** Ni(hmp)(propargylOH)Cl$]_4$•MeOH. Fit shown in red.

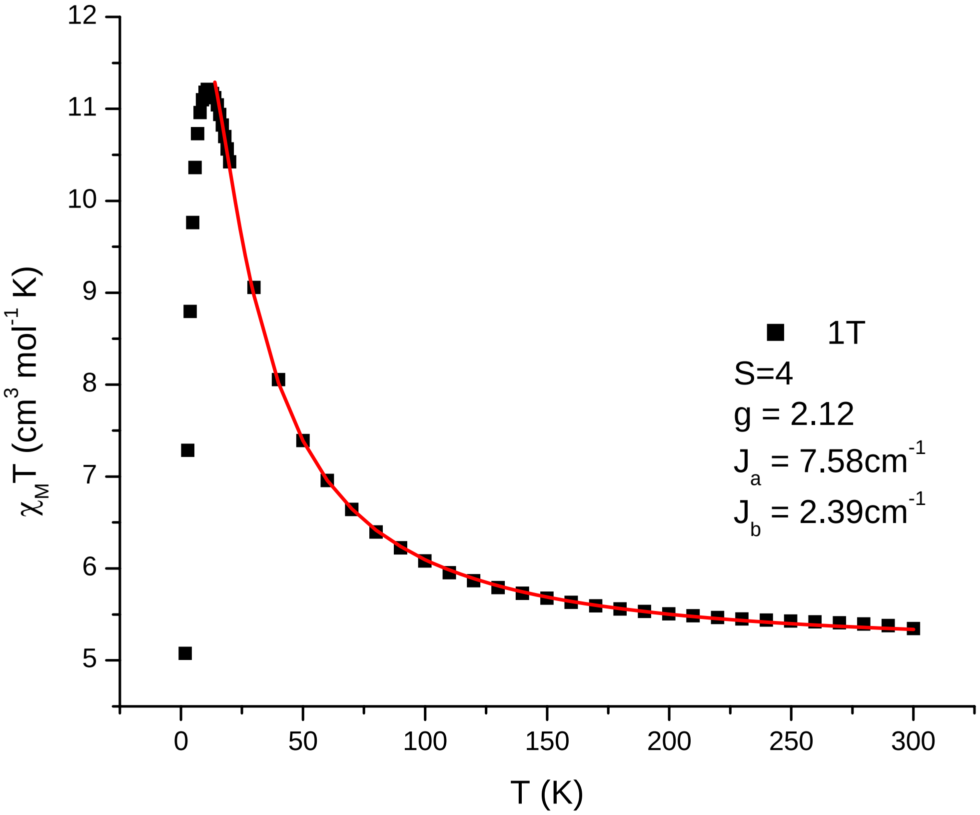

**Figure 13.** DC magnetic susceptibility of complex **5** [Ni(hmp)(benzylOH)Cl]$_4$. Fit shown in red.

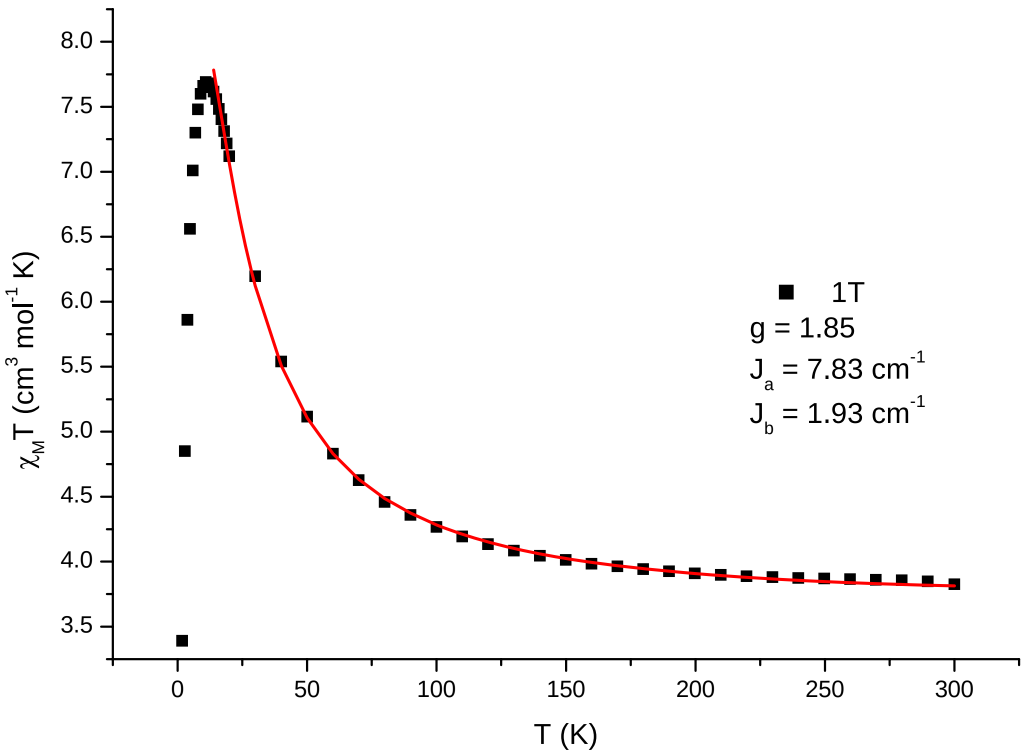

**Figure 14.** DC magnetic susceptibility of complex Complex **6** [Ni(hmp)(TPMeOH)Cl]$_4$. Fit shown in red

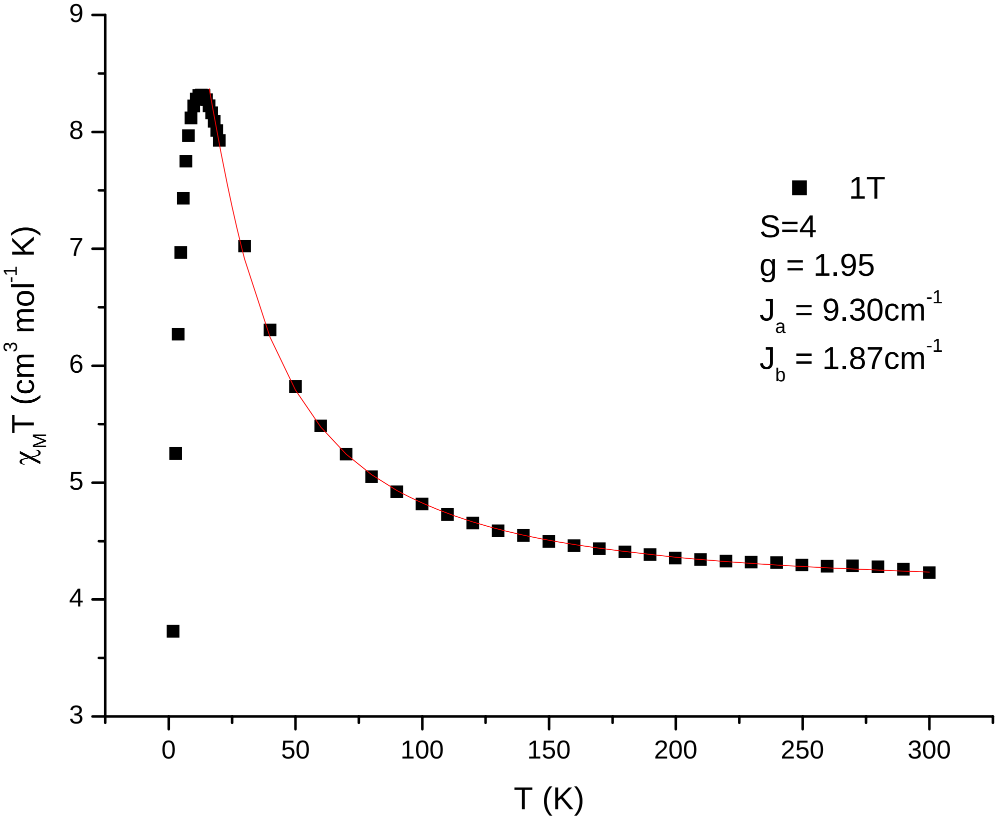

**Figure 15.** DC magnetic susceptibility of complex **7** [Ni(hmp)(MeSEtOH)Cl]$_4$. The fit is shown in red.

The reduced magnetization data can be fit to provide information about g, S, and D. A different spin Hamiltonian is now used to account for both zero-field splitting and Zeeman splitting

$$\hat{H} = \hat{H}_{Zeeman} + \hat{H}_{zfs} \tag{2.6}$$

The terms in this Hamiltonian can be specified as follows:

$$\hat{H} = g\beta H \bullet \hat{S} + D[\hat{S}_z^2 - S(S+1)/3] \tag{2.7}$$

The Hamiltonian matrix (9 x 9) is diagonalized, taking into account the powder average. The eigenvalues obtained are then substituted into the Van Vleck equation:

$$M = \frac{\sum_{i=-S}^{S} (\partial E_i / \partial H) \exp(-E_i / kt)}{\sum_{i=-S}^{S} \exp(-E_i / kt)} \tag{2.8}$$

Utilizing the above equation, the reduced magnetization fit are obtained and are plotted in Figures 15, 16, 17, 18, 19, 20 and 21 for complexes **1-7,** respectively. An important restriction exists for this method of fitting the data; the spin ground state needs to be well-isolated from any excited states as the model assumes a single spin state.

A poor fit of the reduced magnetization data for complexes **1**, **2**, **3** as seen in Figure 16, 17, and 18 is possibly due to mixed composition samples. There are significant deviations in the experimentally determined elemental analysis data for these complexes from their predicted elemental composition based on their X-ray structures. The mixed product would result in reduced magnetization data that is impossible to fit as the model assumes a pure compound. All products in the samples for complexes **1**, **2**, and **3** appear

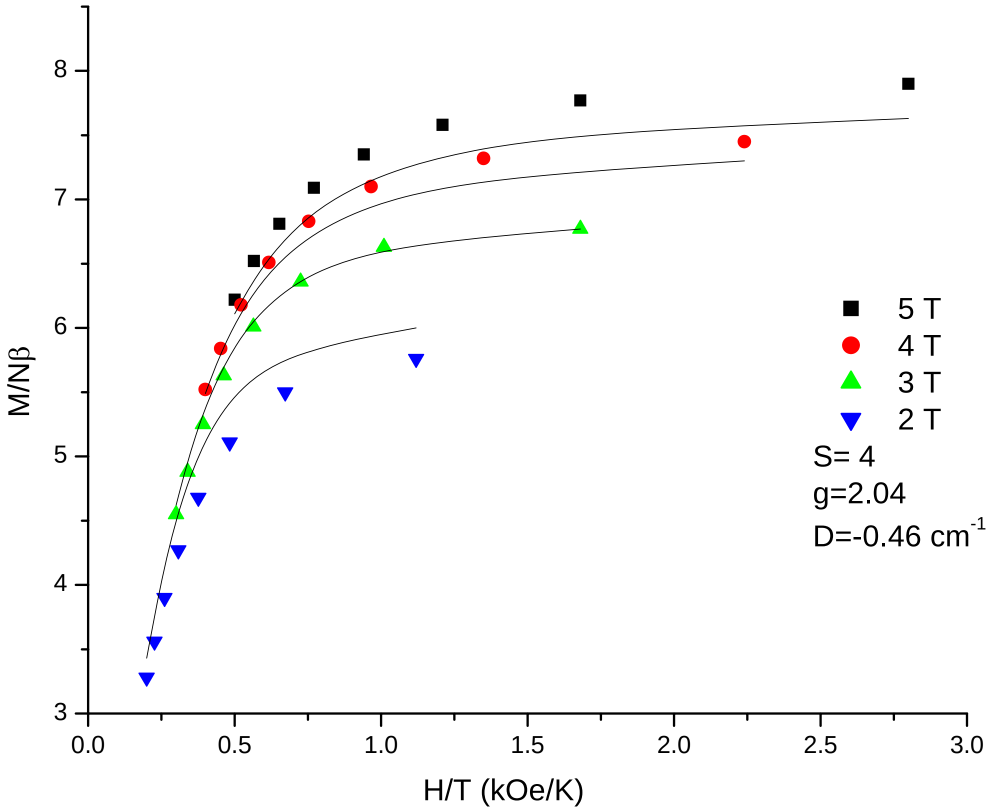

**Figure 16**. Reduced magnetization plot of complex **1** [Ni(hmp)(PrOH)$_{.75}$(H2O)$_{.25}$Cl]$_4$. The fit shown as a black line.

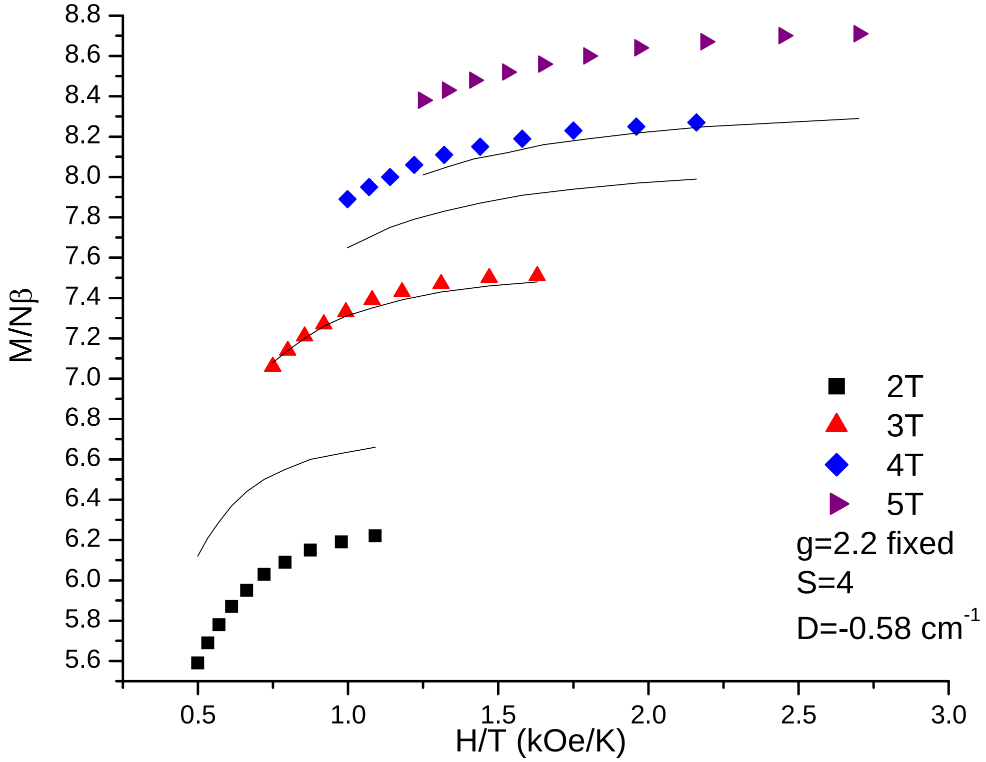

**Figure 17.** Reduced magnetization plot of complex **2** [Ni(hmp)(i-butylOH)Cl]$_4$•2MeOH. The fit shown as a black line.

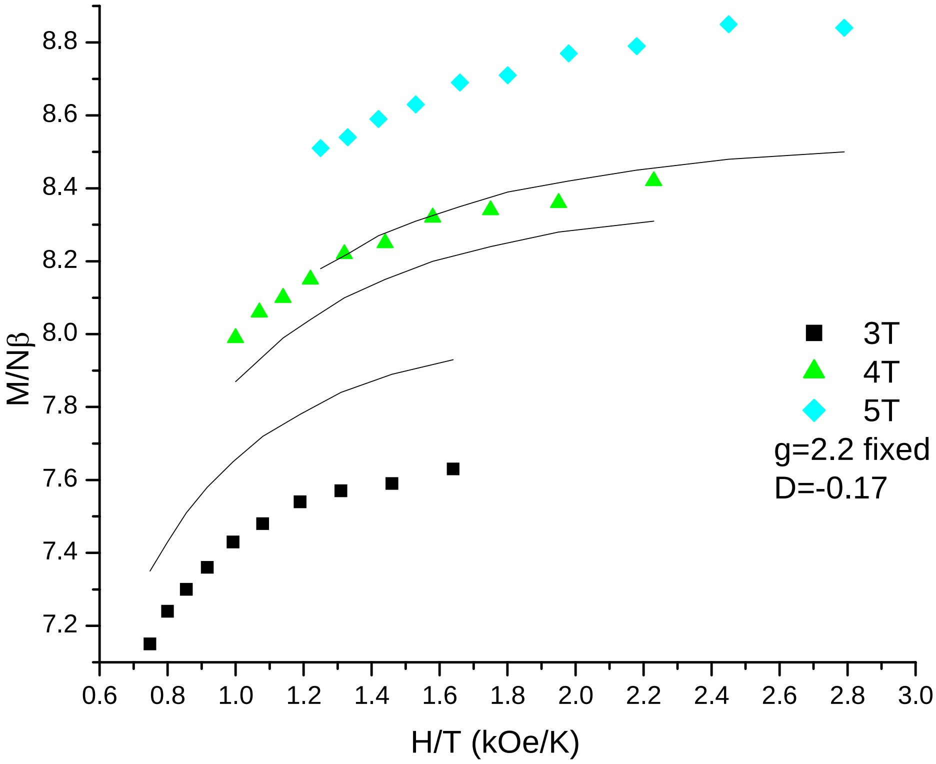

**Figure 18**. Reduced magnetization plot of complex **3** [Ni(hmp)(propargylOH)Cl]$_4$•MeOH. The fit shown as a black line.

crystalline and therefore are impossible to separate. In addition, the molecules have been known to be hygroscopic and additional water could be absorbed from the air during the processing of the SQUID sample. Without the ability to obtain pure products, efforts to fit the reduced magnetization data for complexes **1**, **2**, **3** are futile and optimized parameters carry little meaning. The only information that can be determined from the reduced magnetization data for these complexes is that the isofield lines are not superimposable and therefore there is a nonzero D value. Based on the similarity of complexes **1**, **2,** and **3** to other $Ni_4$ systems, it is likely that there D value is negative.

A good fit of reduced magnetization data were obtained for complexes **4** and **5** as seen in Figures 19 and 20. The optimized parameters obtained for S, g, and D are comparable to the values obtained for the $Ni_4$-dmb complex and other $Ni_4$ SMMs. The reduce magnetization data for these two complexes were fit at all fields and fitted data exhibit little deviation experimental data.

The fit of the reduced magnetization data for complexes **6** and **7** as seen in Figures 21 and 22 appear to be good, but the parameters obtained from fitting are unreasonable. The D value of -1.24 $cm^{-1}$ for complex **6** is much larger than the D values ~0.5 $cm^{-1}$ reported for all other $Ni_4$ complexes. In addition, the g values determined through fitting are lower than all other reported $Ni_4$ molecules which have g values greater than 2. As both sulfur containing complexes exhibit similar behavior, it is likely that this effect is caused by the sulfur atom. It is possible that the origin of the behavior for complexes **6** and **7** is due to intermolecular interactions through sulfur atoms on two adjacent $Ni_4$ complexes. The sulfur atoms for both complexes **6** and **7** are disordered over two positions. Therefore, it is difficult to determine their relative positions to evaluate the extent of possible intermolecular interactions. For both molecules, the sulfur group is protected as is unlikely to form a disulfide bond. As a result, their interactions are more likely to be through space interactions and/or nonclassical hydrogen bonding. Without a X-ray structure that has well defined positions for the sulfur atom, it is currently difficult to determine the nature of the interactions. Ultimately, the values obtained from fitting are highly suspect and should only be taken as crude approximations until additional analytical techniques can decipher the origins of this behavior.

Complexes **1-7** were each analyzed through magnetic susceptibility and reduced magnetization experiments. A summary of the parameters obtained from the fitted data is provided in Table 5. All of the complexes synthesized were determined to have a spin ground state of 4 as supported by fitting of both magnetic susceptibility data as well as reduced magnetization data. All compounds show ferromagnetic coupling of the S=1 $Ni^{II}$ as indicated by their positive J values. In addition, all compounds exhibit a negative D value as evidenced by the splitting of the isofields and fitting of the reduced magnetization data. Together, the high spin ground state and negative D value for complexes **1-7** give rise to the barrier toward magnetization reversal which is necessary for SMM behavior.

The DC magnetization studies offers insight in into the size and characteristics of the barrier for magnetization reversal but hysteresis measurements are necessary to observe tunneling and possible exchange bias. However, due to small barrier of $U \approx 8$ $cm^{-1}$, $Ni_4$ molecules block at very low temperatures. It is currently beyond the capabilities of the SQUID used to conduct meaningful hysteresis measurements.

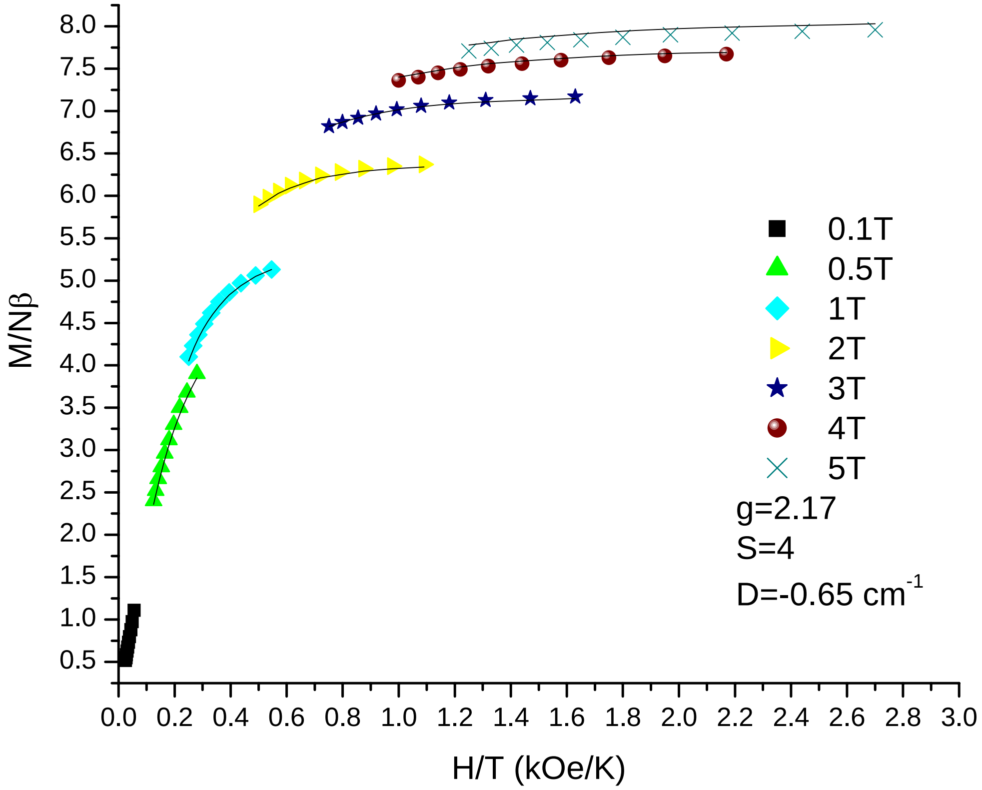

**Figure 19.** Reduced magnetization plot of complex **4** $[Ni(hmp)(H_2O)Cl]_4 \cdot 4(C_4H_8O_2)$. The fit shown as a black line.

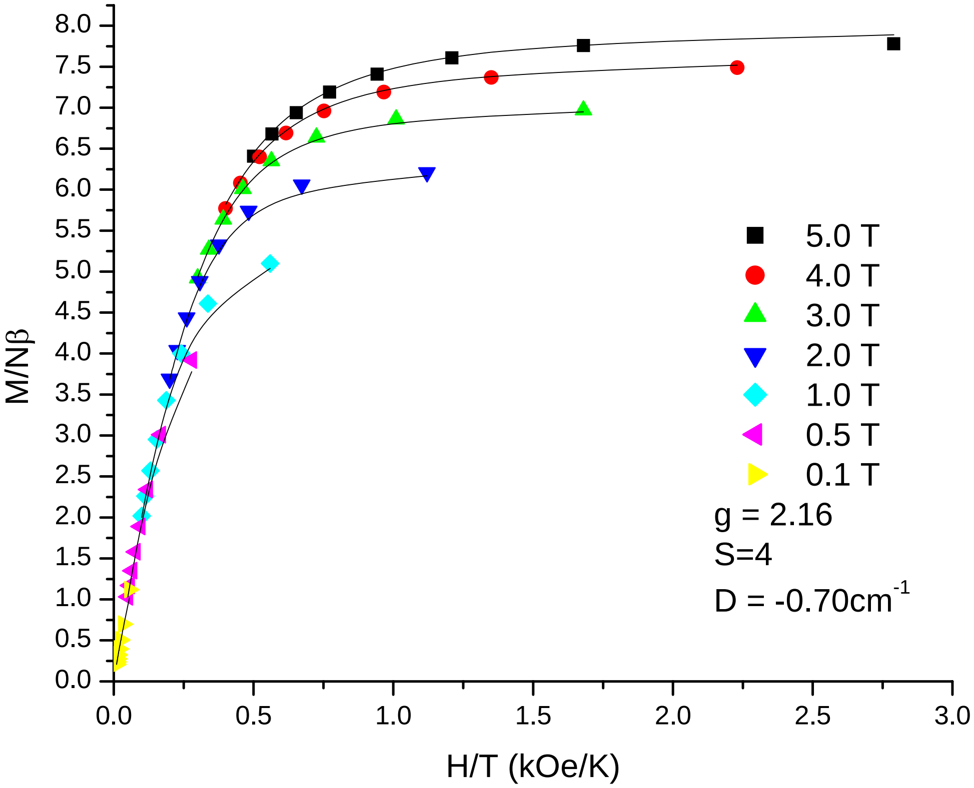

**Figure 20.** Reduced magnetization plot of complex **5** [Ni(hmp)(benzylOH)Cl]$_4$. The fit shown as a black line.

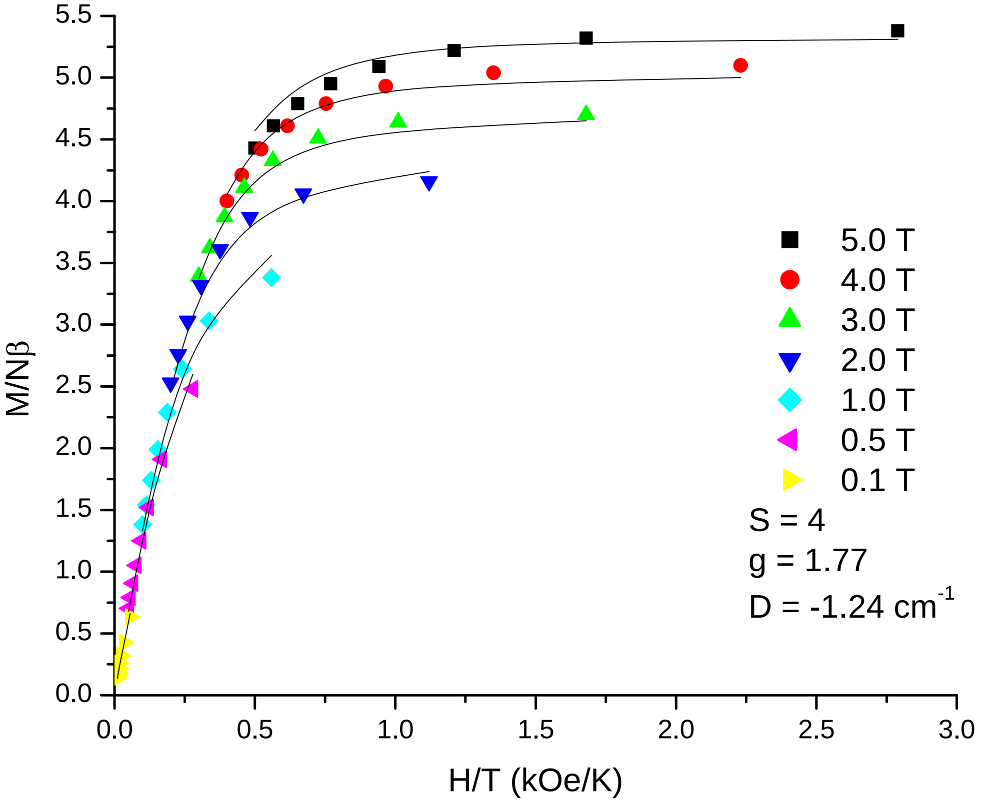

**Figure 21.** Reduced magnetization plot of complex **6** [Ni(hmp)(TPMeOH)Cl]$_4$. The fit shown as a black line.

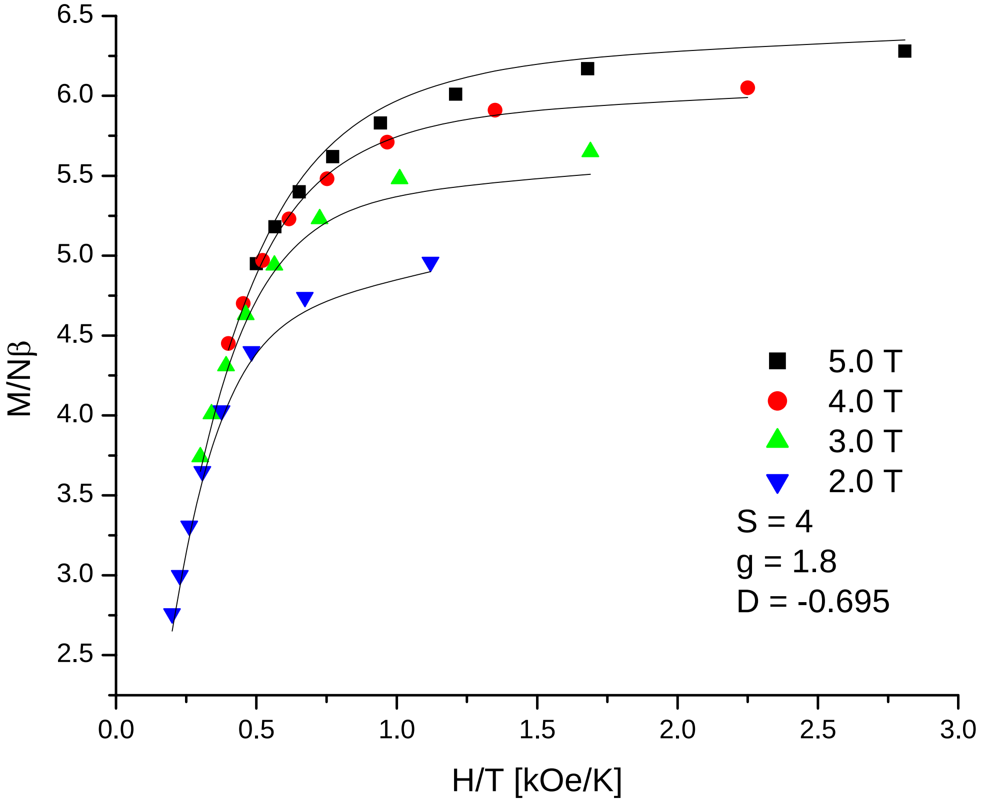

**Figure 22.** Reduced magnetization plot of complex **7** [Ni(hmp)(MeSEtOH)Cl]$_4$. The fit shown as a black line.

**Table 5.** Summary of DC Magnetic Susceptibility and Reduced Magnetization Fit Parameters for **1-7**

| Complex | Formula | Mag. Suceptibility | | | | Reduced Mag. | | |
|---|---|---|---|---|---|---|---|---|
| | | S | g | $J_a$ cm$^{-1}$ | $J_b$ cm$^{-1}$ | S | g | D cm$^{-1}$ |
| 1 | [Ni(hmp)(PrOH)$_{.75}$(H2O)$_{.25}$Cl]$_4$ | 4 | 2.24 | 8.47 | 1.31 | 4 | 2.04 | -0.46 |
| 2 | [Ni(hmp)(tbutylOH)Cl]$_4$•4MeOH | 4 | 2.20* | 3.34 | 6.03 | 4 | 2.2* | -0.58 |
| 3 | [Ni(hmp)(propargylOH)Cl]$_4$•MeOH | 4 | 2.20* | 3.80 | 1.23 | 4 | 2.2* | -0.17 |
| 4 | [Ni(hmp)($H_2O$)Cl]$_4$ •4(1,4Dioxane) | 4 | 2.2 | 3.27 | - | 4 | 2.17 | -0.65 |
| 5 | [Ni(hmp)(benzylOH)Cl]$_4$ | 4 | 2.12 | 7.58 | 2.39 | 4 | 2.16 | -0.70 |
| 6 | [Ni(hmp)(TPMeOH)Cl]$_4$ | 4 | 1.85 | 7.83 | 1.93 | 4 | 1.77 | -1.24 |
| 7 | [Ni(hmp)(MeSEtOH)Cl]$_4$ **(1)** | 4 | 1.95 | 9.30 | 1.87 | 4 | 1.8 | -0.695 |

*parameter held fixed during fitting

## AC Magnetic Susceptibility

AC magnetic susceptibility is another technique that is used to examine SMMs behavior. The presence of a frequency dependent out-of-phase component of the AC signal is one of the identifying characteristics of SMMs as it indicates that there is a barrier toward reversal of magnetization.[8] The out-of-phase signal arises since a SMM is unable to reverse the direction of its magnetization rapidly enough to match the frequency of the applied field due the energy barrier for spin reversal.

The AC magnetic susceptibility experiments were carried out in the range of 5-1.8 K. The molar in-phase susceptibility, $\chi'_M$, and out-of-phase component, $\chi''_M$, are each plotted against temperature. As the temperature decreases, there is an increase in the susceptibility of the compounds. For systems that show an out-of-phase susceptibility, the in-phase component decreases to match any increase in the out-of-phase component of susceptibility.

Compounds **1-7** were measured at AC frequencies of 50, 100, 250, 500, 750, and 1000 Hz. At lower frequencies, SMMs can better match the frequency of spin reversal and are less likely to show an out-of-phase component. At higher frequencies, the role of the barrier of magnetization reversal becomes more significant. Therefore, for SMMs, the out-of-phase component is frequency dependent and increases with increasing frequencies.

In the $[Ni(hmp)(ROH)Cl]_4$ compounds previously synthesized, it was shown that for several compounds that the out-of-phase component was not seen until the 100 mK temperature range.[9] The relatively small spin and D value of these complexes gives rise to a smaller barrier for reversal of magnetization when compared to other higher blocking temperature SMM systems like $Mn_{12}$-Ac[8]. While $Mn_{12}$-Ac shows a pronounced out-of-phase magnetic susceptibility which saturates, it is expected that the onset of the out-of-phase signal for compounds **1-7** will not occur until a much lower temperature and will not reach its peak within the temperature range of the experiments. Furthermore, it is possible that the out-of-phase susceptibility will occur may not occur within the temperature range of the experiment.

Although the $[Ni(hmp)(ROH)Cl]_4$ family of molecules do not show an appreciable out-of-phase signal in the AC susceptibility in the temperature range measured, this does not rule out the presence of a barrier to magnetization reversal. A lower temperature range beyond the capabilities of the SQUID magnetometer employed would be necessary to fully explore the frequency dependence of the AC susceptibility for this family of compounds.

The AC magnetic susceptibility plots of **1-7** are presented in Figures 23-29. Complexes **1**, **2**, **4, 6**, and **7** show a small but measurable out-of-phase response. The in-phase susceptibility rises with decreasing temperatures but fails to reach its peak in all cases. At higher frequencies, the in-phase susceptibility exhibits a greater decrease and there is a corresponding rise in the out-of-phase susceptibility. The out-of-phase susceptibility in complex **1, 2**, **4, 6,** and **7** is small, but exhibits the expected frequency dependent behavior of increasing out-of-phase susceptibilities at higher frequencies. Deviations in the data being superimposed at higher temperatures are due instrument variability and the small scale employed in the plots. The small negative values seen at higher temperatures are not real and can be attributed to the instrument variability and correction terms applied during data processing. The out-of-phase susceptibilities for complexes **1**, **2**, **4**, **6**, and **7** indicate that there is a barrier toward magnetization reversal typical of SMMs. However, due to the fast tunneling of the $Ni_4$ system and its relatively small energy barrier for magnetization reversal, the onset of the out of phase signal is not seen until low temperatures.

The AC susceptibility of **3** exhibits a very strong response. The out-of-phase response value is almost half of the in-phase value which is unprecedented for a $Ni_4$ complex. While the in-phase signal shows the expected frequency dependent behavior of a greater decrease with increasing frequency, the maximum out-of-phase peak does not correspond to the highest frequency. The onset of the AC susceptibility is similar to other complexes examined and occurs just above 2 K. The highest frequency of 1000 Hz has the out-of-phase signal onset at the highest temperature as in the other systems, but fails to serve as the maximum out-of-phase response. In addition, while other systems gradually have a rise in the in-phase and out-of-phase susceptibilities during cooling, this system shows a very sharp response just below 2.3 K. Problems with sample purity makes this result suspect. Until a technique is devised to obtain only a single crystalline product, these results cannot be verified.

Compound **5** as seen in Figure 27 shows no out-of-phase signal within the temperature and frequency range examined. Without additional analysis at lower temperatures and higher frequencies, it is unclear at this point whether not an AC out-of-phase susceptibility signal exists for this complex.

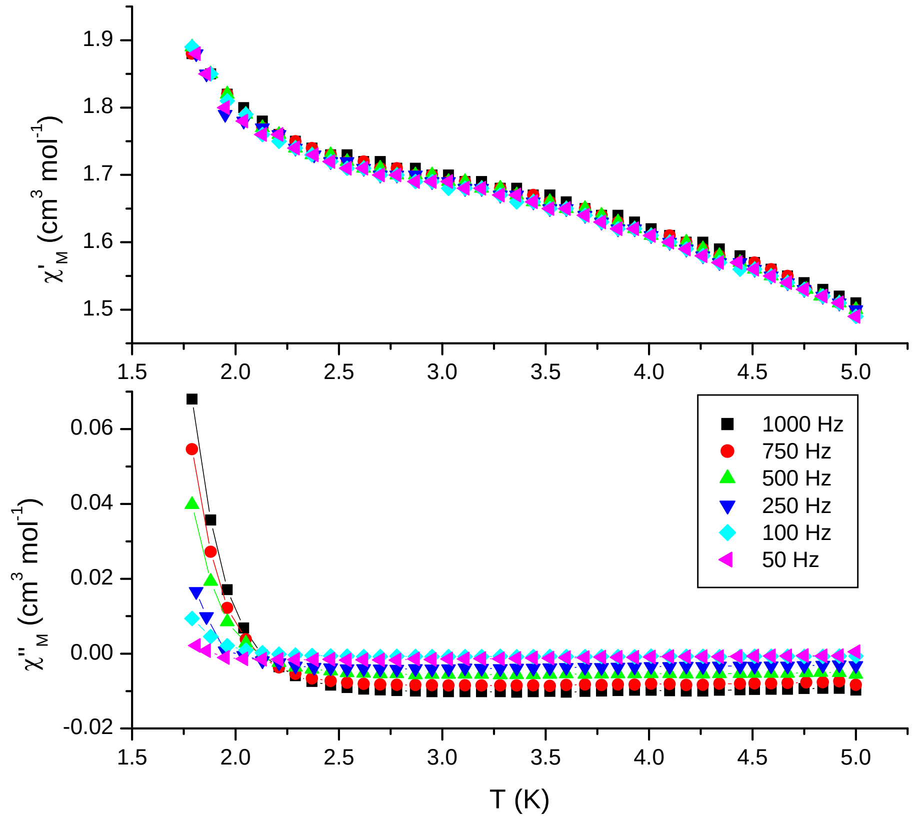

**Figure 23.** AC susceptibility plot of complex **1** [Ni(hmp)(PrOH)$_{.75}$(H2O)$_{.25}$Cl]$_4$.

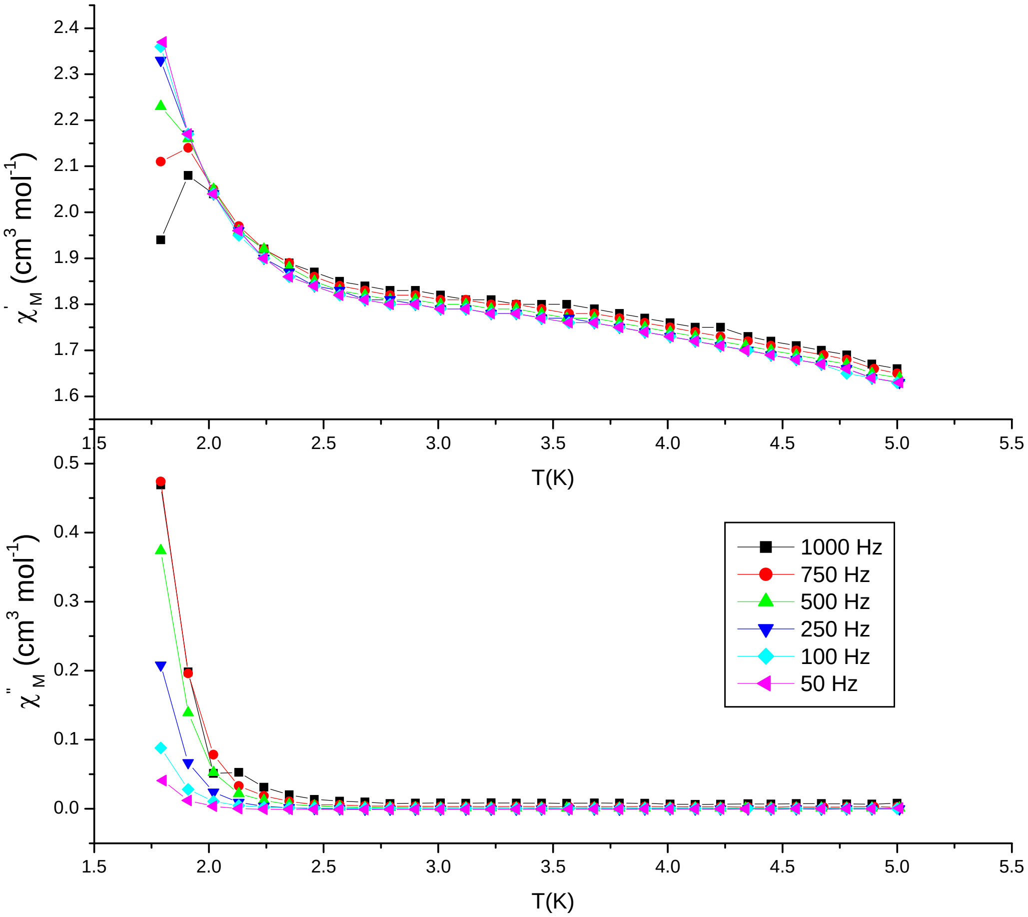

**Figure 24.** AC susceptibility plot of complex **2** **[**Ni(hmp)(i-butylOH)Cl]$_4$•2MeOH.

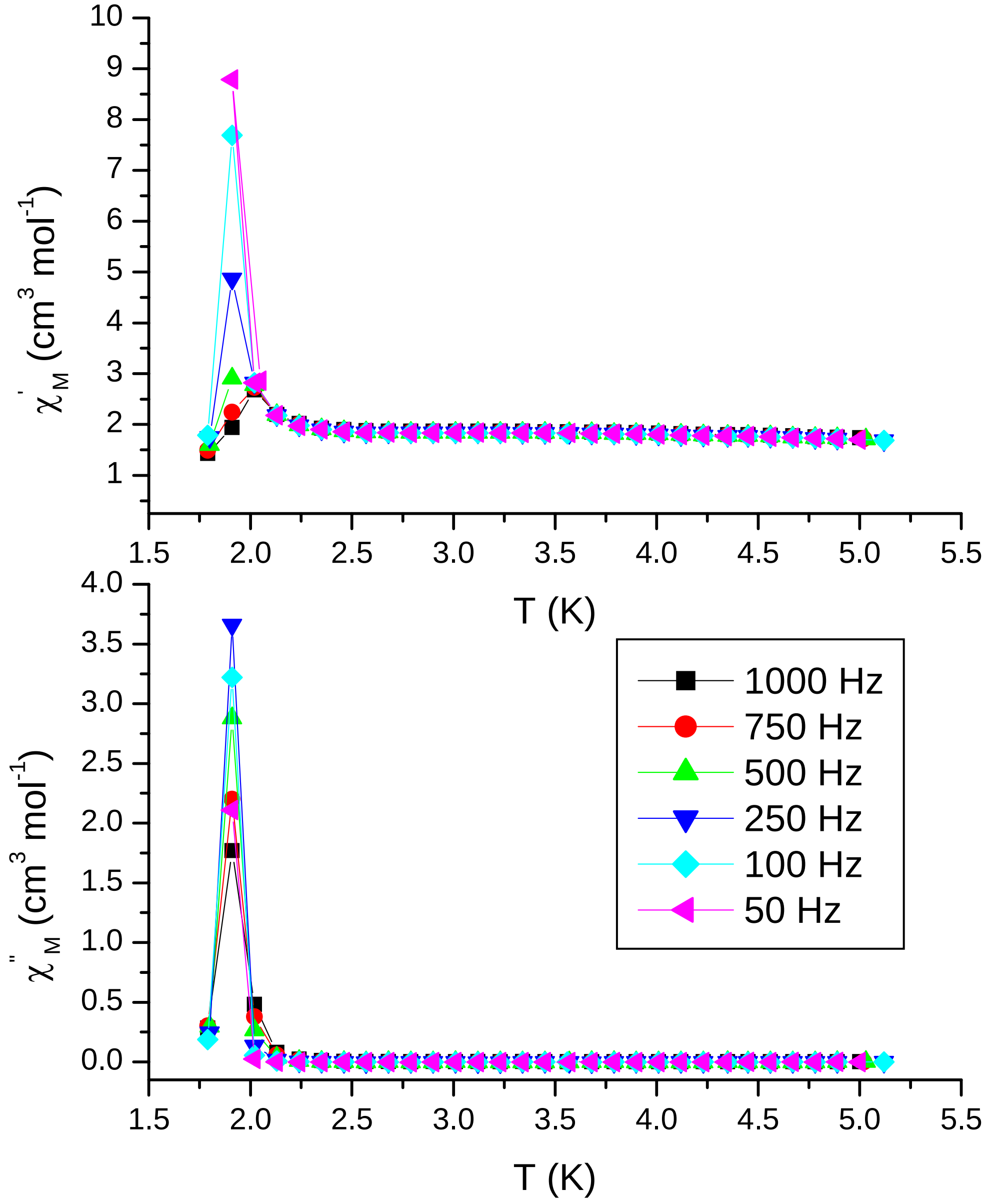

**Figure 25.** AC susceptibility plot of complex **3** [Ni(hmp)($C_3H_3OH$)Cl]$_4$•MeOH.

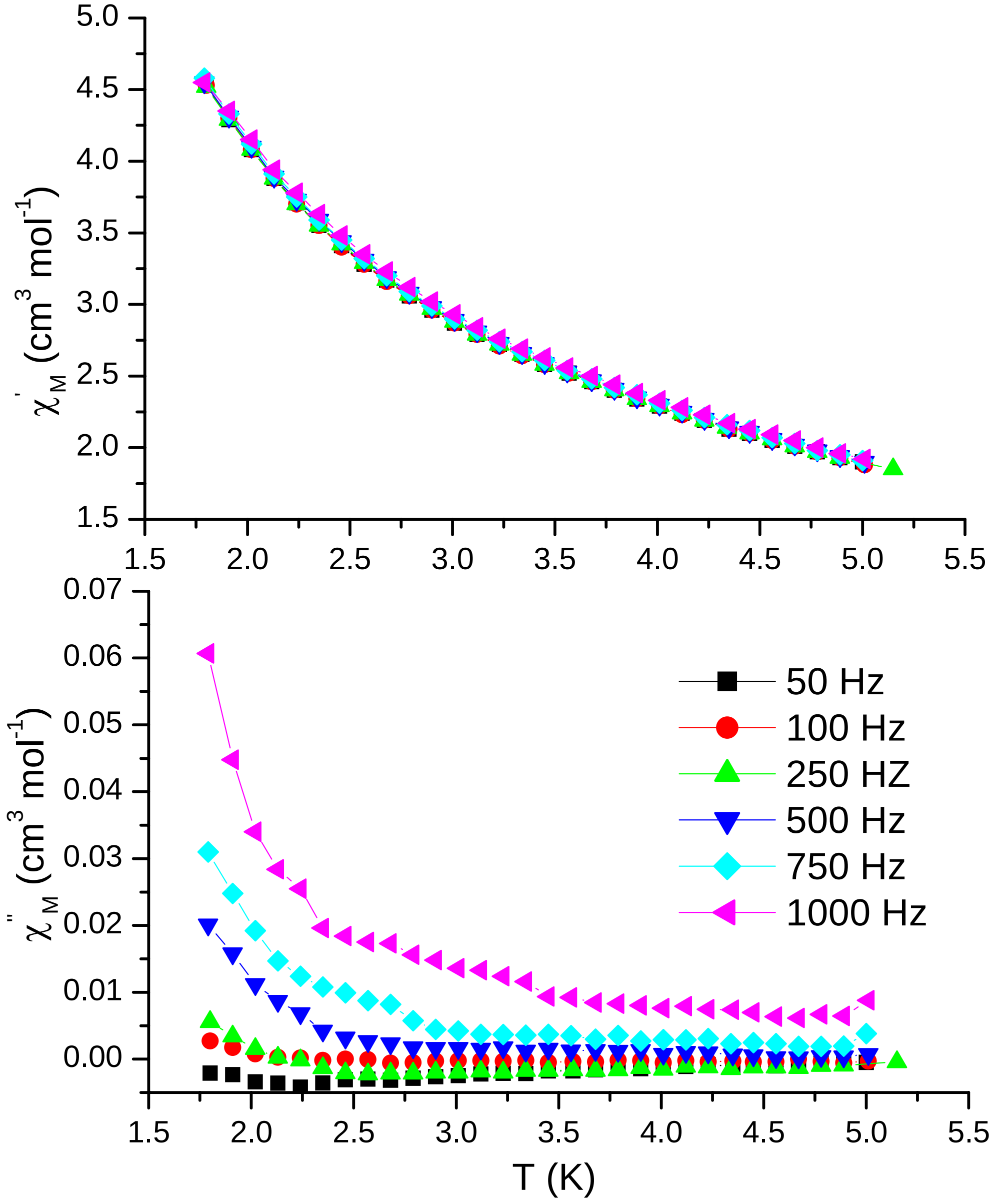

**Figure 26**. AC susceptibility plot of complex **4** $[Ni(hmp)(H_2O)Cl]_4 \cdot 4(C_4H_8O_2)$.

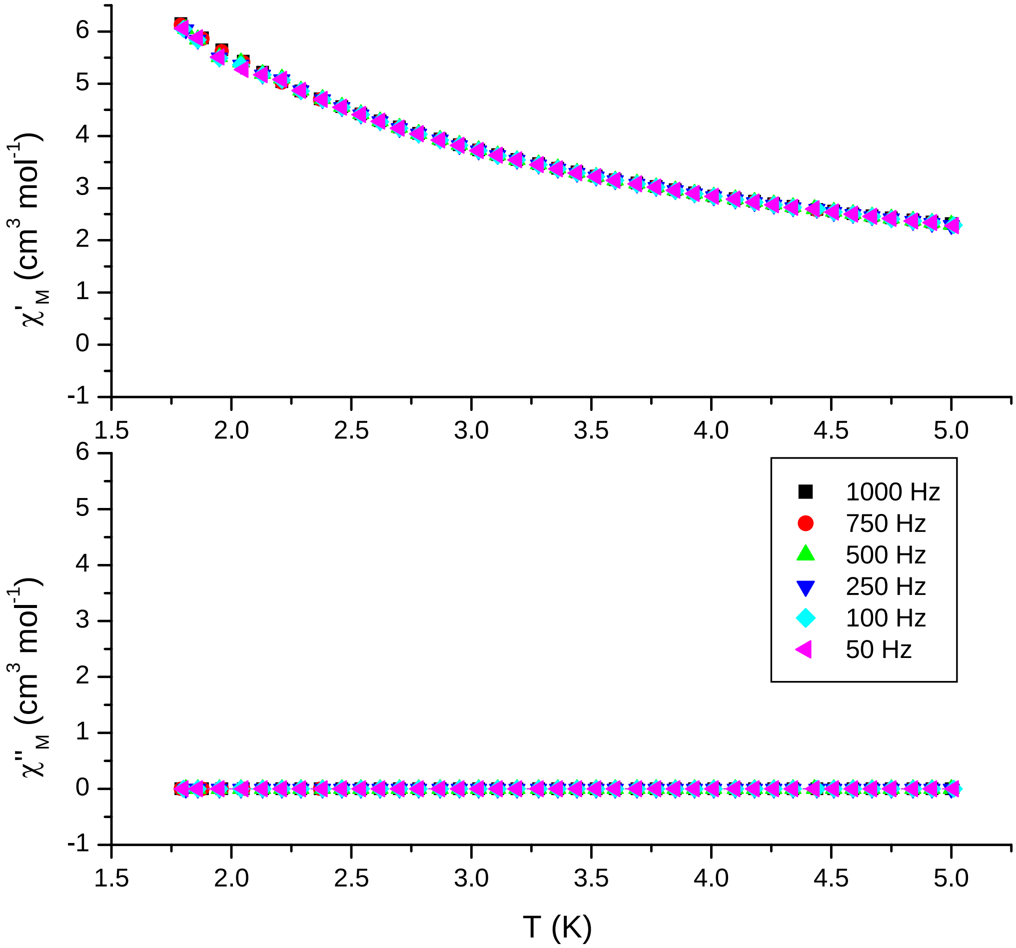

**Figure 27.** AC susceptibility plot of complex **5** [Ni(hmp)(benzylOH)Cl]$_4$.

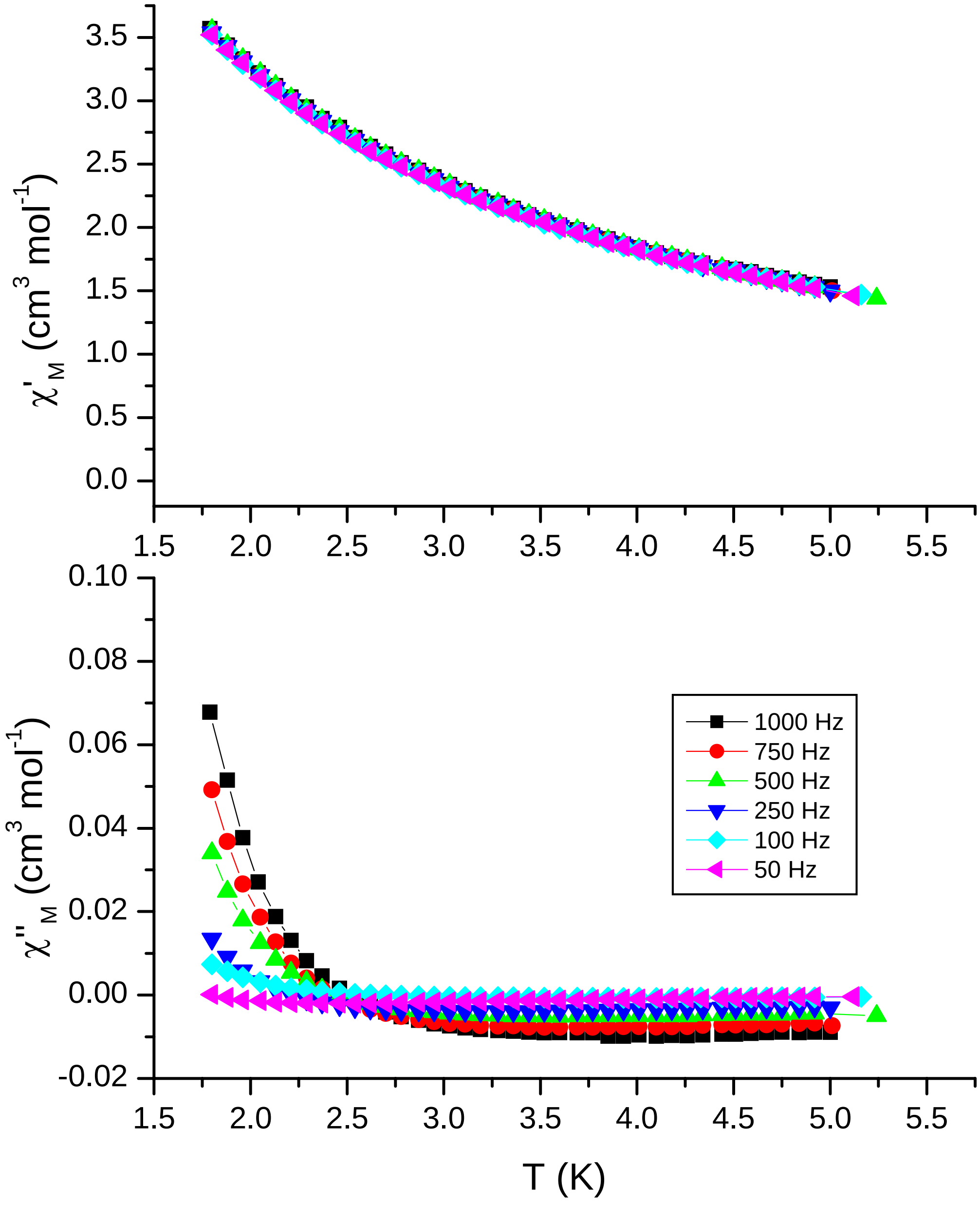

**Figure 28.** AC susceptibility plot of complex **6** [Ni(hmp)(TPMeOH)Cl]$_4$.

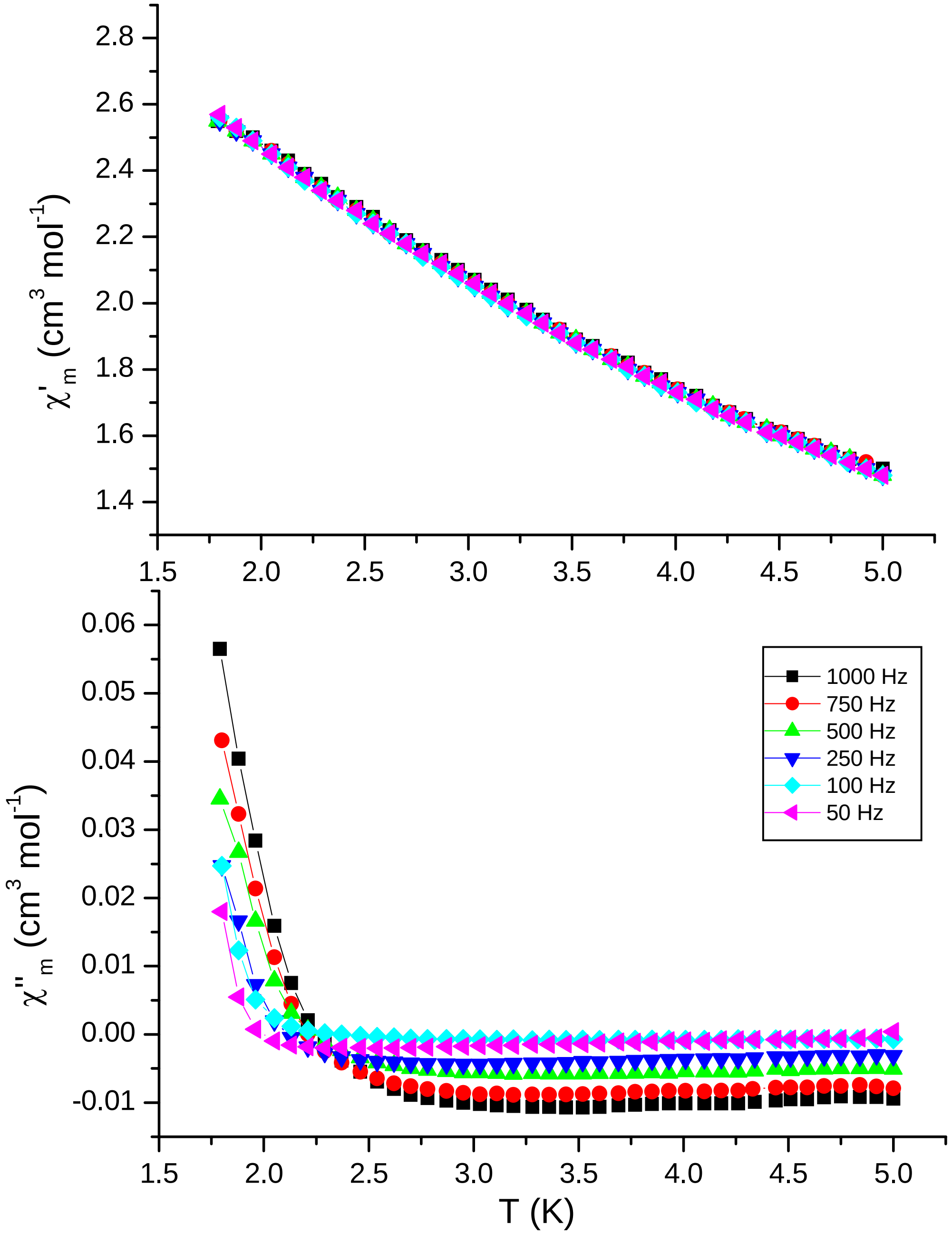

**Figure 29**. AC susceptibility plot of complex **7** [Ni(hmp)(MeSEtOH)Cl]$_4$.

## 2.4 Conclusion

This work provides the groundwork for the structural and magnetic characterization of several interesting classes of $Ni_4$ molecules. A series of 7 $Ni_4$ complexes with the general formula $[Ni(hmp)(ROH)Cl]_4$ where ROH is the modified alcohol group was synthesized. Their X-ray crystal structure was determined and magnetic properties characterized through DC susceptibility, reduced magnetization, and AC susceptibility.

There are problems with sample purity for complexes **1**, **2**, and **3**. Until that is resolved the results obtained from fitting are inaccurate as they represent the mixed bulk sample.

Complex **4** and **5** may be good candidates for HFEPR analysis. They present a significant level of insulation and are unique in that there is insulating solvent or aromatic alcohols attached. An initial study of these compounds is presented but to observe quantum effects and determine their origins will require additional research. Low temperature AC susceptibility or specific heat measurements will be necessary to determine the magnetic ordering temperature to establish the degree of insulation. In addition, magnetization hysteresis measurements are necessary to examine the molecule for exchange bias and the level of exchange bias is also an indicator of molecular insulation.

It was found that the presence of sulfur atoms causes drastically different magnetic properties. $\chi_M T$ max is lower than other $Ni_4$ molecules reported as and there was difficulty in fitting their magnetic data. The sulfur atoms are disordered therefore the S-S distance cannot be established. The S-S pathway may offer a means for interactions between molecules though nonclassical hydrogen bonding and/or through space interactions. Further analyses of these compounds are necessary to observe QTM and to ascertain the origins of this anomalous magnetic behavior.

An attempt was made to chemical modify a $Ni_4$ complex through the propargyl alcohol ligand by utilizing click chemistry. The resulting product removes the alcohol ligand indicating that if chemical modification of fully complexed SMMs were to be successful, it would need to be carried out on a stronger coordinating ligand such as the chelating $hmp^-$.

## References

1. Wernsdorfer, W.; Sessoli, R., Quantum phase interference and parity effects in magnetic molecular clusters. *Science* **1999,** 284, (5411), 133-135.

2. Yang, E.-C.; Wernsdorfer, W.; Hill, S.; Edwards, R. S.; Nakano, M.; Maccagnano, S.; Zakharov, L. N.; Rheingold, A. L.; Christou, G.; Hendrickson, D. N., Exchange bias in Ni4 single-molecule magnets. *Polyhedron* **2003,** 22, (14-17), 1727-1733.

3. Wernsdorfer, W.; Aliaga-Alcalde, N. r.; Hendrickson, D. N.; Christou, G., Exchange-biased quantum tunnelling in a supramolecular dimer of single-molecule magnets. *Nature* **2002,** 416, (6879), 406.

4. del Barco, E.; Kent, A. D.; Hill, S.; North, J. M.; Dalal, N. S.; Rumberger, E. M.; Hendrickson, D. N.; Chakov, N.; Christou, G., Magnetic quantum tunneling in the single-molecule magnet Mn-12-acetate. *Journal of Low Temperature Physics* **2005,** 140, (1-2), 119-174.

5. Wernsdorfer, W.; Bhaduri, S.; Vinslava, A.; Christou, G., Landau-Zener tunneling in the presence of weak intermolecular interactions in a crystal of Mn-4 single-molecule magnets. *Physical Review B* **2005,** 72, (21).

6. Sessoli, R.; Gatteschi, D.; Caneschi, A.; Novak, M. A., Magnetic bistability in a metal-ion cluster. *Nature* **1993,** 365, (6442), 141-143.

7. Sessoli, R.; Tsai, H. L.; Schake, A. R.; Wang, S.; Vincent, J. B.; Folting, K.; Gatteschi, D.; Christou, G.; Hendrickson, D. N., High-spin molecules: $[Mn_{12}O_{12}(O_2CR)_{16}(H_2O)_4]$. *J. Am. Chem. Soc.* **1993,** 115, (5), 1804-1816.

8. Caneschi, A.; Gatteschi, D.; Sessoli, R.; Barra, A. L.; Brunel, L. C.; Guillot, M., Alternating-current susceptibiliy, high-field magnetization, and millimeter band EPR evidence for a ground S=10 state in $[Mn_{12}O_{12}(CH_3COO)_{16}(H_2O)_4]\cdot 2CH_3COOH\cdot 4H_2O$. *Journal of the American Chemical Society* **1991,** 113, (15), 5873-5874.

9. Yang, E. C.; Wernsdorfer, W.; Zakharov, L. N.; Karaki, Y.; Yamaguchi, A.; Isidro, R. M.; Lu, G. D.; Wilson, S. A.; Rheingold, A. L.; Ishimoto, H.; Hendrickson, D. N., Fast magnetization tunneling in tetranickel(II) single-molecule magnets. *Inorganic Chemistry* **2006,** 45, (2), 529-546.

10. Wilson, A.; Lawrence, J.; Yang, E. C.; Nakano, M.; Hendrickson, D. N.; Hill, S., Magnetization tunneling in high-symmetry single-molecule magnets: Limitations of the giant spin approximation. *Physical Review B* **2006,** 74, (14).

11. Edwards, R. S.; Maccagnano, S.; Yang, E. C.; Hill, S.; Wernsdorfer, W.; Hendrickson, D.; Christou, G., High-frequency electron paramagnetic resonance investigations of tetranuclear nickel-based single-molecule magnets. *Journal of Applied Physics* **2003,** 93, (10), 7807-7809.

12. Wilson, A.; Yang, E. C.; Hendrickson, D. N.; Hill, S., On the validity of the giant spin approximation and its application to single-molecule magnets. *Polyhedron* **2007,** 26, (9-11), 2065-2068.

13. Yang, E. C.; Kirman, C.; Lawrence, J.; Zakharov, L. N.; Rheingoid, A. L.; Hill, S.; Hendrickson, D. N., Single-molecule magnets: High-field electron paramagnetic resonance evaluation of the single-ion zero-field interaction in a (Zn3NiII)-Ni-II complex. *Inorganic Chemistry* **2005,** 44, (11), 3827-3836.

14. Carlin, R. L., *Magnetochemistry*. Springer-Verlag: New York, 1986.

15. Kolb, H. C.; Finn, M. G.; Sharpless, K. B., Click chemistry: Diverse chemical function from a few good reactions. *Angewandte Chemie-International Edition* **2001,** 40, (11), 2004-+.

16. Bredas, J. L.; Themans, B.; Fripiat, J. G.; Andre, J. M.; Chance, R. R., Highly conducting polyparaphenylene, polypyrrole, and polythiophene chains- An abinitio study of the geometry and electronic-structure modifications upon doping. *Physical Review B* **1984,** 29, (12), 6761-6773.

17. Roncali, J., Conjugated poly(thiophenes) - synthesis, functionalization, and applications. *Chemical Reviews* **1992,** 92, (4), 711-738.

18. Sirringhaus, H.; Brown, P. J.; Friend, R. H.; Nielsen, M. M.; Bechgaard, K.; Langeveld-Voss, B. M. W.; Spiering, A. J. H.; Janssen, R. A. J.; Meijer, E. W.; Herwig, P.; de Leeuw, D. M., Two-dimensional charge transport in self-organized, high-mobility conjugated polymers. *Nature* **1999,** 401, (6754), 685-688.

19. Aullon, G.; Bellamy, D.; Brammer, L.; Bruton, E. A.; Orpen, A. G., Metal-bound chlorine often accepts hydrogen bonds. *Chemical Communications* **1998**, (6), 653-654.

20. Coronado, E.; Forment-Aliaga, A.; Romero, F. M.; Corradini, V.; Biagi, R.; DeRenzi, V.; Gambardella, A.; delPennino, U., Isolated Mn12 Single-Molecule Magnets Grafted on Gold Surfaces via Electrostatic Interactions. *Inorg. Chem.* **2005,** 44, (22), 7693-7695.

# Chapter Three

# Self Assembled Monolayers of SMMs on Gold

## 3.1 Introduction

Single molecule magnets (SMMs) are nanoscale magnets where individual metal clusters behave as discrete magnets. They exhibit a high spin ground state and significant magnetoanisotropy which gives rise to a barrier to reversal of magnetic spin orientation.[1] SMMs have generated a lot of interest because of their unique quantum and magnetic phenomena. It has been proposed that SMMs can be used as q-bits in quantum computation devices and/or high density magnetic storage devices.[2, 3]

Many hurdles remain in developing these devices such as raising the blocking temperature, coherent tunneling, and information access.[4] Unlike traditional magnetic particles used in information technology, SMMs are crystalline materials. Development of SMM devices requires integration of SMMs into electronic circuitry. SMMs would need to parallel its macro scale counterpart and form ordered structures where information can be stored and accessed without data loss.

Work has been done on attaching the $Mn_{12}$ family of SMMs to gold substrates and break junctions.[5] Methylthiocarboxylate served as the ligand and the authors utilized the strong interaction of gold with sulfur to attach the SMM to the surface to create a self assembled monolayer (SAM).[6, 7] An alternative method involved attaching 11-mercaptoundecanoic acid to a gold surface followed by a ligand exchange of a carboxylate group on $[Mn_{12}O_{12}(O_2C^tBu)_{16}(H_2O)_4]$.[8] A non-sulfur based approach employed highly charged $Mn_{12}$ SMMs composed of the betaine ligand to electrostatically attach the SMM to a charged surface.[9]

While these techniques have worked, they all suffer from a weak interaction of the SMM with the gold. Electrostatic interactions are weaker when compared to a direct bond to the molecule. Methylthiocarboxylate is sterically hindered and the ease of exchange of the carboxylate group on $Mn_{12}$ is an indication of the weaker interactions. A strong direct interaction of the SMM is desired and a possible solution is to exploit coupling reactions. Thus, the goal is to find a means to attach a SMM to a gold surface such that there is an appreciable electronic interaction of the unpaired electrons of the SMM with the electrons in the band structure of gold. "Click Coupling" and Suzuki Coupling are well known techniques to link together azides to acetylenes and halides to boronic acids, respectively.[10, 11] If SMMs were synthesized with these functional groups present; these coupling reactions can be utilized to link the SMM to the surface.

An additional motivation for attaching SMMs to gold surfaces to is explore the Kondo effect. The Kondo effect is a phenomenon where there is a non-zero temperature in which resistivity reaches a minimum for conduction materials. It was originally expected that as a sample cooled, the resistivity of a conducting material will decrease indefinitely as lattice vibrations interfere less with electron transport. However, when a magnetic impurity is introduced to the conductor, it was found that the resistivity of the conductor approaches a minimum at a nonzero temperature due to the interaction of surface charge with the free electron in the magnetic material.[12] The attachment of SMMs to a conducting surface like gold could possibly allow the observation of the Kondo effect. This remains a goal of materials researchers as advances in the understanding of the Kondo effect provides insight into how localized electrons interact with delocalized electrons. This central problem in solid state physics can potentially yield answers regarding electron conduction[13] and superconductivity.[14]

While in previously published work SMMs were attached to planar gold surfaces, other gold surfaces could be employed.. The same coupling strategies can be utilized to couple SMMs to other geometries like spherical nanoparticles. It has been shown that functionalization of gold nanoparticles (AuNP) can be achieved with a variety of organic capping agents. The surface functional groups can be utilized in additional chemical modification and it has been shown that molecules such as the drug Taxol have been successfully attached to AuNP coated with 4-mercaptophenol.[15]

An analogous system will be explored using AuNP coated with 4-mercaptophenylboronic acid to utilize Suzuki coupling. SMMs attached to AuNP will be a novel system to explore the long range interactions between SMMs mediated through a conducting material. An additional benefit is that this system makes it possible to measure the magnetic characteristics of gold coupled to SMMs. Currently no instrument exists which has the sensitivity to measure the magnetic moment of a SMM monolayer on a gold surface. The AuNPs can be prepared as a bulk sample and measured using traditional techniques.

A series of molecules which can be utilized in coupling reactions was explored. Their magnetic and physical properties were characterized to verify that these molecules are SMMs. Attempts were then made to attach these molecules to a planar gold surface and to AuNP.

## 3.2 Experimental

### Synthesis

All manipulations were carried out under aerobic conditions. Regents were purchased from Sigma Aldrich and used without further purification. The POPD-1 catalyst used for Suzuki coupling was purchased from CombiPhos.

Gold substrates were purchased from Arrandee. Their dimensions are 11 mm x 11 mm and have a 250 ± 50 nm thick layer of gold. They are composed of a borosilicate glass support and layered with Cr to assist in adhering Au(111) to the surface. The gold substrate was annealed with 20 passes through a hydrogen flame prior to use. The gold substrate was soaked in a solution of 4-mercaptophenylboronic acid for 24 hrs to generate a monolayer and was verified by surface FT-IR measurements.

4-chloro-2-hydroxymethylpyridine was synthesized by Casey Stephenson in the Hendrickson group. Details of its preparation will be described in a publication in the works.

**4-azidobenzoic acid- CAUTION-** $NaN_3$ is extremely dangerous and needs to be handled with care. It is highly toxic and potentially explosive. Although no problems were encountered in its used, the literature prep which this work is based on has reported to give explosions.

$TfN_3$ was first prepared using a procedure developed by Liu and Tor.[16] 4-aminobenzoic acid (0.41g 3mmol) was dissolved in 2 mL of $CH_2Cl_2$ to which $Et_3N$ (0.91g, 9mmol) and $CuSO_4$ (0.024g, 0.15mmol, in 0.5mL $H_2O$) were added. $TfN_3$ was then added to the reaction and brought to homogeneity with MeOH (ca. 2 mL). The reaction was mixed for 3 hrs whereupon the solution turns from black to dark green.

Next, 40 mL of a 1:1 mixture of $CH_2Cl_2$:HCl (1 M) was added to the reaction which resulted in a suspension. An additional 30 mL of $CH_2Cl_2$ was added to the flask to dissolve the precipitate. The mixture was washed with brine and the organic phase was recovered. Silica gel column chromatography (1g prod:20g silica gel) eluted with a 1:9 mixture of MeOH/$CH_2Cl_2$ was used to purify the compound. Progress was monitored by TLC and the pure product was verified by NMR and FT-IR.

[Ni(hmp-Cl)(MeOH)Cl]$_4$ •1/3MeOH **(1** • 1/3MeOH**)** - The procedure was adapted from Yang, et al.[17] $NiCl_2$ (1 mmol, 0.237g) was combined with 4-chloro-2-hydroxymethylpyridine (1 mmol, 0.133g) in 30 mL of methanol. Sodium methoxide (1mmol, 0.54g) was dissolved in 10 mL of methanol and added slowly to the reaction. The reaction was refluxed for 20 minutes, filtered, and allowed to crystallize in a sealed flask. Dark green crystal formed after 24 hours. Select IR peaks 3400 $cm^{-1}$(s), 1595 $cm^{-1}$(s), 1471 $cm^{-1}$(w), and 1070 $cm^{-1}$(m). Elemental Analysis calculated: 31.35 %C 3.47 %H 5.16 %N experimental: 31.48 %C 2.78 %H 4.98 %N.

[$Mn^{II}_2Mn^{III}_2$(mdea)$_2$(Hmdea)$_2$($O_2$CPhBr)$_2$$Cl_2$] • $Et_2O$ **(2** • $Et_2O$**)**– $MnCl_2$ (1 mmol, 0.197g), 4-bromobenzoic acid (1 mmol, 0.201g), and methyldiethanol amine (mdea) (2 mmol, 0.228 mL) were dissolved in 60 mL of a 2:1 mixture of $CH_2Cl_2$/MeOH. Triethylamine (0.5 mmol, 0.0505g, 0.07 mL) was slowly added to the solution as a base. The mixture was stirred for 30 minutes. Brown rod-like crystals were obtained from $Et_2O$ diffusion after 2 weeks. Select IR peaks 3363 $cm^{-1}$(m), 2849 $cm^{-1}$(m), 1616 $cm^{-1}$(s), 1345 $cm^{-1}$(s), 1095 $cm^{-1}$(s), and 911 $cm^{-1}$(m). Elemental Analysis calculated: 38.52 %C 5.70 %H 4.28 %N experimental: 35.31 %C 3.54 %H 3.34 %N.

$[Mn^{II}_2Mn^{III}_2(mdea)_2(Hmdea)_2(O_2CPhN_3)_4]$ **(3)-** $MnCl_2$ (1 mmol, 0.197g), 4-azidobenzoic acid (1 mmol, 0.163g), and methyldiethanol amine (2 mmol, 0.228 mL) were dissolved in 40 mL of a 2:1 mixture of $CH_2Cl_2$/MeOH. Triethylamine (0.5 mmol, 0.0505g, 0.07 mL) was slowly added to the solution as a base. The solution was stirred for 30 minutes. Brown rod-like crystals were obtained from $Et_2O$ diffusion after 2 weeks. Select IR peaks 3356 $cm^{-1}$(m), 2850 $cm^{-1}$ (m), 2120 $cm^{-1}$(s), 1601 $cm^{-1}$(s), 1366 $cm^{-1}$(s), and 1096 $cm^{-1}$(m). Elemental Analysis calculated: 43.06 %C 4.67 %H 16.74 %N experimental: 40.06 %C 4.39 %H 14.66 %N.

**AuNP-B(OH)$_2$-** The gold nanoparticles were synthesized adopting a strategy developed by Brust et al.[18] $HAuCl_4 \cdot 3H_2O$ (0.150g, 0.38 mmol) and 4-mercaptoboronic acid (0.139g, 0.9mmol) was dissolved in 75 mL of MeOH with ~1 mL acetic acid to prevent deprotonation. A 15 mL aqueous solution of 0.4 mol/dm$^3$ of $NaBH_4$ (0.227g) was added to added drop wise to the gold solution under vigorous stirring. Stirring was stopped after 30 min whereupon the solvent was removed under reduced pressure. The residue was washed with $Et_2O$ 3 x 25 mL. The $Et_2O$ was removed under reduced pressure and the nanoparticles were then washed with $H_2O$. The AuNP were filtered and then dissolved with EtOH to remove AuNP adhered to the glassware. The solvent was removed under reduced pressure to yield the final product. Elemental Analysis experimental: 33.74 %C 6.74 %H 6.35 %S.

Suzuki Coupling of **1** to gold substrate was carried out on the gold substrate functionalized with 4-mercaptophenylboronic acid. Approximately 10 mg of compound **1** was dissolved in dry THF with ca. 2 mg of $Pd(PPh_3)4$ and ca. 2 mg of $NH_4F$. The gold substrate was allowed to soak in the solution for 24 hours.

Suzuki Coupling of **1** to AuNP-$B(OH)_2$ was carried out by dissolving 100 mg of AuNP-$B(OH)_2$ and 110 mg of compound **1** in 15 mL of 2:1 mixture of dry THF:DMF. An additional 5 mL of EtOH was added to bring the solution into homogeneity. Approximately 2 mg of POPD-1 was added as the catalyst along with 0.035 g of $K_2CO_3$. The solution was allowed to stir for 24 hours after which the solvent was removed upon reduced pressure. The black powder was washed with THF and dried.

### X-ray Crystallography

Diffraction data was collected at 100 K using a Bruker Smart Apex CCD diffractometer. The data were integrated using the Bruker SAINT software and SADABS was employed to correct for absorption differences. The structures were solved using direct methods (SIR-2004 for **1** and SHELXS-97 for **2,3**), developed by successive difference Fourier syntheses, and refined by full matrix least-squares on all $F^2$ data. The non-hydrogen atoms were refined anisotropically and the hydrogen atoms were idealized based on 1.2-1.5 times the equivalent isotropic U values for the C atoms to which they were bound.

A disordered solvent molecule in **1** was treated by the PLATON program SQUEEZE, the details of which can be found in the cif. The electron density accounted for 1 methanol solvate molecules per 3 $Ni_4$ cubanes in the unit cell in compound **1**. The $Et_2O$ solvate molecule in complex **2** is ordered and was refined anisotropically.

Compound **1** **[Ni(hmp-Cl)(MeOH)Cl]$_4$** •1/3MeOH crystallized as a twinned crystal and was refined to a final BASF parameter of 0.43991. In complex **2** and **3,** the mdea ligands were disordered. It was modeled with a Part instruction in both cases. For compound **2,** it was assigned twp parts (Part 1 = C14, C16, C17; Part 2 = C14A, C16A, C17A) and was refined to 88% occupancy of Part 1 vs. Part 2. For compound **3,** the ligand was assigned two parts (Part 1 = C16A, C18A, C19A; Part 2 = C16, C18, C19) and was refined to 20% occupancy of Part 1 vs. Part 2.

## Magnetic Studies

DC magnetic susceptibility data were collected on ground microcrystalline samples locked in eicosane to prevent torquing of the sample in the magnetic field. A Quantum Design MPMS-5 SQUID magnetometer equipped with a 5.5 T magnet was used to analyze the samples. The experiments were done between 300-1.8 K and with fields ranging from 0.1-50 kG. Magnetic susceptibility data were corrected for the sample holder, sample rod, and eicosane. A diamagnetic correction was applied to the observed magnetic susceptibilities using Pascal's constants.[19]

DC magnetic susceptibility measurements for AuNP-$B(OH)_2$ and the AuNP-$Ni_4$ after Suzuki Coupling were measured at 5 T due to the small moment of sample used. For comparison, complex **1** was also measured at 5 T. For both nanoparticles measurements, no eicosane was used as there is no preferred directionality in their magnetic moment.

AC magnetic susceptibility data were collected with a 3 G AC field from 10-997Hz. No DC field was applied and the experiments were done from 1-5 K using a Quantum Design MPMS-2 SQUID magnetometer equipped with a 3 T magnet.

## Other Physical Measurements

IR spectra were collected samples on powder samples locked in a KBr pellet on a Thermo-Nicolet Avatar 360 spectrometer.

PM-IRRAS surface infrared spectra was colleted using a Bruker Equinox 55 infrared spectrometer with a PMA 37 photoelastic modulator (PEM) fitted with a nitrogen cooled MCT detector and a resolution of 4 $cm^{-1}$. The experiments were carried out with the PEM set to 2000 $cm^{-1}$ and the detector set at an angle of $45^o$. The sample orientation was optimized by rotating the sample stage such that the detector signal was maximized.

Elemental analysis data were collected by Numega Resonance Laboratories (San Diego, CA). TEM measurements were done by Dr. Steve Barlow at the Electron Microscope Facility of San Diego State University using a FEI Tecnai 12 Transmission Electron Microscope set to 120 kV. XPS experiments were conducted by Dr. Tom Mates at the University of California, Santa Barbara using a Kratos Axis Ultra XPS system.

## 3.3 Results and discussion

### Description of Structure

Complex **1** is structurally analogous to the $[Ni(hmp)(MeOH)Cl]_4$ previously published.[20] An ORTEP can be seen in Figure 1. The core of each complex is 4 $Ni^{2+}$ ions occupying alternating positions of a distorted cube with $\mu_3$-oxo atoms occupying the remaining 4 vertices. Each octahedral $Ni^{2+}$ ions is coordinated by 3 $\mu_3$-oxo atoms originating from the deprotonated arms of the $hmp^-$-Cl ligands, a nitrogen atom from $hmp^-$-Cl, a $Cl^-$ ion, and the oxygen from the propargyl alcohol. There are 3 symmetry independent molecular orientations in the unit cell unlike $[Ni(hmp)(MeOH)Cl]_4$ which has a 2 orientations. The addition of Cl to hmp reduces the ability of the molecule to pack efficiently with few molecular orientations because of the high electron density of Cl on

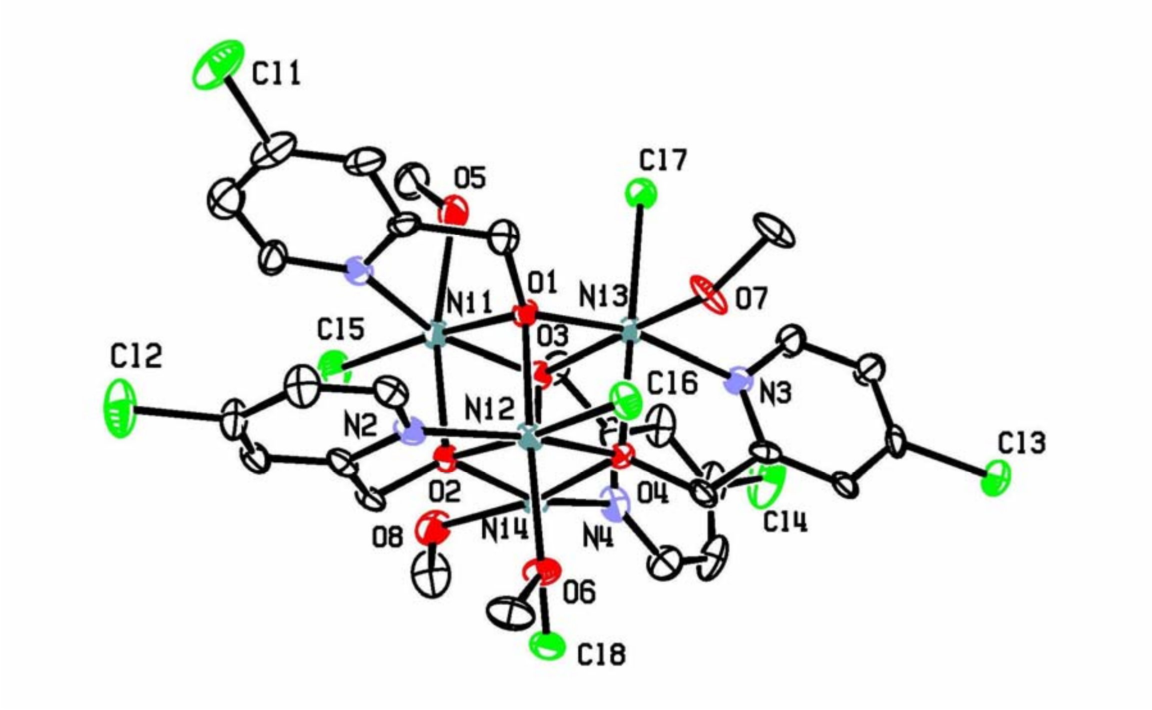

**Figure 1.** ORTEP of **[**Ni(hmp-Cl)(MeOH)Cl]$_4$ • 1/3MeOH (**1** • 1/3MeOH) with thermal ellipsoids at the 30% probability level. Hydrogen and solvate atoms omitted for clarity.

the periphery of the molecule The chlorination of the hmp reduces the crystal symmetry of $[Ni(hmp)(MeOH)Cl]_4$ with space group I-42d to the much lower symmetry space group of P-1. The molecule symmetry is unaffected and the point group of **1** is $S_4$.

The asymmetric unit of compound **2** (Figure 2) consists of half the cluster, the 4-bromobenzoate ion, and the $Et_2O$ solvate molecule. An ORTEP of complex **2** can be seen in Figure 2. Its cores consist of 2 $Mn^{II}$ and 2 $Mn^{III}_2$ ions bridged by 6 $\mu_3$-oxo ligands from the mdea ligands. Assignment of Mn oxidation states was made through examination of Jahn-Teller distortion. The Jahn-Teller distortion resides on Mn(1) and can be seen on the O(4)-Mn(1)-N(1) axis. The two bonds lengths, Mn(1)-O(4) 2.22 Å and Mn(1)-N(1) 2.25 Å, are distinctly longer than the other bond lengths ranging between 1.86-1.97 Å. Therefore, Mn(1) is $Mn^{3+}$ and Mn(2) is $Mn^{2+}$. Mn(2) displays a longer Mn-ligand average bond distance of 2.41 Å when compared to the average Mn(1)-ligand bond distance of 2.01 Å. There is a $Cl^-$ ion coordinated to Mn(2) that participates in hydrogen bonding to O(6) of the neighboring molecule at a distance of 3.13 Å. Two types of mdea ligands are present in the complex. Type A coordinates N(1)-Mn(1) with a bond distance of 2.25 Å and is composed of O(3) and O(4). Type B mdea coordinates N(2)-Mn(2) with a bond distance of 2.42 Å and is composed of O(5) and O(6). One arm of type B mdea is protonated and coordinates O(6)-Mn(2) with a bond distance of 2.28 Å. The uncoordinated arm of the 4-bromobenzoate forms a hydrogen bond with O(2)···O(6) 2.83 Å and O(2)···O(3) 2.85 Å.

The asymmetric unit of complex **3** (Figure 3) encompasses half the cluster with the 4-azidobenzoate ion. An ORTEP can be seen in Figure 3. The core for complex **3** is structurally similar to complex **2**. There are no $Cl^-$ ions in this case but instead there are 4

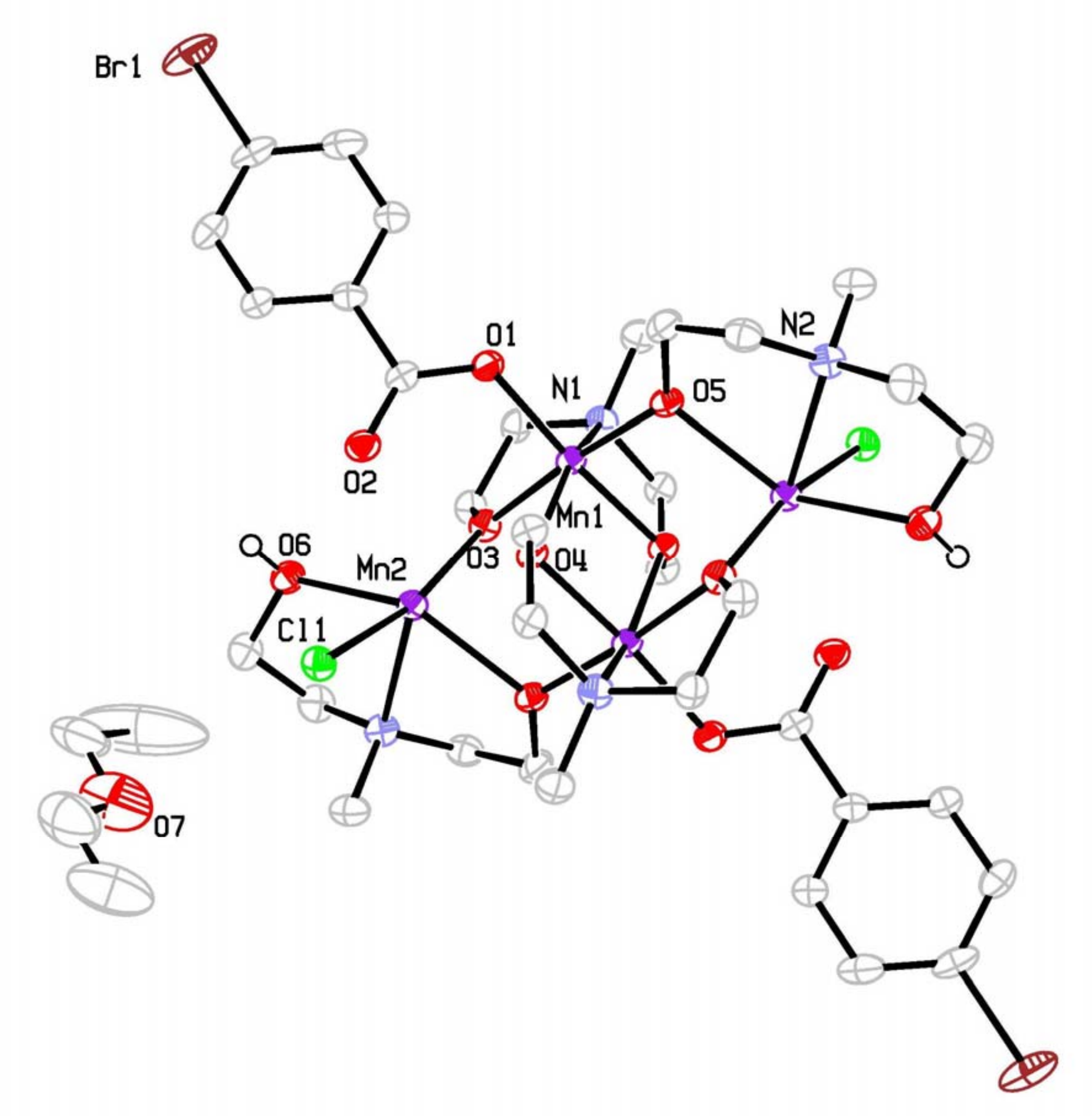

**Figure 2.** ORTEP of [$\mathrm{Mn^{II}_2Mn^{III}_2(mdea)_2(Hmdea)_2(O_2CPhBr)_2Cl_2}$] • $\mathrm{Et_2O}$ (**2** • $\mathrm{Et_2O}$) with thermal ellipsoids at the 30% probability level. Hydrogen atoms omitted for clarity.

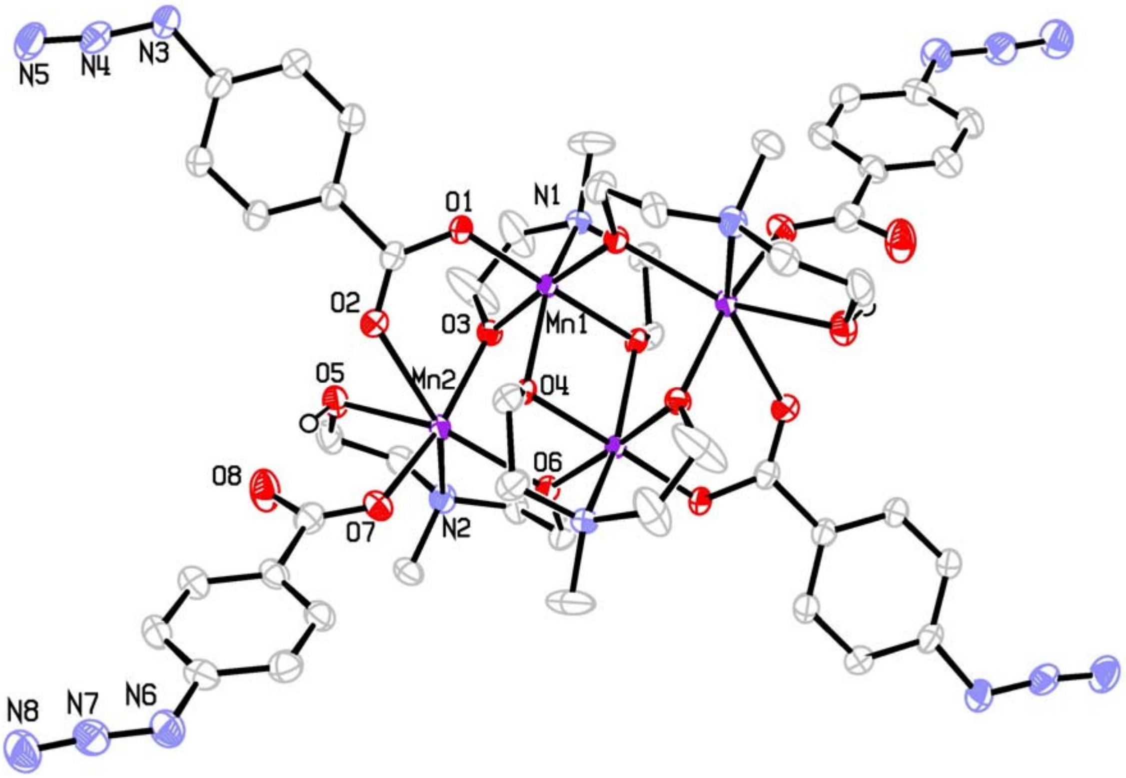

**Figure 3.** ORTEP of [$Mn^{II}_2Mn^{III}_2(mdea)_2(Hmdea)_2(O_2CPhN_3)_4$] (3) with thermal ellipsoids at the 30% probability level. Hydrogen atoms omitted for clarity.

4-azidobenzoate ligands. The uncoordinated arm of the 4-azidobenzoate ligands bound to Mn(2) is hydrogen bonded to the mdea ligand O(2)···O(6) at a distance of 2.59 Å. The 4-azidobenzoate ligand bound to Mn(1) is hydrogen bound to 3 different mdea ligands at distances O(3)···O(6) 2.93Å, O(3)···O(7) 2.89 Å, and O(3)···O(8) 2.96 Å. The azide group on 4-azidobenzoate participates in hydrogen bonding with the azide group of the 4-azidobenzoate group on the adjacent molecule N(1)···N(5). A summary of complexes **1-3** crystal data and refinement parameters can be found in Table 1.

### DC Susceptibility Measurements

Powdered samples of complexes **1-3** were locked in eicosane and were measured using a 1T DC field between 300-1.8 K.. The $\chi_M$T versus temperature plot for complex **1** is shown in Figure 4. $\chi_M$T was measured as 5.4 cm$^3$ mol$^{-1}$ K at 300 K and increases to a maximum of 10.1 cm$^3$ mol$^{-1}$ K at 12 K. These values are comparable to the values determined for [Ni(hmp)(MeOH)Cl]$_4$ of ~4.9 cm$^3$ mol$^{-1}$ K at 300 K and the maximum of 10.4 cm$^3$ mol$^{-1}$ K at 12 K.[20] The decrease below 12 K is likely due to Zeeman effects.

Figure 4 for complex **1** suggests that there is ferromagnetic coupling between the four S=1 Ni$^{2+}$ ions which would suggest a S=4 ground state. Modeling of the $\chi_M$T is necessary to definitively establish the spin ground state and to ascertain the strength of the coupling between the molecules. Complex **1** was analyzed in a manner similar to [Ni(hmp)(MeOH)Cl]$_4$. To account for the S$_4$ symmetry of the molecule, 2 coupling parameters were used to model the molecule. The spin Hamiltonian takes the form:

$$\hat{H} = -2J_a(\hat{S}_1 \bullet \hat{S}_2 + \hat{S}_3 \bullet \hat{S}_4) - 2J_b(\hat{S}_1 \bullet \hat{S}_3 + \hat{S}_1 \bullet \hat{S}_4 + \hat{S}_2 \bullet \hat{S}_3 + \hat{S}_2 \bullet \hat{S}_4) \qquad (3.1)$$

**Table 1.** Crystal Data and Structure Refinement Parameters for Complexes **1-3**

| | **1** | **2** | **3** |
|---|---|---|---|
| Empirical formula | C85 H112 Cl24 N12 Ni12 O25 | C42 H74 Br2 Cl2 Mn4 N4 O14 | C48 H62 Mn4 N16 O16 |
| Formula weight | 3257.19 | 1309.53 | 1338.90 |
| Temperature | 100(2) K | 100(2) K | 100(2) K |
| Wavelength | 0.71073 Å | 0.71073 Å | 0.71073 Å |
| Crystal system | Triclinic | Triclinic | Triclinic |
| Space group | P-1 | P-1 | P-1 |
| Unit cell dimensions | a = 15.658(4) Å | a = 10.6339(15) Å | a = 8.3438(9) Å |
| | b = 16.904(4) Å | b = 10.7073(15) Å | b = 12.1002(13) Å |
| | c = 24.772(6) Å | c = 13.0743(19) Å | c = 14.4143(15) Å |
| | α= 94.682(4)°. | α= 82.162(2)°. | α= 91.6940(10)°. |
| | β= 106.565(3)°. | β= 80.964(2)°. | β= 98.5420(10)°. |
| | γ = 90.281(4)°. | γ = 65.871(2)°. | γ = 99.6730(10)°. |
| Volume | 6261(3) Å$^3$ | 1337.4(3) Å$^3$ | 1416.5(3) Å$^3$ |
| Z | 2 | 1 | 1 |
| Density (calculated) | 1.728 g/cm$^3$ | 1.626 g/cm$^3$ | 1.570 g/cm$^3$ |
| Absorption coefficient | 2.339 mm$^{-1}$ | 2.580 mm$^{-1}$ | 0.953 mm$^{-1}$ |
| F(000) | 3300 | 670 | 690 |
| Crystal color/habit | green plate | brown rod | brown needle |
| θ range for data collection | 1.36 to 28.37°. | 1.58 to 28.13°. | 1.43 to 28.38°. |
| Reflections collected | 62910 | 33187 | 16084 |
| Independent reflections | 62910 [R(int) = 0.0000] | 6074 [R(int) = 0.0581] | 6362 [R(int) = 0.0471] |
| Completeness to θ = 25.00° | 96.1 % | 100.0 % | 98.0 % |
| Data / restraints / parameters | 62910 / 0 / 1440 | 6074 / 0 / 336 | 6362 / 0 / 411 |
| Goodness-of-fit on F2 | 1.013 | 1.040 | 1.057 |
| Final R indices [I>2sigma(I)] | R1 = 0.0686, wR2 = 0.1395 | R1 = 0.0488, wR2 = 0.1025 | R1 = 0.0476, wR2 = 0.1089 |
| R indices (all data) | R1 = 0.1251, wR2 = 0.1690 | R1 = 0.0709, wR2 = 0.1111 | R1 = 0.0623, wR2 = 0.1173 |
| Largest diff. peak and hole | 1.502 and -0.900 e.Å$^{-3}$ | 1.626 and -0.885 e.Å$^{-3}$ | 0.641 and -0.538 e.Å$^{-3}$ |

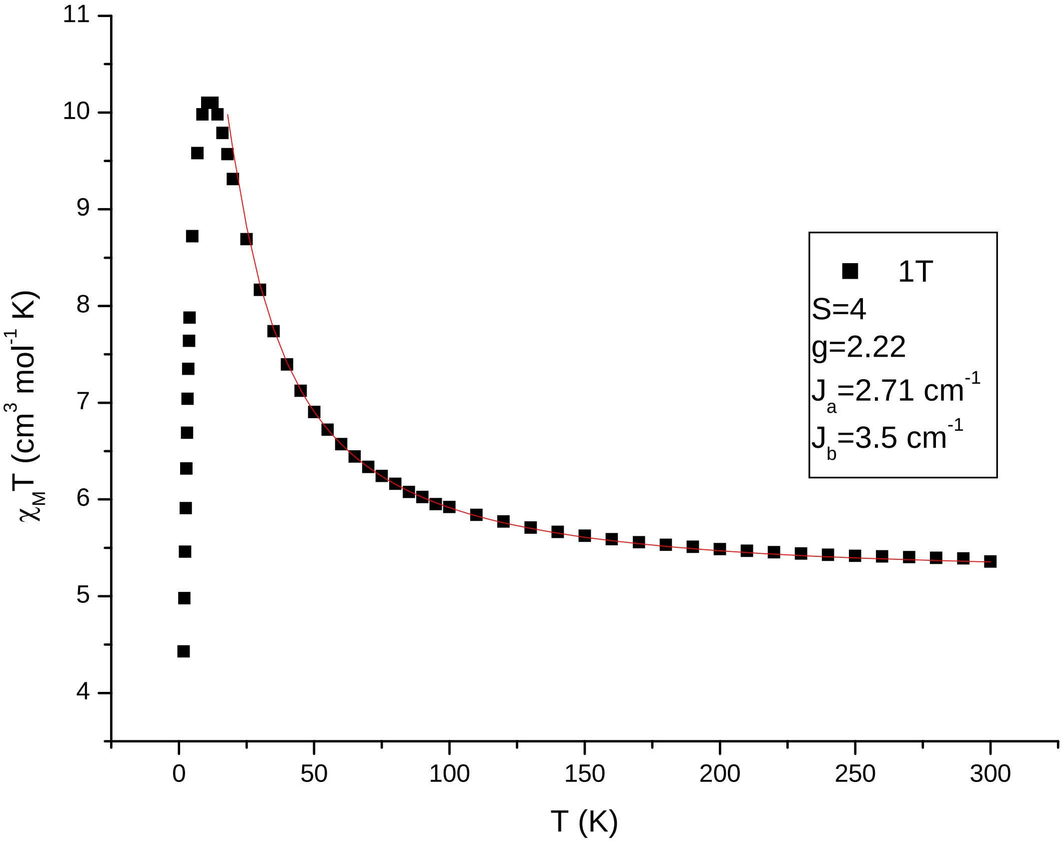

**Figure 4.** Magnetic susceptibility of $[Ni(hmp\text{-}Cl)(MeOH)Cl]_4 \cdot 1/3MeOH$ (**1**•1/3MeOH**).** Fit shown in red.

The spin Hamiltonian can be simplified by utilizing Kambe vector coupling such that $S_A = S_1 + S_2$, $S_B = S_3 + S_4$, and $S_T = S_A + S_B$. Using these definitions, the energy of the 19 spin states can be expressed as:

$$\begin{aligned} E(S_T, S_A, S_B) = -J_A[S_A(S_A+1) + S_B(S_B+1)] \\ - J_2[S_T(S_T+1) - S_A(S_A+1) - S_B)(S_B+1)] \end{aligned} \quad (3.2)$$

The energies can be substituted into the Van Vleck equation to fit the $\chi_M$T results. The fit is shown as the solid red line and the experimental data as the black points in Figure 4. The temperature independent paramagnetism (TIP) contribution to magnetic susceptibility for 4 $Ni^{2+}$ was taken into account for the fit and is fixed at 400 x $10^{-6}$ $cm^3$ $mol^{-1}$. The fit yielded g=2.22 which is on the higher end for a $Ni_4$ complex. The optimized magnetic exchange parameters are $J_a$=2.7 $cm^{-1}$ and $J_b$= 3.5 $cm^{-1}$. The g value is higher than the g=2.02 found for $[Ni(hmp)(MeOH)Cl]_4$ and the coupling constants are lower than the fitted values of $J_a$=9.2 $cm^{-1}$ and $J_b$=2.8 $cm^{-1}$.[20] Like the $Ni_4$-MeOH complex, complex **1** was also fitted to a S=4 ground state.

A different model from complex **1** was employed to fit the $\chi_M$T of complexes **2** and **3**. A model was adapted from a previously published approach used to analyze analogous molecules.[22] Figure 5 depicts the coupling scheme used in this model. A 2 J values model is use for complexes **2** and **3**. The $Mn^{III}(1)$ ions in the center of the molecule are labeled $S_1$ and $S_3$. The spins are symmetry equivalent and the interaction $J_{13}$ and $J_{31}$ are approximated to be equivalent. These two interactions are now assign the parameter $J_{bb}$. The interactions between $Mn^{III}(1)$ and $Mn^{II}(2)$ in the wings of the molecule ($J_{12}$, $J_{21}$, $J_{14}$, $J_{41}$, $J_{23}$, $J_{32}$, $J_{34}$, and $J_{43}$) are also approximated to be equivalent and the parameter $J_{wb}$ is used to account for all of the wing-body interactions. Interactions

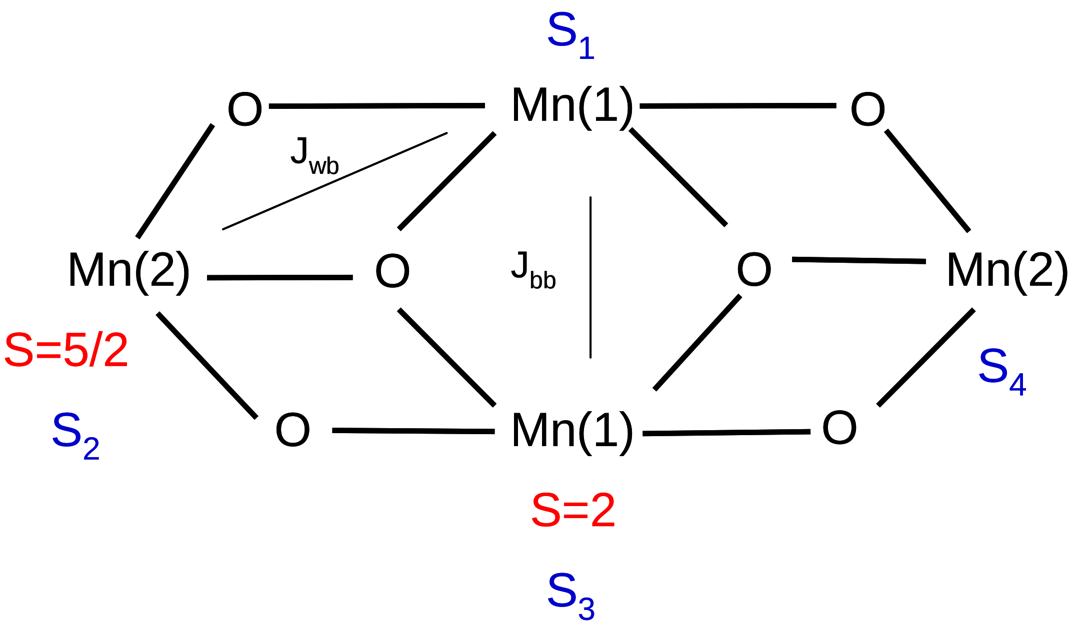

**Figure 5.** Diagram showing the definition of atom number and magnetic exchange parameters for complex **2** and **3**.

between $Mn^{II}(2)$ and $Mn^{II}(2)$ on the opposite ends of the molecule are negligible due to the long pathway necessary for exchange. This enables the use of Kambe vector coupling to express the spin Hamiltonian:

$$\hat{H} = -J_{wb}(\hat{S}_T^2 - \hat{S}_A^2 - \hat{S}_B^2) - J_{bb}(\hat{S}_A^2 - \hat{S}_1^2 - \hat{S}_3^2) \tag{3.3}$$

where $\hat{S}_A = \hat{S}_1 + \hat{S}_3, \hat{S}_B = \hat{S}_2 + \hat{S}_4$, and $\hat{S}_T = \hat{S}_A + \hat{S}_B$. The corresponding eigenvalue expression can be expressed as:

$$E(S_T) = -J_{wb}[S_T(S_T+1) - S_A(S_A+1) - S_B(S_B+1)] - J_{bb}[S_A(S_A+1)] \tag{3.4}$$

There are a 110 possible spin states to account for the total spin of the complex ranging from 0 to 9 with the two S = 2 and two S = 5/2 interacting spins in $Mn_4$.

The eigenvalue expression and Van Vleck equation were used to obtain a least squares fit to experimental $\chi_M T$ data. The plots of $\chi_M T$ versus temperature for the fitted and experimental data of complex **2** and **3** are shown in Figures 6 and 7, respectively.

The optimized parameters for complex **2** are S=9, g=1.62, $J_{bb}$=3.16 $cm^{-1}$, and $J_{wb}$=0.26 $cm^{-1}$. The optimized parameters for complex **3** are S=9, g=1.91, $J_{bb}$=0.65 $cm^{-1}$, and $J_{wb}$=4.23 $cm^{-1}$. The J parameters fall within range of other $Mn_4$ complexesof a similar architecture. The positive J values indicate that there is ferromagnetic coupling between all 4 Mn ions. Magnetic exchange between the two $Mn^{III}$ ions is the predominate magnetic exchange as the J value between $Mn^{II}$ and $Mn^{III}$ is small in both cases. The g value for complex **3** is similar to other $Mn_4$ complexes but the g value for complex **2** is significantly lower than the g≈1.9 reported for similar complexes. It is possible that poor separation of the ground state from excited states is a cause of this problem. Fitting of the $\chi_M T$ data resulted in a energy separation of ~5 $cm^{-1}$ between the S=9 ground state and the

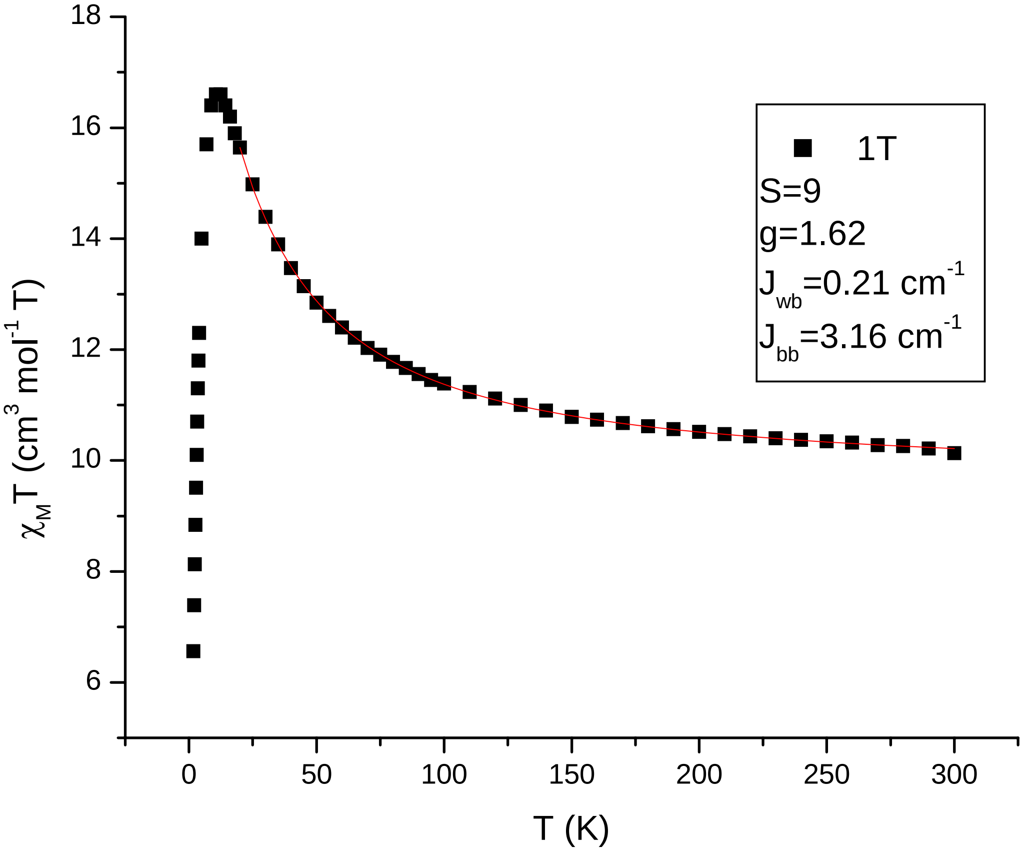

**Figure 6.** Magnetic susceptibility of $[Mn^{II}_2Mn^{III}_2(mdea)_2(Hmdea)_2(O_2CPhBr)_2Cl_2] \bullet Et_2O$ (**2** • $Et_2O$). Fit shown in red.

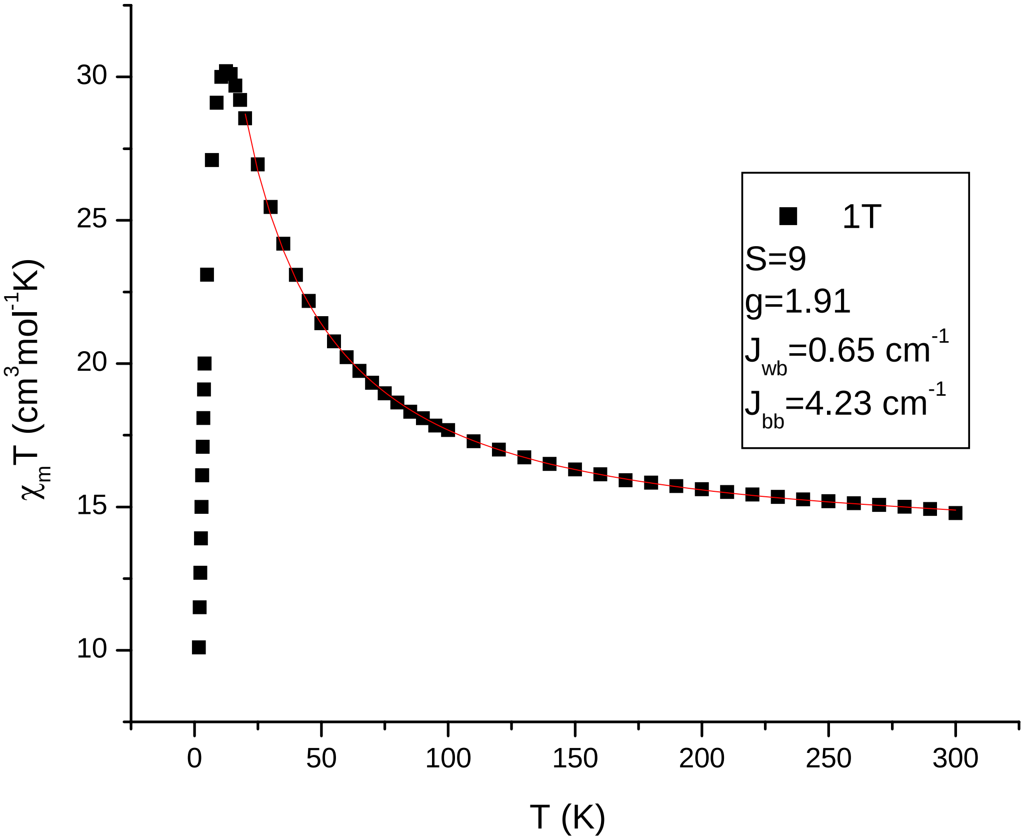

**Figure 7.** Magnetic susceptibility of $[Mn^{II}_2Mn^{III}_2(mdea)_2(Hmdea)_2(O_2CPhN_3)_4]$ (**3**). Fitted data shown in red.

closest excited state of S=8. Although the fitted data for complex **2** indicates a ground state of S=9. It is possible that the ground state is lower as other $Mn_4$ compounds of a similar architecture have been reported to have lower than a S=9 ground state. This is also evidenced in the lower $\chi_M T$ max for compound **2** versus compound **3**. The $\chi_M T$ value for **2** at 300 K is 10 cm$^3$ mol$^{-1}$ K and rises to a maximum of 17 cm$^3$ mol$^{-1}$ K at ~15 K. The $\chi_M T$ value for **3** at 300 K is 17 cm$^3$ mol$^{-1}$ K and rises to 30 cm$^3$ mol$^{-1}$ K at ~15 K. Below 15K, the drop in $\chi_M T$ is likely due to zero-field splitting and/or Zeeman effects. The discrepancies between the values for compounds **2** and **3** are indicative of a lower spin state for compound **2.** Spin states lower than S=9 have been seen for the $Mn_4$ dicubane type of compounds with lower $\chi_M T$ max values.[21] Further analysis is necessary to decipher the spin ground state of compound **2**.

Complex **1** was also analyzed using the reduced magnetization experiment. The sample was measured in the range of 4-1.8 K at different magnetic field strengths varying between 0.1 and 5 T. The results are plotted as M/Nβ versus H/T where M is the magnetization, N is Avogadro's number, β is the Bohr magneton, H is the magnetic field, and T is the absolute temperature. For systems where there is no D value, the iso-fields will be superimposed and will saturate at the value of gS at high magnetic fields. On the contrary, if a D value does exist for the complex, the iso-field data will be split.

The reduced magnetization data can be fit to provide information about g, S, and D. A different spin Hamiltonian is now used to account for both zero-field splitting and Zeeman splitting:

$$\hat{H} = \hat{H}_{Zeeman} + \hat{H}_{zfs} \qquad (3.5)$$

The spin Hamiltonian for these terms can be expressed as:

$$\hat{H} = g\beta H \bullet \hat{S} + D[\hat{S}_z^2 - S(S+1)/3] \tag{3.6}$$

The Hamiltonian operator was diagonalized, taking into account the orientations of the powder average. The eigenvalues obtained are then substituted into the Van Vleck equation:

$$M = \frac{\sum_{i=-S}^{S} (\partial E_i / \partial H) \exp(-E_i / kt)}{\sum_{i=-S}^{S} \exp(-E_i / kt)} \tag{3.7}$$

Utilizing the above equation, the reduced magnetization data is fit and the data for complex **1** is presented in Figure 8 with the fit shown as the solid black line. An important restriction exists for this method of fitting the data; the spin ground state needs to be well-isolated from any excited states as the model assumes a single spin state.

The parameters determined from the fit of the reduced magnetization data of complex **1** to the above model are S=4, g=2.06, and D=-0.55. The values are comparable to the previously determined values for $[Ni(hmp)(MeOH)Cl]_4$ of S=4, g=2.09, and D=-0.60 $cm^{-1}$. This result indicates that there is roughly the same barrier toward reversal of magnetization in complex **1** to its analogous compound. The g value as determined my magnetic susceptibility fit optimization differs from the g value reduced magnetization data but both fits are not good. The fit to the reduced magnetization data deviates from the experimental data as seen by the failure of solid lines to superimpose upon the points in Figure 5. This is possibly due to the invalid assumption of a well isolated spin state. Fitting of $\chi_M T$ predicted an energy separation of the spin ground state to the first excited state of 15.4 $cm^{-1}$. At 5 K, the ambient thermal energy is 3.5 $cm^{-1}$. Although small when compared to the barrier to the next state, the $\chi_M T$ fit resulted in a high g parameter and the

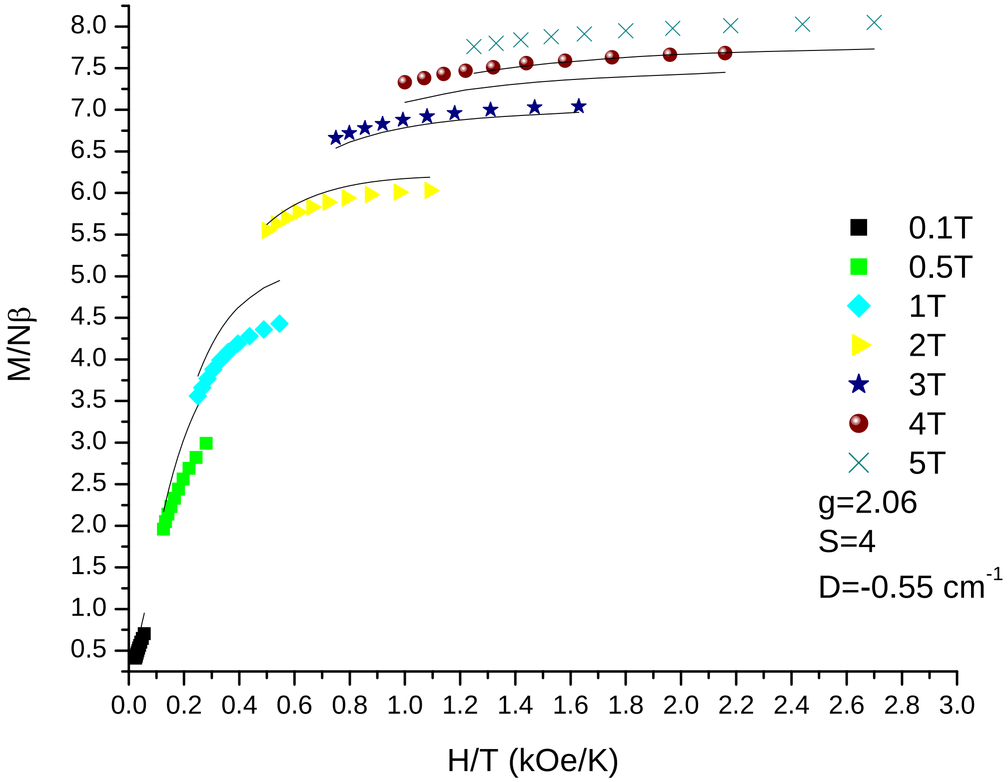

**Figure 8.** Reduced magnetization plot of [Ni(hmp-Cl)(MeOH)Cl]$_4$ • 1/3MeOH (**1**•1/3MeOH**).** Fit shown in black.

energy barrier may be smaller. Therefore, it is possible that there is a distribution of spin state within the temperature range of the experiment. Additional analysis is necessary to accurately determine the g value.

Reduced magnetization analysis was done for complexes **2** and **3** using the same model as before and is presented in Figures 9 and 10. The D values for complex **2** and **3** are comparable at $D=-0.16\ cm^{-1}$ and $D=-0.18\ cm^{-1}$, respectively. The g values determined from magnetic susceptibility fitting are different from the values obtains for reduce magnetization fitting for **2** and **3** with $g=1.24$ and $g=1.63$, respectively. The maximum value in the reduced magnetization plot for complex **2** is lower than that in complex **3** which follows the trend of lower values seen in the reduced magnetization plot. A summary of the optimized parameters for all compounds can be seen in Table 2.

### AC Susceptibility Measurements

Evidence that complexes **1-3** are SMMs was obtained through measurement of AC susceptibilities. Prerequisites of SMMs are that they must have a large spin ground state and negative magnetoanisotropy to generate a barrier to reversal of magnetization between spin up and spin down states. When such a barrier exists, a sluggish magnetization response occurs in an oscillating AC field at low temperatures. The molecule is unable to reverse its magnetization at the frequency of the applied AC field and an out-of-phase ($\chi''_M$) response is seen with a corresponding drop in the in-phase susceptibility ($\chi'_M$). Frequency dependence should be seen in their AC susceptibilities. The drop for the in-phase component and rise in the out-of-phase component of the signal should be greater and begin at higher temperatures for the higher frequencies.

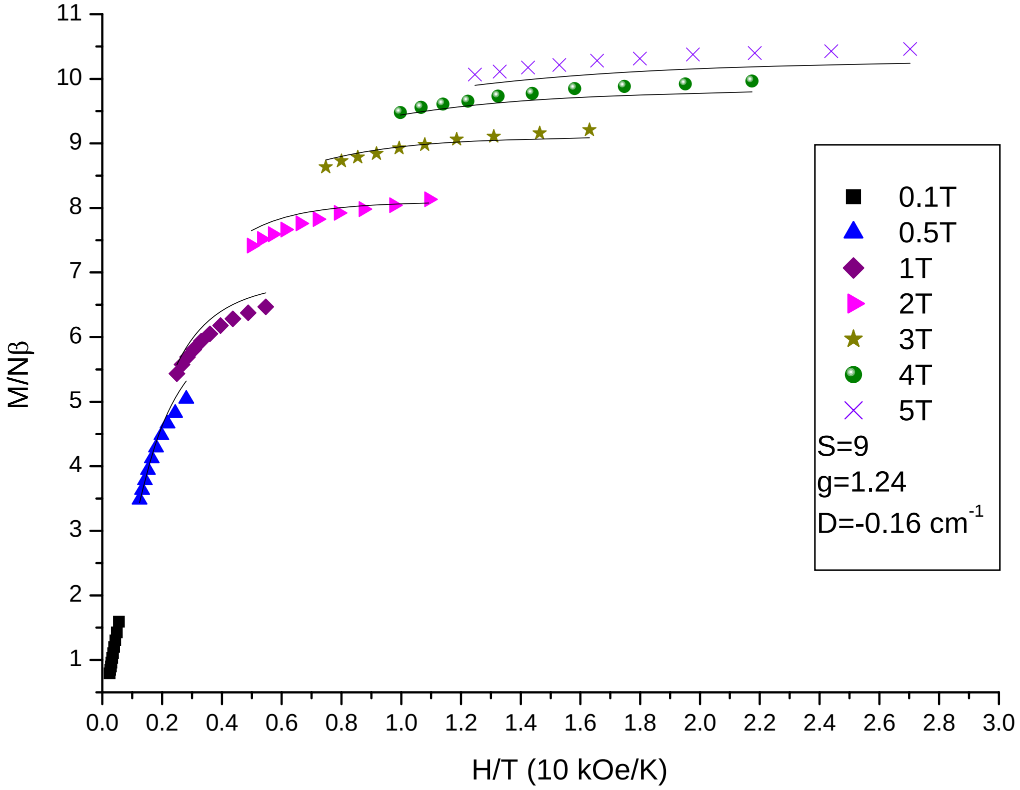

**Figure 9.** Reduced magnetization plot of $[Mn^{II}_2Mn^{III}_2(mdea)_2(Hmdea)_2(O_2CPhBr)_2Cl_2]$ • $Et_2O$ (**2** • $Et_2O$). Fit shown in black.

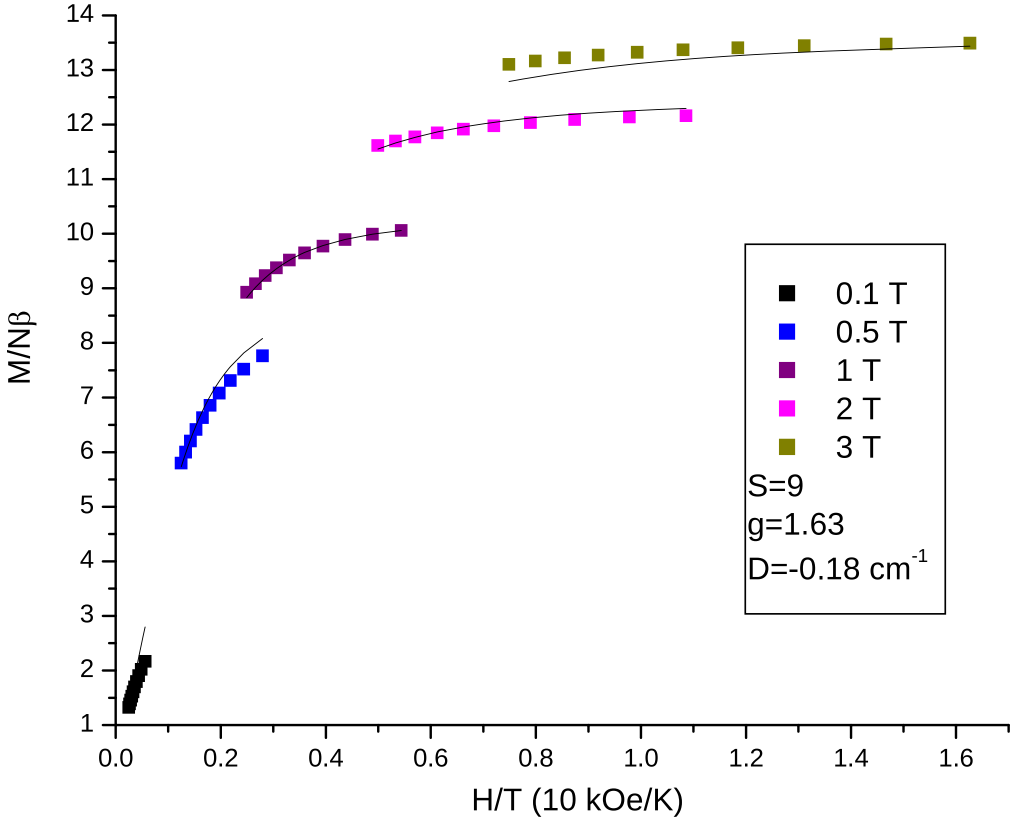

**Figure 10.** Reduced magnetization plot of of $[Mn^{II}_2Mn^{III}_2(mdea)_2(Hmdea)_2(O_2CPhN_3)_4]$ (**3**). Fit shown in black.

**Table 2.** Summary of Parameters Obtained from Fitting DC Magnetization Data

| **Complex** | **Formula** | **Mag. Suceptibility** | | | | **Red. Mag.** | | |
|---|---|---|---|---|---|---|---|---|
| | | **g** | **S** | **$J_{wb}$ cm$^{-1}$** | **$J_{bb}$ cm$^{-1}$** | **S** | **g** | **D cm$^{-1}$** |
| **1** | $[Ni(hmp\text{-}Cl)(MeOH)Cl]_4$ •1/3MeOH | 2.22 | 4 | 2.71 | 3.5 | 4 | 2.06 | -0.55 |
| **2** | $[Mn^{II}_2Mn^{III}_2(mdea)_4(O_2CPhBr)_2Cl_2]$ | 1.62 | 9 | 0.21 | 3.16 | 9 | 1.24 | -0.16 |
| **3** | $[Mn^{II}_2Mn^{III}_2(mdea)_4(O_2CPhN_3)_4]$ | 1.91 | 9 | 0.65 | 4.23 | 9 | 1.63 | -0.18 |

Powdered microcrystalline samples were measured between 5 and 1.8 K with a 3 G AC field. The oscillation frequencies studied were 250 Hz, 500 Hz, 750 Hz, and 1000 Hz. The AC susceptibility measurements are plotted as their in-phase and out-of-phase components versus temperature. The plots for complexes **1-3** can be seen in Figures 11-13, respectively.

Complex **1** exhibits an AC response typical of $Ni_4$ compounds. Due to their lower spin and anisotropy, only a small barrier for reversal of magnetization exists. Therefore, the onset of an out-of-phase response occurs at a much lower temperature (< 2.5 K) and is less pronounced. Although only exhibiting a small signal, the proper frequency dependence is seen in this complex. The out-of-phase component for higher frequencies starts at a higher temperature and has a greater absolute value. The AC susceptibility of $Ni_4$ fails to reach a peak in the temperature range explored due to the small energy barrier of the system.

Complex **2** and **3** **(**Figures 12 and 13) have a larger barrier for reversal of magnetization than complex **1** due to their larger spin (S=9 versus S=4). Their signals saturate just above 2 K and the expected frequency dependence is seen with increased sluggishness at higher frequencies of oscillation. In addition, that larger barrier allows for the onset of the out-of-phase AC response to occur at a higher temperature (< 3 K) and makes up a larger portion of their in-phase signals (~10 %).

The establishment of a barrier toward reversal of magnetization as seen through AC and DC magnetization susceptibility is evidence that complexes **1-3** are SMMs. Given that, attempts were made to use Suzuki coupling to attach complex **1** to gold surfaces and AuNP-$B(OH)_2$. Complex **1** was chosen as the first candidate because of its

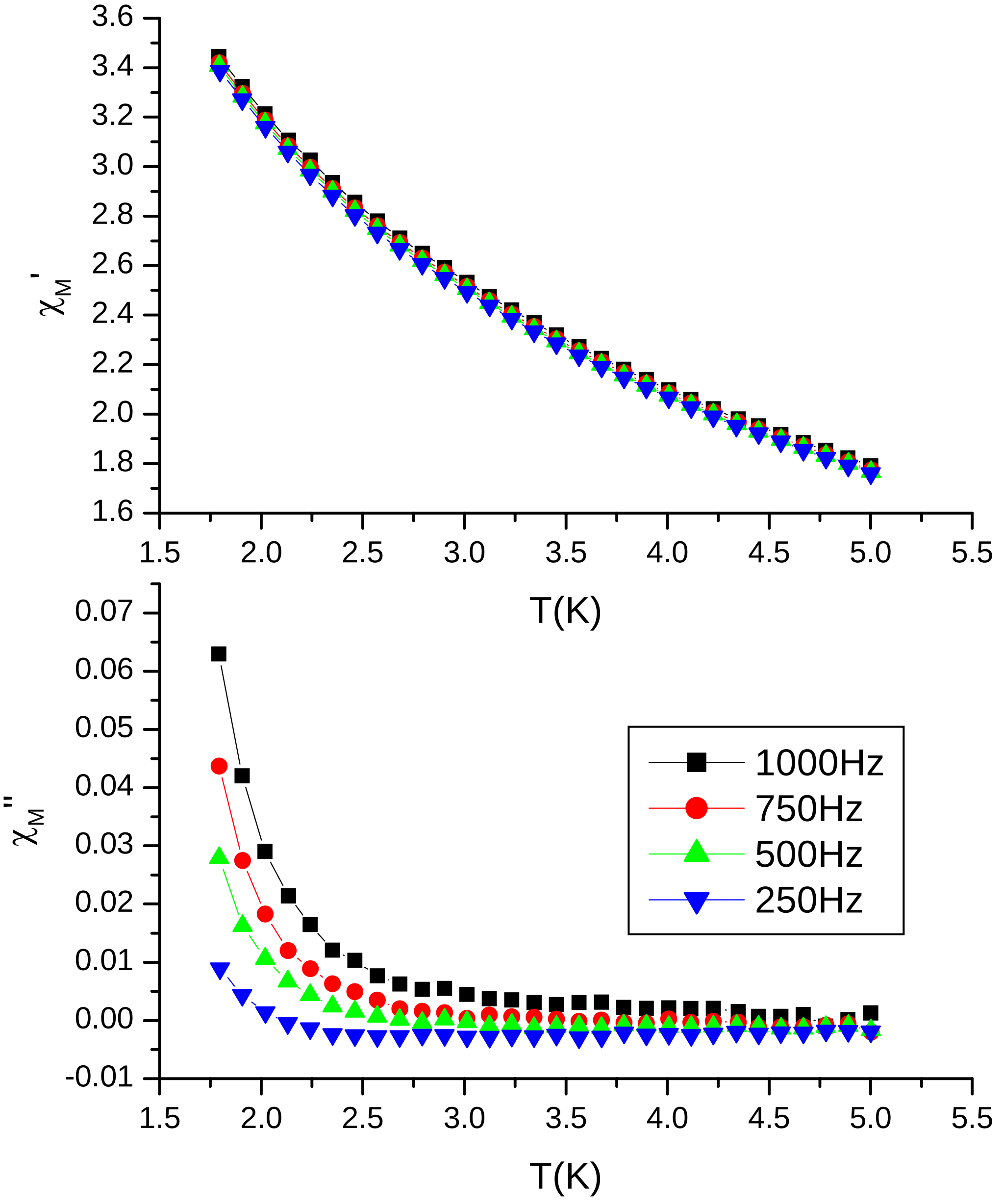

**Figure 11.** AC susceptibility plot of [Ni(hmp-Cl)(MeOH)Cl]$_4$ • 1/3MeOH (**1**•1/3MeOH**)**. The in phase and out of phase susceptibility are plotted on the top and bottom respectively.

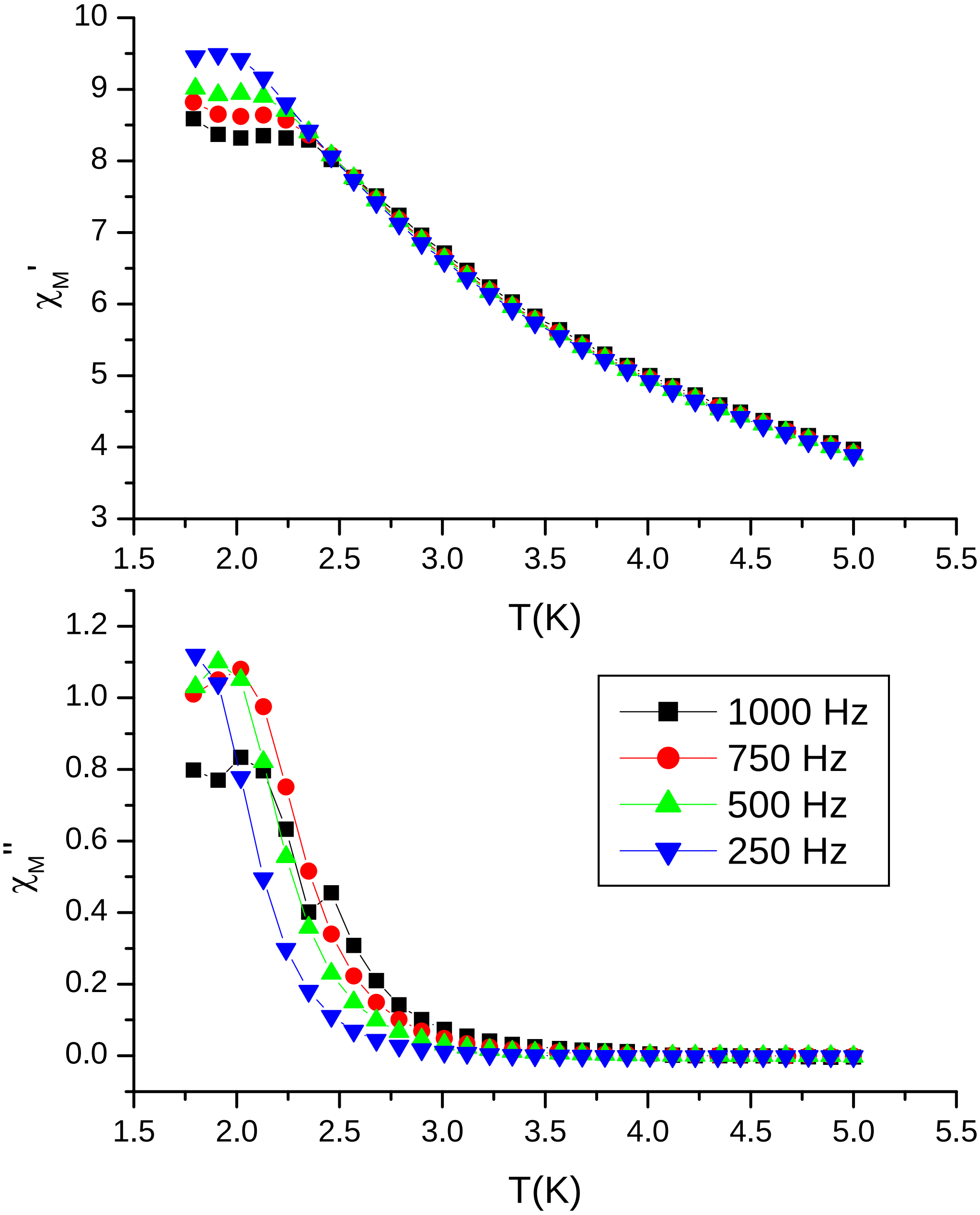

**Figure 12.** AC susceptibility plot of $[\mathrm{Mn^{II}}_2\mathrm{Mn^{III}}_2(\mathrm{mdea})_2(\mathrm{Hmdea})_2(\mathrm{O_2CPhBr})_2\mathrm{Cl_2}] \bullet \mathrm{Et_2O}$ (**2** • $\mathrm{Et_2O}$**).** The in phase and out of phase susceptibility are plotted on the top and bottom respectively.

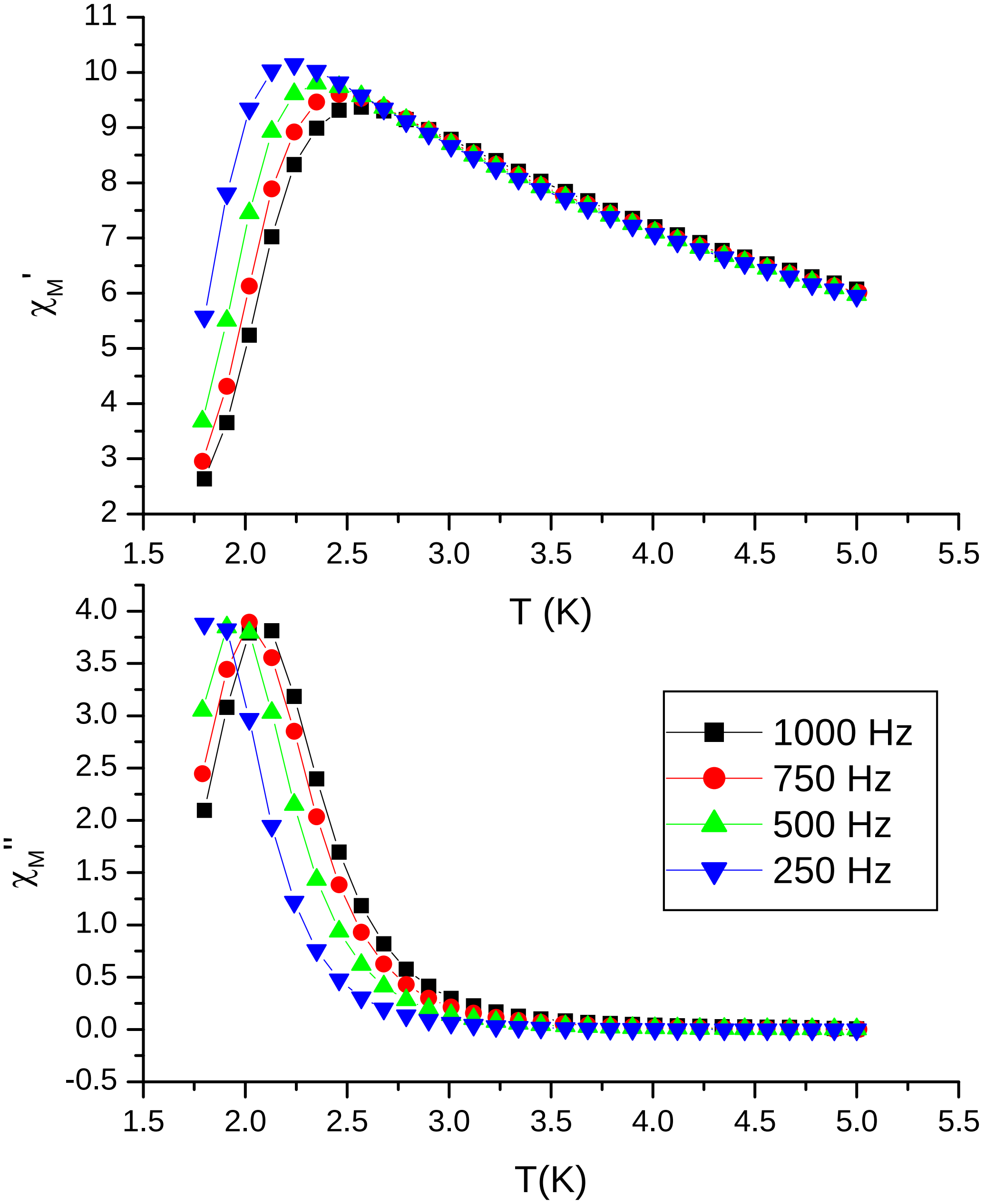

**Figure 13.** AC susceptibility plot of $[Mn^{II}_2Mn^{III}_2(mdea)_2(Hmdea)_2(O_2CPhN_3)_4]$ (**3**). The in phase and out of phase susceptibility are plotted on the top and bottom respectively.

greater simplicity with fewer metal centers and the higher stability of the $Ni^{II}$ oxidation state. In addition, hmp-Cl is a stable chelating ligand for the $Ni_4$ systems and does not as readily exchange as the carboxylate ligands do in the $Mn_4$ systems.

### Suzuki Coupling to Gold Surface and Surface FT-IR

Surface FT-IR measurements were used to monitor the progress of the Suzuki coupling reactions. The gold substrate was removed from the reaction solution after 24 hrs, rinsed with dry THF, and dried under a $N_2$ stream before measurements with the spectrometer. A background spectrum was taken for comparison with a monolayer of 4-mercaptophenyl boronic acid on gold. The two attempts are designated S1 and S2. The surface FT-IR results are presented in Figures 14 and 15 respectively.

The peak used to monitor reaction progress was the B-O stretching peak at 1370 $cm^{-1}$ and the hmp C=C aromatic stretch at 1600 $cm^{-1}$.[23] As the reaction progresses, the B-O peak should decrease in intensity as boronic acid is eliminated with Cl in the Suzuki coupling reaction. The background spectrum shows a peak 1600 $cm^{-1}$ before Suzuki Coupling due to the C=C aromatic stretch of the phenyl ring for the monolayer of 4-mercaptophenyl boronic acid on gold. This peak intensifies after Suzuki Coupling due to the hmp. FT-IR analysis of the free ligand and complex **1** verifies the occurrence of the peak at 1600 $cm^{-1}$ as seen in Figure 16.

### XPS Results

X-ray photoelectron spectroscopy has been one of the standard techniques for verifying the presence of SMMs attached to gold substrates and was used here as well.[8, 9] Experiments were run on a bulk sample of complex **1** (Figure 17), S1 (Figure 18), and S2

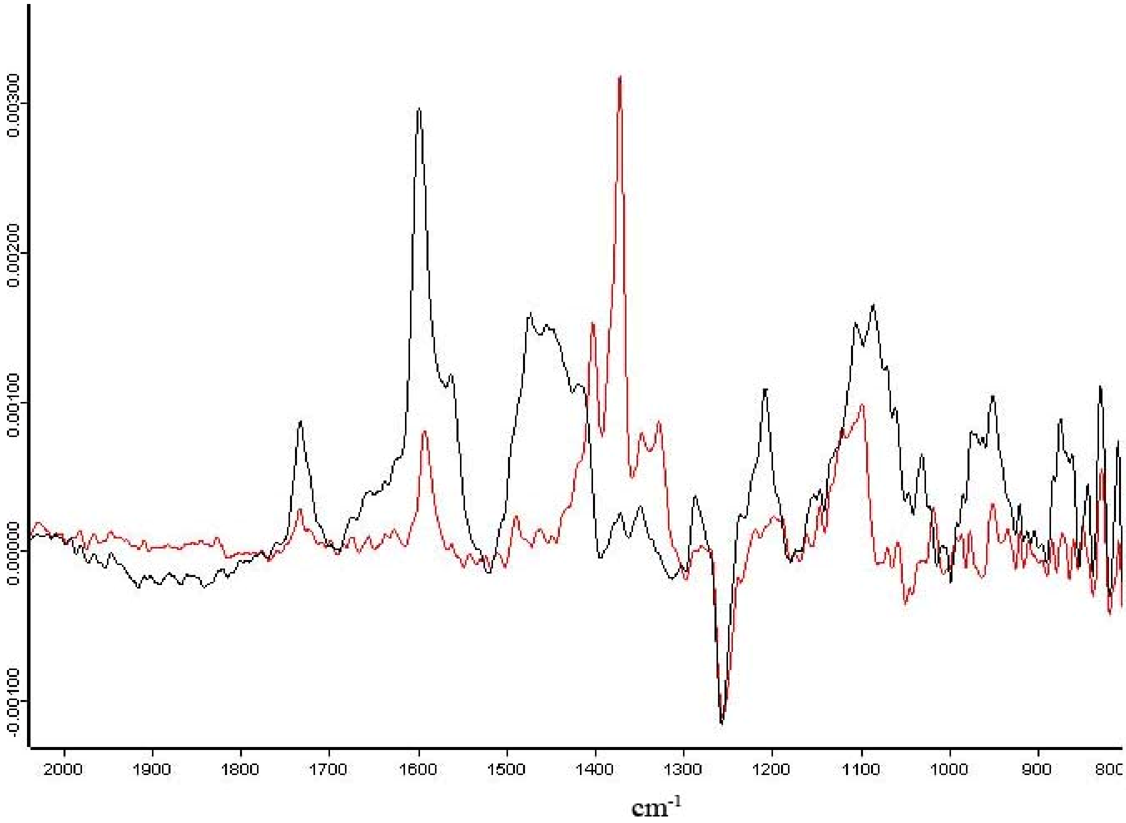

**Figure 14.** Sample S1 surface FT-IR results of Suzuki coupling to complex **1**. The initial sample with 4-mercaptophenyl boronic is shown in red and the Suzuki Coupling reaction after 24 hours in black.

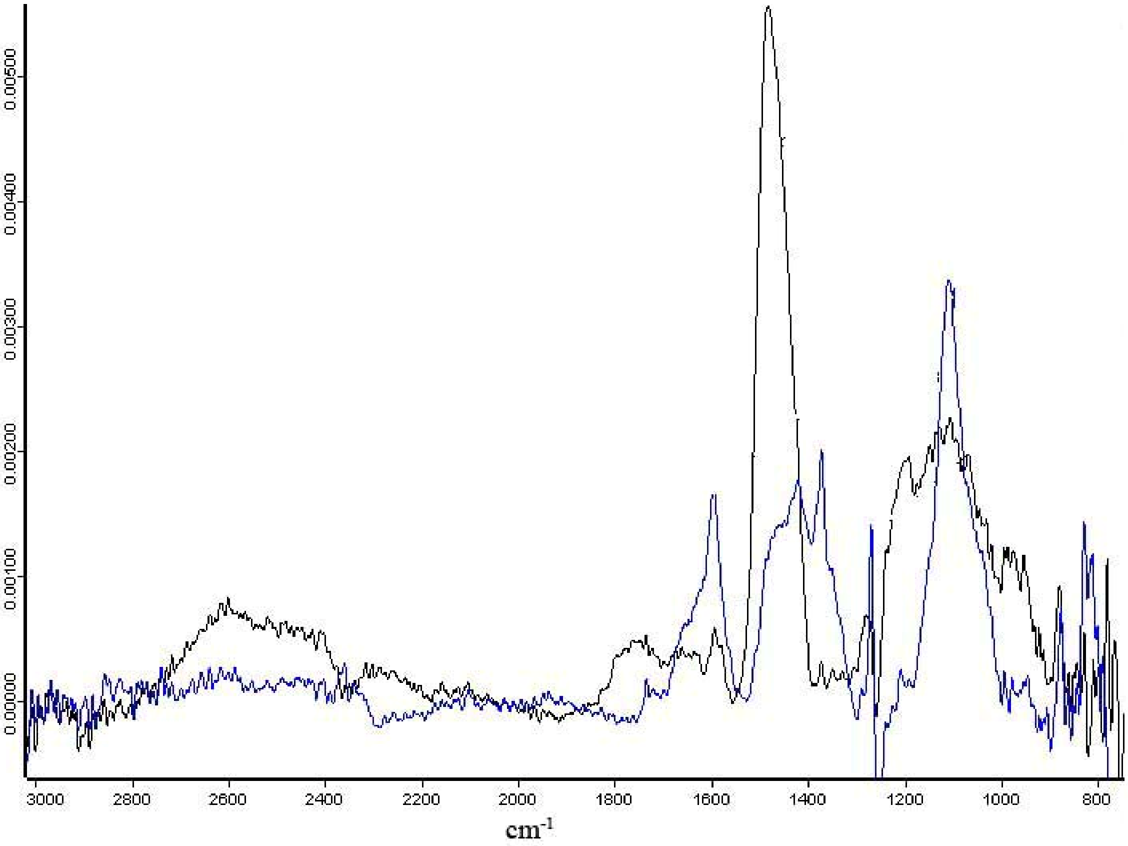

**Figure 15.** Sample S2 surface FT-IR results of Suzuki coupling to complex **1**. The initial sample with 4-mercaptophenyl boronic is shown in blue and the Suzuki Coupling reaction after 24 hours in black.

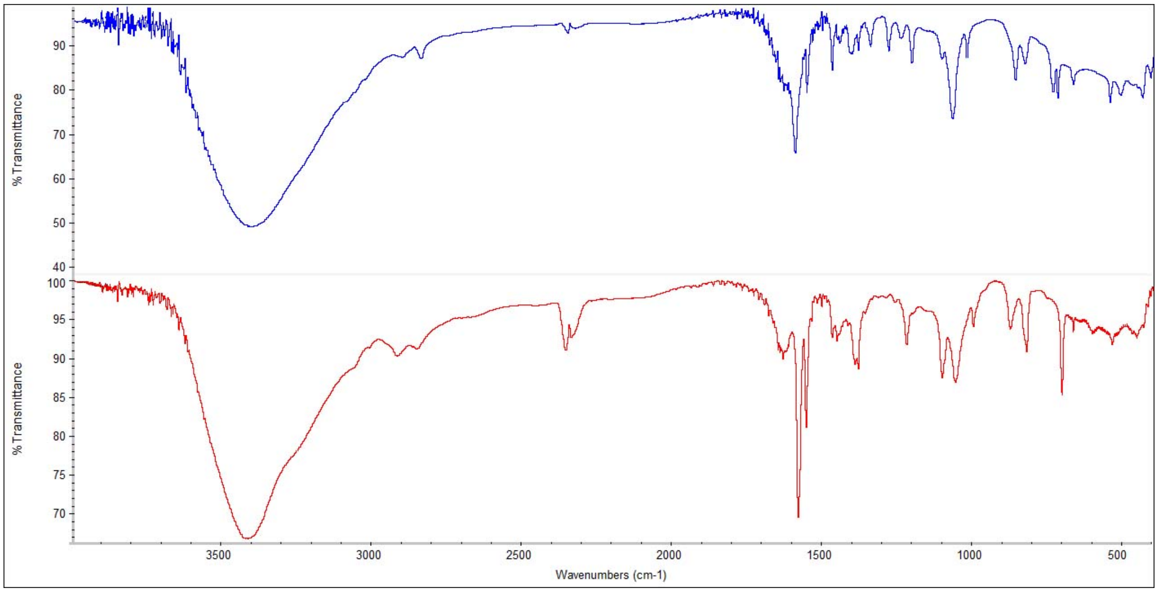

**Figure 16.** FT-IR in KBr spectra of Complex **1** shown on top in blue and 4-chloro-2-hydroxymethyl pyridine shown in red on the bottom.

(Figure 19). The characteristic binding energies of the excited core electrons were used to verify the presence of $Ni^{2+}$ and the other elements in the $Ni_4$ complex. The XPS analysis on the bulk sample of complex **1** confirms the X-ray crystallography results. $Ni^{2+}$ is present in the molecule as well as Cl, N, O, and C originating from the ligands.

A problem arises when analyzing the two samples S1 and S2. The XPS experiment detects the presence of $Ni^{2+}$, N, O, and C from complex **1** on the surface of the gold substrate. However, Cl is absent from both samples. While it is expected and desired that the Cl group is removed from hmp-Cl during the coupling reaction, Suzuki coupling should not interact with Cl coordinated to $Ni^{2+}$. Suzuki coupling is a cross coupling reaction between a boronic acid and an aryl chloride. Coordinated $Cl^-$ lacks the activity to react with the boronic acid through the Suzuki pathway. Without the existence of the $Cl^-$ peak, it cannot be definitively established that complex **1** attached to the surface of the gold intact.

Further analysis needs to be done to determine whether complex 1 attaches as an intact molecule to gold. Surface FT-IR measurements show the disappearance of the peak attributed to boronic acid at 1370 $cm^{-1}$ and the rise of a C=C aromatic peak at 1600 $cm^{-1}$ which can be attributed to the hmp. XPS results show that $Ni^{2+}$ is on the surface of the gold but the molecule may not be intact. The spectrum has the noticeable lack of a peak attributed to Cl. Results indicate that Suzuki coupling is happening on the surface but it is unclear what is happening to the $Cl^-$ on complex **1**. Without additional analytical techniques, it cannot be accurately determined what happened to complex **1** on the surface.

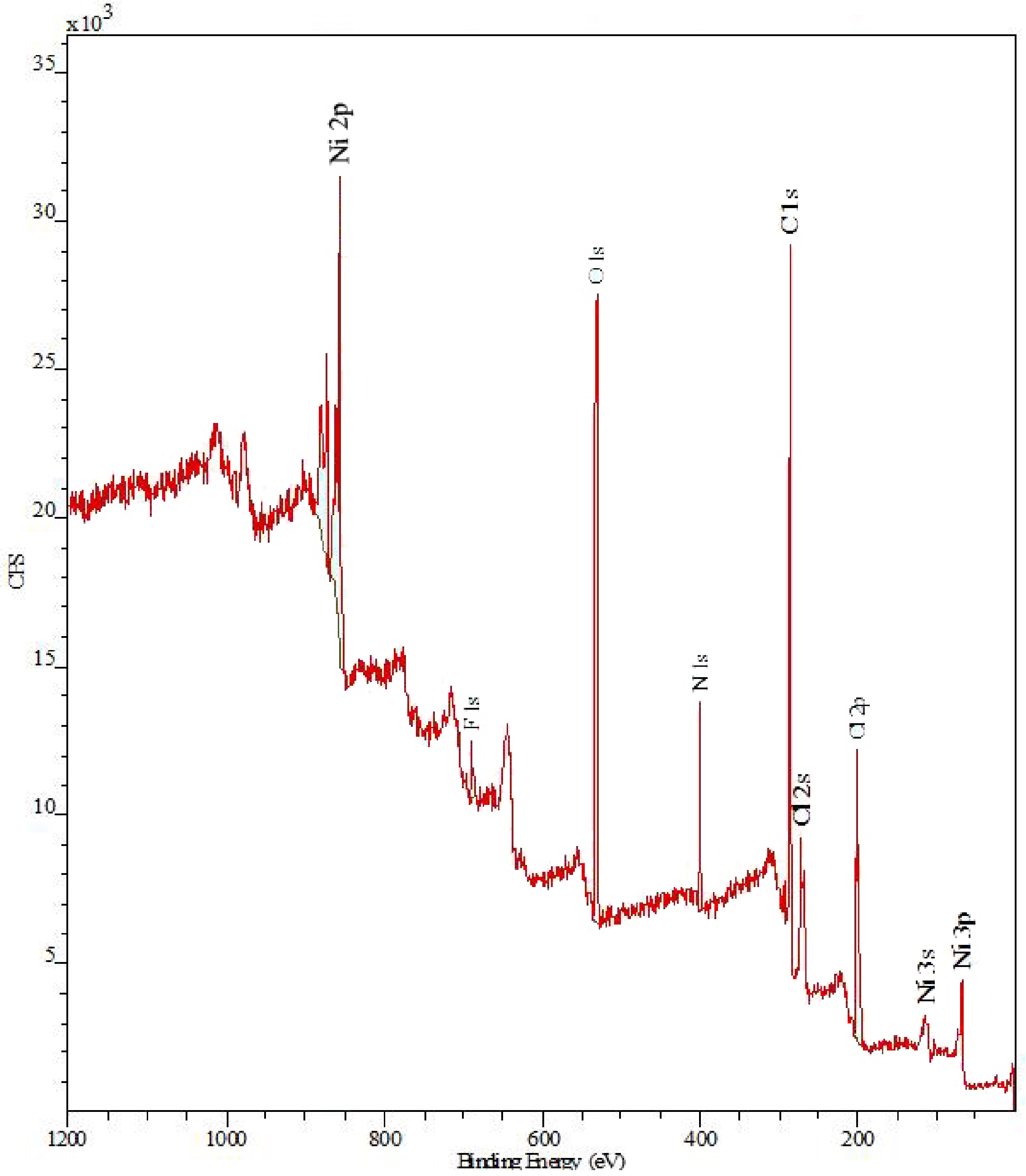

**Figure 17.** XPS measurements on the bulk sample of [Ni(hmp-Cl)(MeOH)Cl]$_4$ (**1**).

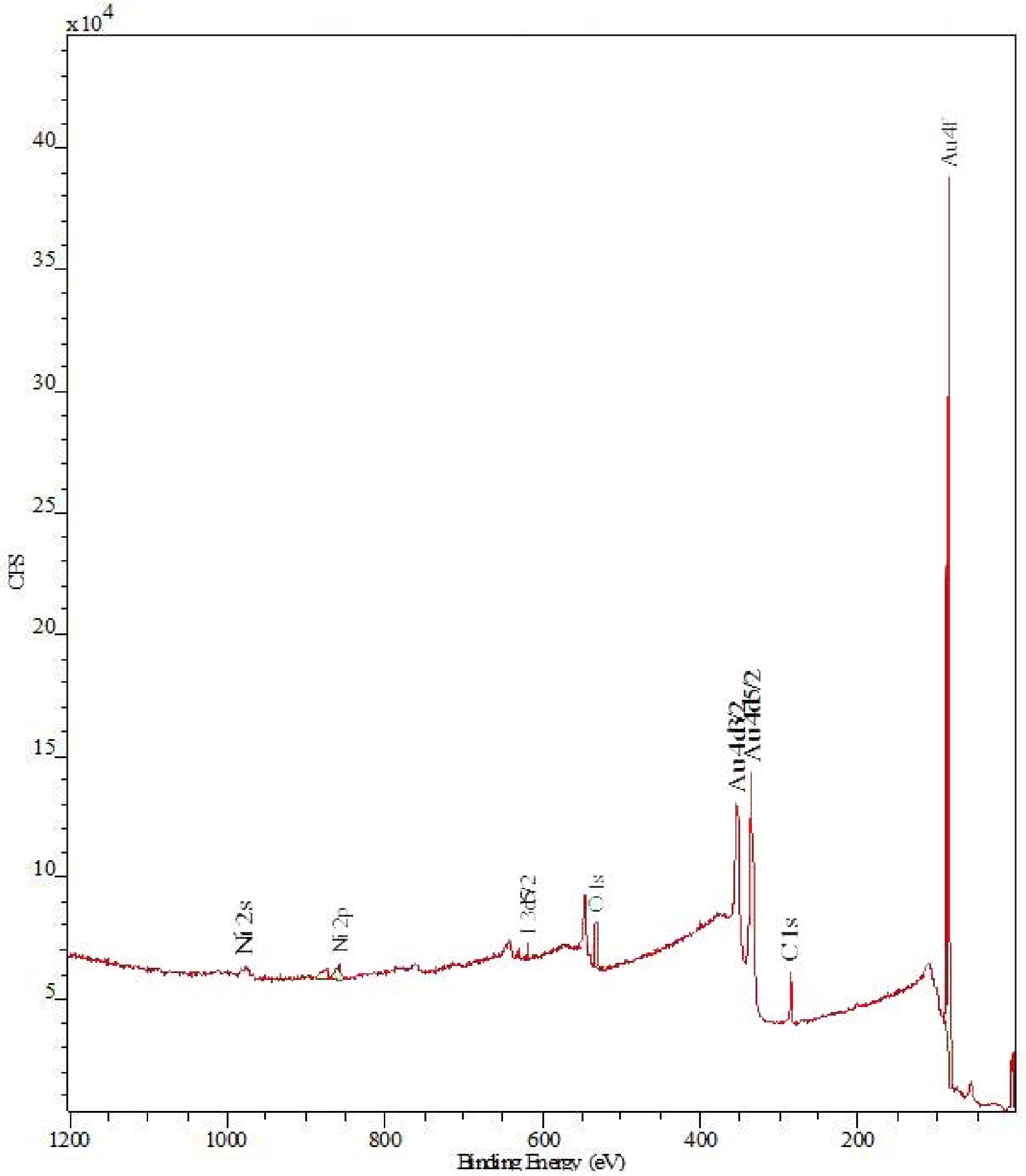

**Figure 18.** XPS measurements on sample S1 after Suzuki coupling with complex **1.**

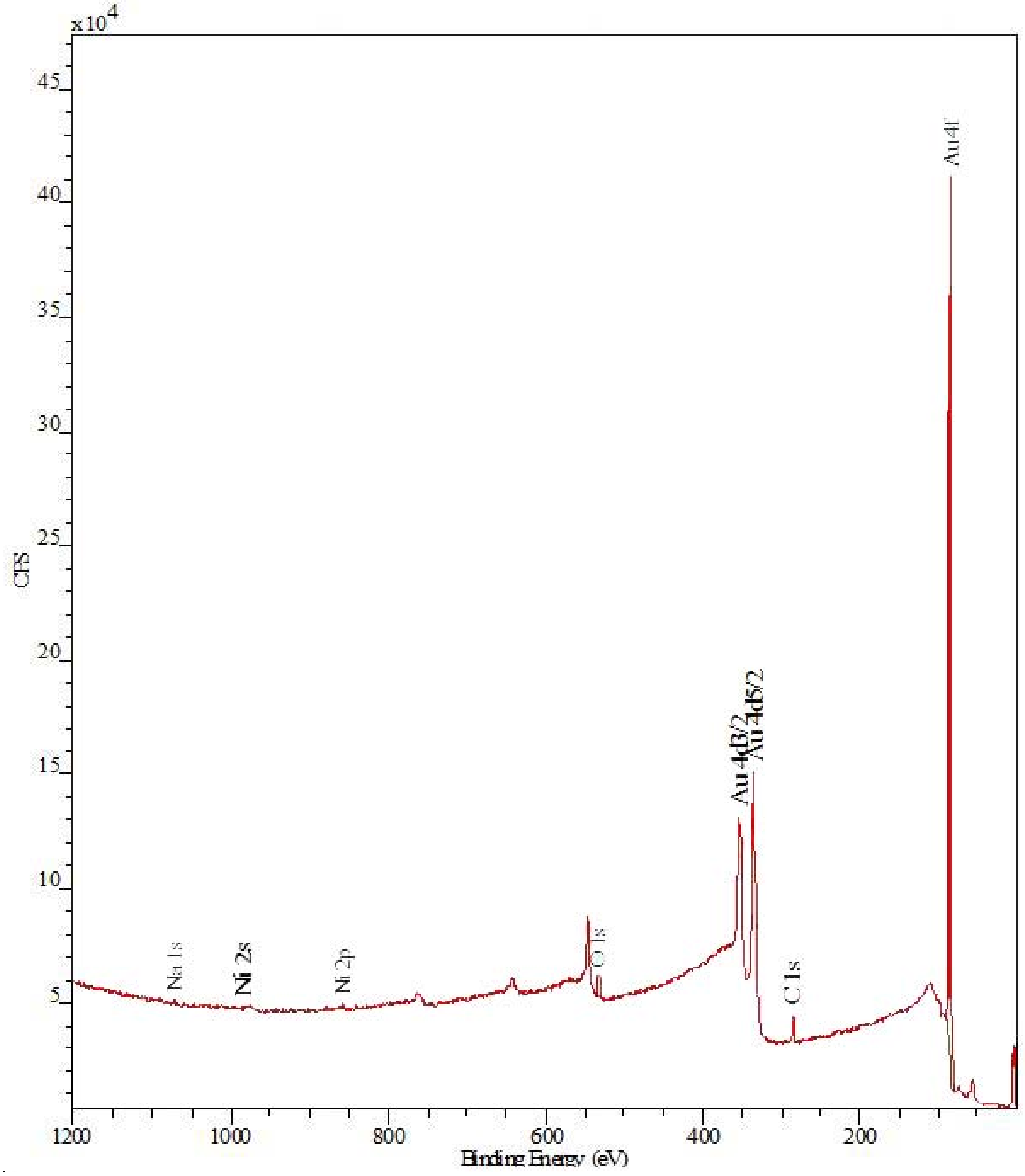

**Figure 19.** XPS measurements on sample S2 after Suzuki coupling with complex **1.**

No magnetic susceptibility instrument currently exists which has the sensitivity to detect the presence of a monolayer of SMMs on a planar substrate.[24] There are approximately ~1.6 x $10^8$ molecules of complex **1** on the surface which is translates into ~2.8 x $10^{-13}$ g. Therefore, magnetic measurements are currently not possible for this system. As a solution, coupling SMMs to gold nanoparticles was explored as a means to examine whether the magnetic moment of SMMs attached to gold can be detected.

### AuNP-B(OH)$_2$

The synthesis of the AuNP-B(OH)$_2$ yielded a fine black powder that was soluble in EtOH. FT-IR analysis on the nanoparticles and the organic capping agent indicated that 4-merceptophenyl boronic acid was present on the nanoparticles. The spectrum of the free capping agent and the nanoparticle can be seen in Figure 20. The IR spectrum of the two indicates that the characteristic peaks of B-O stretching at 1370 cm$^{-1}$ and C=C aromatic ring stretching at 1600 cm$^{-1}$ are present in both compounds. The IR peaks indicate that 4-mercaptophenyl boronic acid is present on the surface of the nanoparticles as desired.

TEM was used analyzed the size and distribution of particles and an image of the particles is presented in Figure 21. The particles were found to be in the size range of ~7 nm. This puts the nanoparticles in the scope of sizes found for other reported nanoparticles of this type.[15, 18]

EDS was used to characterize the elements present in AuNP-B(OH)$_2$. Unfortunately, the TEM used did not have these capabilities and an SEM microscope

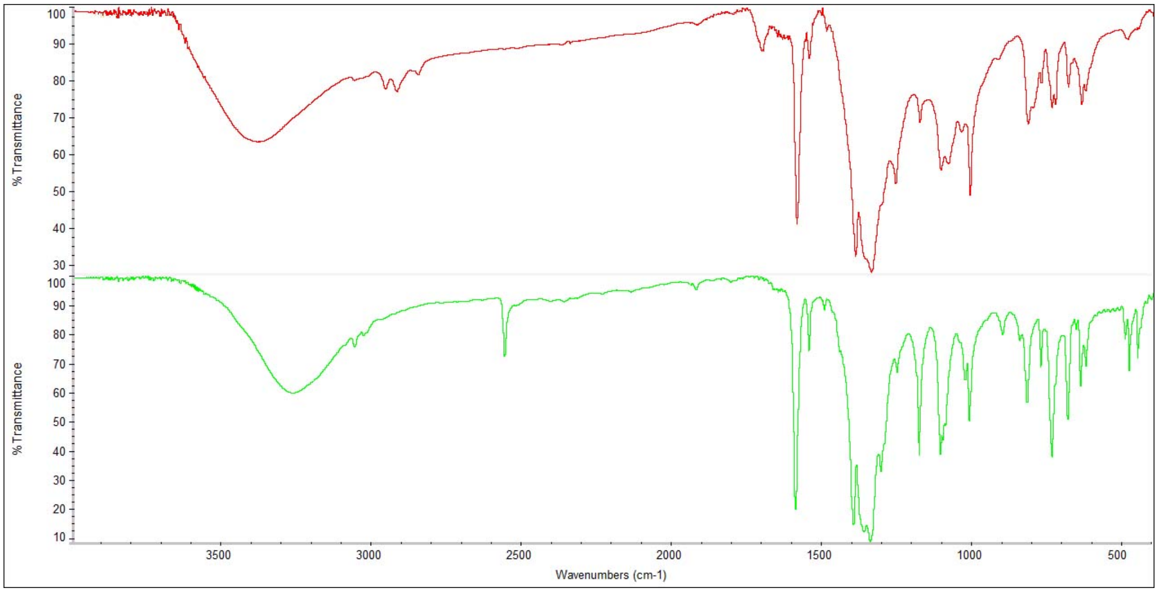

**Figure 20.** Baseline corrected FT-IR spectra of AuNP-B(OH)$_2$ (top) and 4-mercaptophenyl boronic acid (bottom).

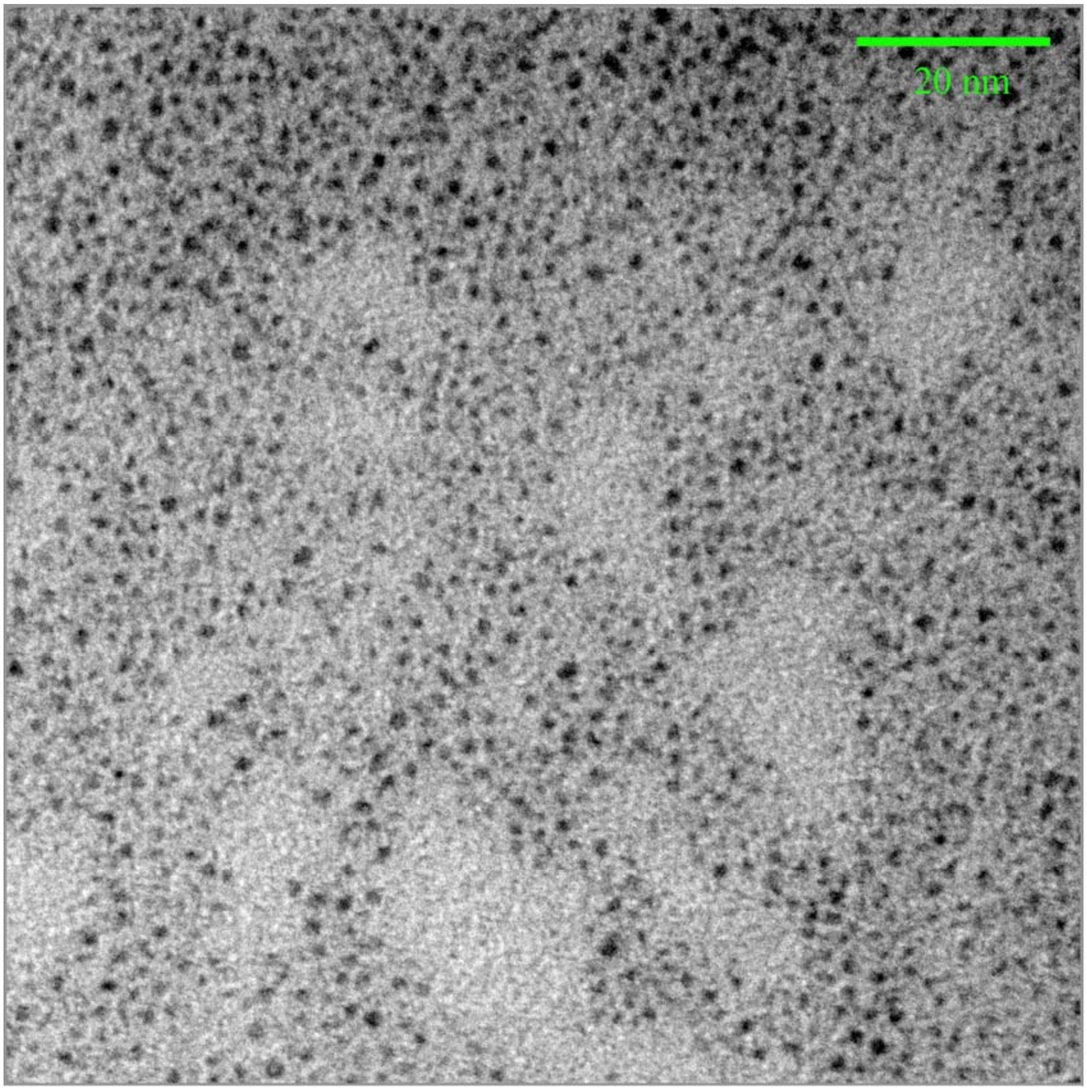

**Figure 21.** TEM image of AuNP-B$(OH)_2$ at 220,000x zoom.

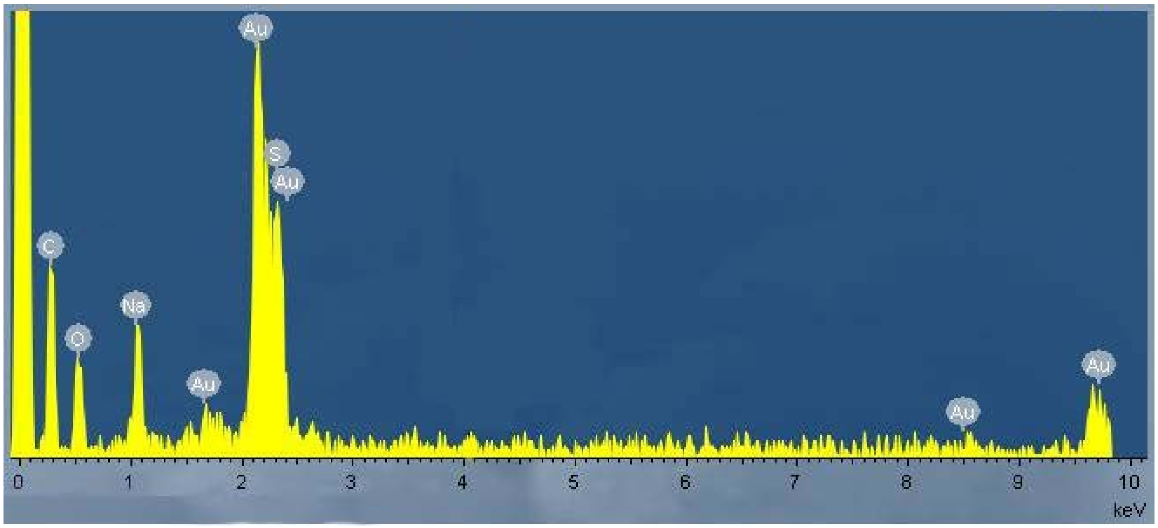

**Figure 22.** EDS results on AuNP-B$(OH)_2$ obtained from a bulk sample using a SEM. The expected heavy elements of Au, S, and O are present. EDS is less capable of detecting lighter elements.

equipped with an EDS probe was used on a bulk sample of the nanoparticles. The EDS results are present in Figure 22. The expected elements of Au, S, and O were observed in the spectrum as desired. Lighter elements C, B, and H cannot be accurately determined through EDS.

These results collectively indicate that AuNP-$B(OH)_2$ was properly synthesized. Their particle size is in the nanoscale regime. Elemental analysis and EDS confirm their correct composition. FT-IR spectroscopy indicates that the correct functional groups are present for Suzuki coupling. Therefore coupling reactions of complex **1** to AuNP-$B(OH)_2$ proceeded.

A modified Suzuki Coupling scheme was employed for coupling complex **1** to AuNP-$B(OH)_2$. POPD-1 was used as the Pd catalyst because it generates higher yields than $Pd(PPh_3)_4$ under aerobic conditions.[10] Completeness of reaction is becomes a larger factor in the case of the nanoparticles as opposed to the gold substrate because there is significantly more reactions necessary. Reactions were also done with less of an excess of complex **1**. After reaction, the solvent was removed under reduced pressure. Excess complex **1** was removed through a washing with THF. The final product was a black precipitate that was no longer soluble in EtOH.

Magnetic measurements were done on the coupled nanoparticles. A background of AuNP-$B(OH)_2$ was measured in addition to coupled AuNP-SMM. The magnetic data for both is presented in Figure 23. Assuming the average 7 nm diameter for each nanoparticle, it is estimated that there are ~11,000 Au atoms per AuNP. This translates into a surface area of ~620 $nm^2$ allowing for an ideal total coverage population of 64 $Ni_4$ molecules per AuNP. This in turn results in nanoparticle samples that are approximately

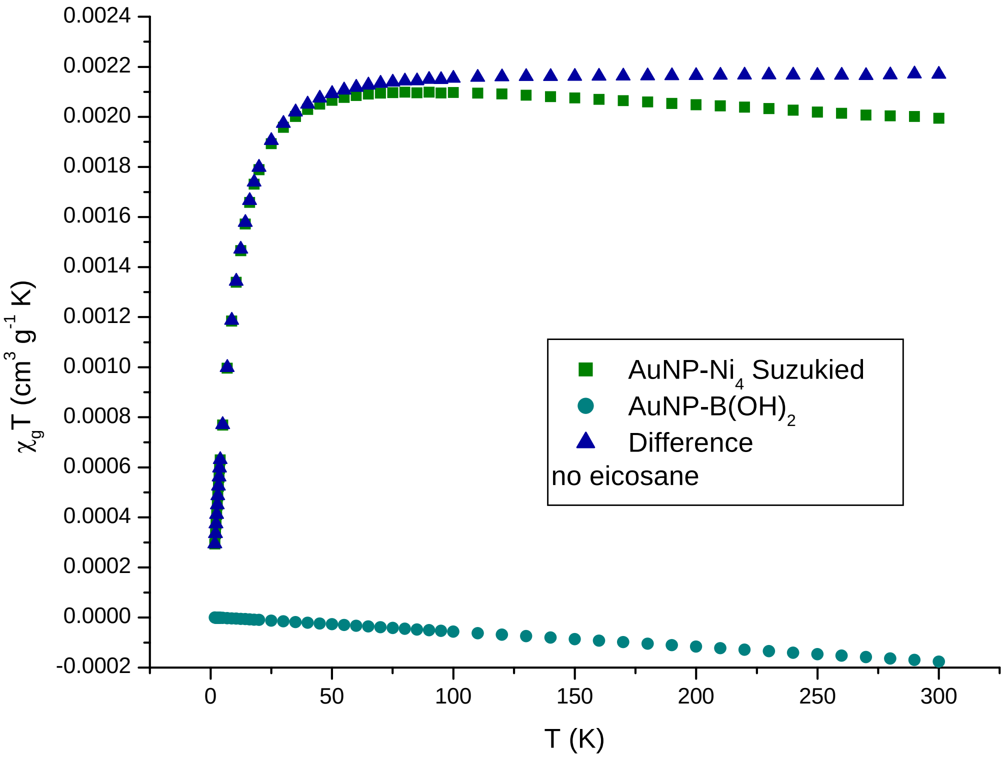

**Figure 23.** DC magnetic susceptibility data on AuNP-B(OH)$_2$ and AuNP functionalized with complex **1**.

3 wt% $Ni_4$. So although small, there is significantly more $Ni_4$ atoms than on a planar gold surface. The addition of complex **1** results in a drastically different magnetic susceptibility plot. The susceptibility measurement of AuNP-$B(OH)_2$ alone indicates diamagnetic behavior. A potential complication arises due to the potential ferromagnetic behavior of certain AuNP. Depending upon the size distribution and the capping agent employed, AuNP have been observed to exhibit ferromagnetic behavior due to the interaction of the gold surface molecules with the sulfur based capping agent.[25-27] However, in this case the magnetic susceptibility of AuNP-$B(OH)_2$ does not suggest ferromagnetic behavior. The addition of complex **1** to AuNP-$B(OH)_2$ through Suzuki coupling gave rise to a response with a positive $\chi_gT$ value. The $\chi_gT$ value is ~0.0022 $cm^3$ $g^{-1}$ K at high temperatures until 50 K whereupon the value rapidly decreases. This decline at low temperatures is similar to the behavior seen in $Ni_4$ complexes and is attributed to Zeeman splitting. For comparison, the DC magnetic susceptibility data for complex **1** collected at 5 T is provided for comparison in Figure 24. At large magnetic fields, the maximum values for $\chi_gT$ is significantly lower due to Zeeman interactions. However, the data maintains the same temperature response behavior. The large correction terms for eicosane at high temperatures lead to the non-single value for $\chi_gT$ data at high temperatures.

For the coupled nanoparticles, its magnetic susceptibility behavior represents a system much more complicated than the isolated complex **1** as there is no ferromagnetic rise in the susceptibility. The drastic difference from the uncoupled nanoparticles is an indicator that there is likely spin containing molecules on the surface of the nanoparticles. A likely explanation for this difference is that the molecules are interacting through

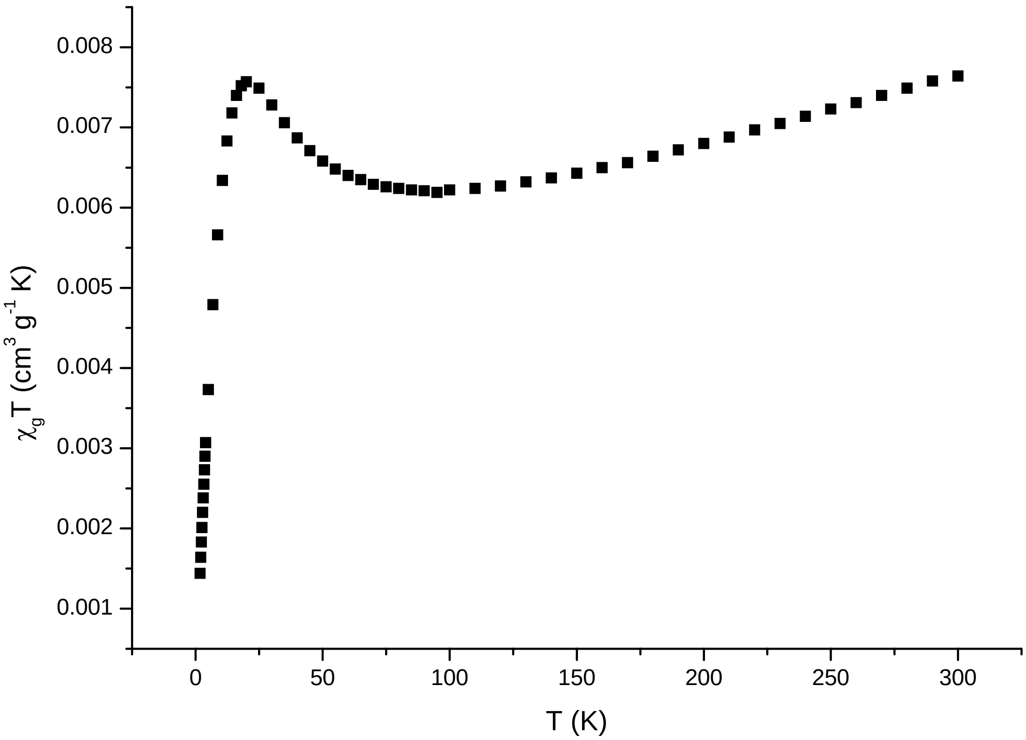

**Figure 24.** DC magnetic susceptibility data on of complex **1** collected at 5 T.

the conducting material. Each $Ni_4$ complex may be interacting with the spins of its neighboring molecules or with the delocalized electrons of the Au surface. It is possible that there is no longer a well defined high spin ground state even at low temperatures. The population of a high spin ground state is responsible for the rise in the DC magnetic susceptibility in the $Ni_4$ cubane family of SMMs. Further analysis needs to be conducted to determine the exact nature of the complex **1** on the gold nanoparticles.

## 3.4 Conclusion

A $Ni_4$ cubane and two $Mn_4$ dicuabne complexes were synthesized that can possibly utilize Suzuki or Click coupling reactions to attach to gold. Their magnetic behavior was characterized and indicates SMM behavior. From fitting of magnetic susceptibility data and reduced magnetization data it was determined that their spin ground states were S=4, S=9, and S=9 for complexes **1, 2**, and **3**, respectively. The spin state of complex **2** is suspect as it exhibits a lower $\chi_M T$ maximum than complex **3** and other S=9 dicubanes. Suzuki coupling was done on complex **1** to gold surfaces and gold nanoparticles. Physical measurements were done both systems in to verify the presence of the intact compound on the surface but results remain inconclusive. Magnetic measurements indicate a change of the magnetic susceptibility of the AuNP after the coupling reaction.

## References

1. Wernsdorfer, W.; Aliaga-Alcalde, N. r.; Hendrickson, D. N.; Christou, G., Exchange-biased quantum tunnelling in a supramolecular dimer of single-molecule magnets. *Nature* **2002,** 416, (6879), 406.

2. Affronte, M.; Troiani, F.; Ghirri, A.; Carretta, S.; Santini, P.; Corradini, V.; Schuecker, R.; Muryn, C.; Timco, G.; Winpenny, R. E., Molecular routes for spin cluster qubits. *Dalton Transactions* **2006**, (23), 2810-2817.

3. Leuenberger, M. N.; Loss, D., Quantum computing in molecular magnets. *Nature* **2001,** 410, (6830), 789-793.

4. Affronte, M.; Troiani, F.; Ghirri, A.; Candini, A.; Evangelisti, M.; Corradini, V.; Carretta, S.; Santini, P.; Amoretti, G.; Tuna, F.; Timco, G.; Winpenny, R. E. P., Single molecule magnets for quantum computation. *Journal of Physics D-Applied Physics* **2007,** 40, (10), 2999-3004.

5. Ni, C.; Shah, S.; Hendrickson, D.; Bandaru, P. R., Enhanced differential conductance through light induced current switching in Mn-12 acetate molecular junctions. *Applied Physics Letters* **2006,** 89, (21), 3.

6. Zobbi, L.; Mannini, M.; Pacchioni, M.; Chastanet, G.; Bonacchi, D.; Zanardi, C.; Biagi, R.; Del Pennino, U.; Gatteschi, D.; Cornia, A.; Sessoli, R., Isolated single-molecule magnets on native gold. *Chemical Communications* **2005**, (12), 1640-1642.

7. Pineider, F.; Mannini, M.; Sessoli, R.; Caneschi, A.; Barreca, D.; Armelao, L.; Cornia, A.; Tondello, E.; Gatteschi, D., Solvent Effects on the Adsorption and Self-Organization of Mn12 on Au(111). *Langmuir* **2007,** 23, (23), 11836-11843.

8. Abdi, A. N.; Bucher, J. P.; Rabu, P.; Toulemonde, O.; Drillon, M.; Gerbier, P., Magnetic properties of bulk Mn(12)Pivalates(16) single molecule magnets and their self assembly on functionnalized gold surface. *Journal of Applied Physics* **2004,** 95, (11), 7345-7347.

9. Coronado, E.; Forment-Aliaga, A.; Romero, F. M.; Corradini, V.; Biagi, R.; DeRenzi, V.; Gambardella, A.; delPennino, U., Isolated Mn12 Single-Molecule Magnets Grafted on Gold Surfaces via Electrostatic Interactions. *Inorg. Chem.* **2005,** 44, (22), 7693-7695.

10. Anderson, K. W.; Buchwald, S. L., General catalysts for the Suzuki-Miyaura and Sonogashira coupling reactions of aryl chlorides and for the coupling of challenging substrate combinations in water. *Angewandte Chemie-International Edition* **2005,** 44, (38), 6173-6177.

11. Evans, R. A., The rise of azide-alkyne 1,3-dipolar 'click' cycloaddition and its application to polymer science and surface modification. *Australian Journal of Chemistry* **2007,** 60, (6), 384-395.

12. Goldhaber-Gordon, D.; Shtrikman, H.; Mahalu, D.; Abusch-Magder, D.; Meirav, U.; Kastner, M. A., Kondo effect in a single-electron transistor. *Nature* **1998,** 391, (6663), 156-159.

13. Kouwenhoven, L.; Glazman, L., Revival of the Kondo effect. *Physics World* **2001,** 14, (1), 33-38.

14. Steglich, F., Superconductivity and magnetism: From antagonism to mutual interplay. *Physica C-Superconductivity and Its Applications* **2007,** 460, 7-12.

15. Gibson, J. D.; Khanal, B. P.; Zubarev, E. R., Paclitaxel-functionalized gold nanoparticles. *Journal of the American Chemical Society* **2007,** 129, (37), 11653-11661.

16. Liu, Q.; Tor, Y., Simple conversion of aromatic amines into azides. *Organic Letters* **2003,** 5, (14), 2571-2572.

17. Yang, E.-C.; Wernsdorfer, W.; Hill, S.; Edwards, R. S.; Nakano, M.; Maccagnano, S.; Zakharov, L. N.; Rheingold, A. L.; Christou, G.; Hendrickson, D. N., Exchange bias in Ni4 single-molecule magnets. *Polyhedron* **2003,** 22, (14-17), 1727-1733.

18. Brust, M.; Fink, J.; Bethell, D.; Schiffrin, D. J.; Kiely, C., Synthesis and reactions of functionalized gold nanoparticles. *Journal of the Chemical Society-Chemical Communications* **1995**, (16), 1655-1656.

19. Carlin, R. L., *Magnetochemistry*. Springer-Verlag: New York, 1986.

20. Yang, E. C.; Wernsdorfer, W.; Zakharov, L. N.; Karaki, Y.; Yamaguchi, A.; Isidro, R. M.; Lu, G. D.; Wilson, S. A.; Rheingold, A. L.; Ishimoto, H.; Hendrickson, D. N., Fast magnetization tunneling in tetranickel(II) single-molecule magnets. *Inorganic Chemistry* **2006,** 45, (2), 529-546.

21. Beedle, C. C.; Heroux, K. J.; Nakano, M.; DiPasquale, A. G.; Rheingold, A. L.; Hendrickson, D. N., Antiferromagnetic tetranuclear manganese complex: Wheel or dicubane? *Polyhedron* **2007,** 26, (9-11), 2200-2206.

22. Yoo, J.; Brechin, E. K.; Yamaguchi, A.; Nakano, M.; Huffman, J. C.; Maniero, A. L.; Brunel, L. C.; Awaga, K.; Ishimoto, H.; Christou, G.; Hendrickson, D. N., Single-molecule magnets: A new class of tetranuclear manganese magnets. *Inorganic Chemistry* **2000,** 39, (16), 3615-3623.

23. Barriet, D.; Yam, C. M.; Shmakova, O. E.; Jamison, A. C.; Lee, T. R., 4-mercaptophenylboronic acid SAMs on gold: Comparison with SAMs derived from thiophenol, 4-mercaptophenol, and 4-mereaptobenzoic acid. *Langmuir* **2007,** 23, (17), 8866-8875.

24. Waldmann, O.; Guidi, T.; Carretta, S.; Mondelli, C.; Dearden, A. L., Elementary excitations in the cyclic molecular nanomagnet Cr-8. *Physical Review Letters* **2003,** 91, (23), 4.

25. Dutta, P.; Pal, S.; Seehra, M. S.; Anand, M.; Roberts, C. B., Magnetism in dodecanethiol-capped gold nanoparticles: Role of size and capping agent. *Applied Physics Letters* **2007,** 90, (21).

26. Michael, F.; Gonzalez, C.; Mujica, V.; Marquez, M.; Ratner, M. A., Size dependence of ferromagnetism in gold nanoparticles: Mean field results. *Physical Review B* **2007,** 76, (22).

27. Garitaonandia, J. S.; Insausti, M.; Goikolea, E.; Suzuki, M.; Cashion, J. D.; Kawamura, N.; Ohsawa, H.; de Muro, I. G.; Suzuki, K.; Plazaola, F.; Rojo, T., Chemically induced permanent magnetism in Au, Ag, and Cu nanoparticles: Localization of the magnetism by element selective techniques. *Nano Letters* **2008,** 8, (2), 661-667.